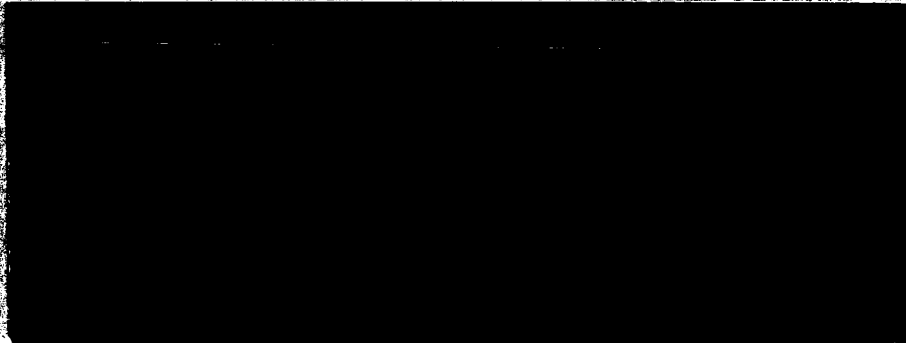


Contract No. 950136



FACILITY FORM 602

N65-20111	
(ACCESSION NUMBER)	(THRU)
107	1
(PAGES)	(CODE)
CR 57526	14
(NASA CR OR TRS OR AD NUMBER)	(CATEGORY)

GPO PRICE \$ \_\_\_\_\_  
C.S.F.T.  
~~GPO~~ PRICE(S) \$ \_\_\_\_\_

Hard copy (HC) 4.00  
Microfiche (MF) 75

Betty J. Conway 4/5/65

PR 57526

FINAL REPORT ON  
ULTRA-HIGH SPEED ELECTRO-OPTICAL SYSTEMS  
EMPLOYING FIBER OPTICS

by  
N. S. Kapany, Principal Investigator  
J. J. Burke  
D. F. Capellaro  
N. A. Peppers

Prepared for  
JET PROPULSION LABORATORY  
under Contract No. 950136  
(Subcontract under NASA Contract NASw - 6 )

This work was performed for the Jet Propulsion Laboratory,  
California Institute of Technology, sponsored by the  
National Aeronautics and Space Administration under  
Contract NAS7-100.

Submitted by  
OPTICS TECHNOLOGY, INC.  
248 Harbor Boulevard  
Belmont, California

November 30, 1962

## ULTRA-HIGH SPEED ELECTRO-OPTICAL SYSTEMS EMPLOYING FIBER OPTICS

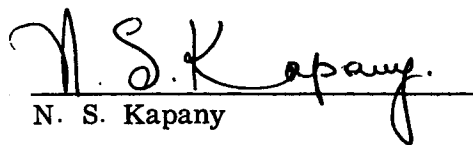
This report describes a comprehensive program aimed at the design and development of high photographic speed, wide angle and high resolution optical systems using fiber optics image correctors. The use of fiber optics field flattener, distortion corrector and conical condenser is shown to give some valuable extra degree of freedom to the lens designer. The preliminary third order design study phase of this program showed that a marked improvement is achievable in the performance of five different types of systems, i. e., cemented and uncemented telescope doublets, landscape doublet, symmetric Hypergon and Pantoskop. A considerable improvement in performance is also achievable in a two element reflector system using a decentered stop at the center of curvature which is capable of working in the ultraviolet, visible and infrared regions of the spectrum. However, further work along these lines is required.

The fabrication and testing of a refracting and a reflecting system using fiber optics field flattener and conical condenser was undertaken. The experimental and analytical studies show that a Sutton lens ( $f/3.5$ ) used in conjunction with a fiber optics field flattener is capable of 150-200 lines/mm resolution over a  $60^\circ$  field angle. When used with a conical condenser such a system is capable of yielding an effective f-ratio less than  $f/1$  and resolution of 70-100 lines/mm. Further developments on a Fresnelized field flattener, high quality conical condenser and distortion corrector should yield optical systems with some unusual performance characteristics. The experimental model of a reflecting system with decentered stop was constructed and only preliminary testing could be accomplished.

During this program evaluation of various optical systems designs with a known amount of aberrations was undertaken using image synthesizer techniques. The importance of taking due account of diffraction effects in high quality systems is demonstrated and the limitations of geometrical optics pointed out. Details of this study are included in Appendix A. On the other hand, the two optical systems constructed were evaluated on a frequency response measuring apparatus capable of measuring up to 500 lines/mm.

Various investigations described in this report point toward the promising new direction in the field of lens design using fiber optics image correctors. However, further design studies and component development work is required to fully exploit the various unusual possibilities.

November 30, 1962

  
N. S. Kapany



## TABLE OF CONTENTS

SUMMARY	i
I. INTRODUCTION	1
II. GENERAL CONSIDERATIONS	4
A. Interrelations Between Overall Resolution and Effective Photographic Speed	4
B. Correction of Aberrations in Cameras Employing Fiber Optics, Image Corrector	9
C. Selection of Merit Evaluation Function Root Mean Square Deviation as a Criterion for Comparison	12
D. Algebraic Formulation of Merit Function for Third Order Study	14
III. RESULTS OF DESIGN STUDY	20
A. Cemented Telescope Doublet	24
B. Uncemented Telescope Doublet	28
C. Cemented Doublet Landscape Lens	30
D. Hypergon	33
E. Pantoskop	36
F. Wide Angle Reflecting System	40
G. Improvement of Performance of Wide Angle Reflecting System Using a Cylindrical Reflector	48
IV. EXPERIMENTAL DATA	52
A. Refracting System	52
B. Camera	58
C. Reflecting System	58

V. FIBER OPTICS	67
A. Fiber Optics Field Flatteners	67
B. Fiber Optics Conical Condenser	68
C. Distortion Corrector	71
 APPENDIX A	 A-1
IMAGE SYNTHESIS STUDIES	
 APPENDIX B	 B-1
APPARATUS FOR MEASURING VERY HIGH SPATIAL FREQUENCY RESPONSE	

# LIST OF FIGURES

<u>Figure No.</u>		<u>Page</u>
1	Resolution vs. f/number of Lens for Various Conical Fiber and Conventional Compound Systems	7
2	Cemented Telescope Doublet Working at f/11.5	25
3	Average Resolution over 16° Full Field as a Function of Effective f/number - Cemented and Uncemented Doublets	27
4	Resolution vs Field Angle for Uncemented Doublet - Spherical Image Surface with Fiber Optics and Best Flat Image Surface	29
5	Mean Square Deviation of All Rays from Center of Gravity, Averaged Over the Field as a Function of Bending for Semi Fields 30°, 10°, 8°, 4°, 2°	31
6	Landscape Objective, a Cemented Doublet Working at f/11.5	32
7	Resolution vs. Effective f/number for Landscape Doublet	34
8	Hypergon at f/10, Best Correction with Bending as a Function of Field Angle	35
9	Resolution vs. Effective f/number for Hypergon for f/10 30° Semi-Field Angle Alone and with Fiber Optics	37
10	Pantoskop at f/10, Best Correction Attainable with Bending as a Function of Semi-Field Angle	38
11	Resolution vs. Effective f/number for Pantoskop Designed for f/10 and 30° Semi- Field Angle	39
12	f/8 Wide Angle Reflecting Camera with Decentered Elliptical Aperture	41
13	RMS Deviation for Axial Imaging by Decentered Reflector with Elliptical Stop	45

14	RMS Deviation for 400 Rays as a Function of Full Field Angle for Elliptical Apertures at f/8 and f/12	47
15	Sutton Lens Specification	53
16	Summary of Frequency Response Data	54
17	Frequency Response of Sutton Lens at Gaussian Focal Plane	55
18	Frequency Response of Sutton Lens - Field Flatteners Combination	56
19	Suttons Lens Camera	59
20	Suttons Lens Camera Exploded View	60
21	San Carlos Homes Taken with Sutton Lens Camera	61
22	Test Object Taken with Sutton Lens Camera	62
23	Test Object Taken with Sutton Lens without Field Flatteners	63
24	Reflecting System Camera	65

#### APPENDIX A

A-1	Image Synthesizer	A-3
A-2	Laboratory Image Synthesizer	A-10
A-3	Schematic of Laboratory Image Synthesizer	A-11
A-4	Magnification of Spot Diagram vs. Dial Reading	A-13
A-5	Magnification of Target vs. Dial Reading	A-14
A-6	Relative Transmitted Intensity vs. Angles From Normal to Screen	A-15
A-7	Spot Diagrams and Synthesized Images	A-18
A-8	Synthesized Image Using Airy Disc Spot Diagram.	A-19
A-9	Real Image Using Sutton Lens	A-20

## APPENDIX B

- |     |   |     |
|-----|---|-----|
| B-1 | Optical Apparatus for Measurement of Frequency Response of Image Forming System | B-2 |
| B-2 | Optical Setup for Measurement of Frequency Response of Image Forming System     | B-3 |

# ULTRA-HIGH SPEED ELECTRO-OPTICAL SYSTEMS EMPLOYING FIBER OPTICS

## I. INTRODUCTION

This study and development program is aimed at the coupling of conventional optical and fiber optics elements to meet the need, in future space exploration projects, for relatively simple, rugged optical systems capable of fast, high resolution performance over wide angular fields. Conventional systems only approximating the desired performance are generally made of many reflecting and/or refracting elements, and therefore present imposing problems in alignment, mechanical stability and index of refraction variations with temperature. It is believed that many such problems may be eliminated using the field-flattening, light-condensing, and distortion correcting properties of fiber optics components. The principal objectives of this program were the design and development of fiber optics elements that would have the above-mentioned properties, and the theoretical and experimental determination of the magnitude of the improvements to be derived in visible, ultraviolet and infrared imaging systems.

Prior to the commencement of this study, the field-flattening, light condensing, and distortion-correcting capabilities of fiber optical components had all been demonstrated experimentally.<sup>(1)</sup> However, the size of the components and, in the case of distortion correctors, their quality were inadequate for wide angle photographic uses. Considerable developmental work was needed to provide large, high resolution field flatteners and conical condensers while a broader research effort was required for producing desired distortions

to close tolerances. During the program improvements in fiber optics component fabrication were made. Good quality field flatteners 3 inches in diameter were produced by methods readily extendable to the production of flatteners up to 5 inches in diameter. A conical condenser of good quality, with entrance and exit diameters of 2 inches and 1/2 inch, respectively, was fabricated. Methods for obtaining known amounts of distortion were studied, and although no large high-quality distortion correctors were made, the data gathered should facilitate future studies considerably. A discussion of work performed on the fabrication of fiber optics components is found in Section V of this report.

The design studies ranged from a generalized first order analysis of coupled lens-fiber optics systems through a third order comparative study of five simple 2-, 3- and 4- element lens systems, with and without fiber optics, to a trigonometric analysis of a mirror system with decentered stop. The first order analysis resulted in graphs showing the interrelations between resolution, aperture dimensions, and effective photographic speeds for diffraction-limited systems employing fiber optics components. These are discussed in Section II. The third order studies of cemented and uncemented telescope doublets, a landscape doublet, and the symmetric Hypergon and Pantoskop objective, as reported in Section III, show the considerable enhancement in the resolution of these systems which is obtainable through the use of fiber optics field flatteners and conical condensers. A factor of two or more in resolution is often achievable. The detailed analysis of a decentered reflecting system, reported at the end of Section III, indicates that a system

that consists of a spherical mirror and a correcting cylindrical mirror may provide resolution of about 40 lines/mm over a 16 x 60 degree field, working at f/8 without a conical condenser or at f/2 or less with a conical condenser.

Early in the program an experimental camera, which incorporated a wide angle (120°) Sutton lens designed by Dr. J. Baker, and a fiber optics field flattener were fabricated. The Sutton lens, made of two concentric spheres of glass, provides diffraction-limited resolution over its entire spherical focal surface. The lens system and field flattener are rugged and stable and, except for weight, appear to satisfy many criteria outlined for this program. The performance of the camera has been evaluated by spatial frequency response measurement and image synthesis methods. The details of this camera and the tests made are found in Section IV, which also includes a report on the preliminary experimental study of the reflecting system mentioned earlier.

The image synthesis studies carried out with a view toward the final evaluation of the merits of the various diffraction-limited lens designs considered on the program, are discussed in the appendix.



## II. GENERAL DESIGN CONSIDERATIONS

In this section the first order properties of conventional lens or mirror optics and fiber optics combinations are initially considered with the view of determining the ultimate limitations in resolution for systems of various photographic speeds. The geometrical aberration theory is then used to determine the improvements expected with the use of fiber optics. Finally, a discussion of the merit function employed to assess the system and the computational methods used to evaluate this function are given.

### A. Interrelations Between Overall Resolution and Effective Photographic Speed

A camera which covers a 20 to 40 degree field and works at photographic speeds greater than f/1 is specified in the contract. It is important, at the outset, to examine the criteria in terms of resolution that can be obtained with fiber optics components.

In aerial reconnaissance or photographic work, the desired angular resolution is specified. This quantity is governed by the wavelength and the aperture dimensions and is independent of the focal length. Since the contract calls for a "diffraction-limited" system, it is meaningful to discuss resolution in terms of the dimensions of Airy disc images of stars. Assuming for the moment that the wavelength is fixed, one may obtain in principle any desired angular resolution by selecting a suitably large aperture, according to the formula:

$$R_{\text{Ang}} = \frac{d}{1.22 \lambda}$$

In cameras without fiber optics components, one then selects the focal length according to the desired photographic speed, which is proportional to  $(d/f)^2 = (1/F)^2$ . The linear resolution is then given by:

$$R_{\text{Lin}} = \frac{1}{1.22 F \lambda}$$

where F is the f/ number of the camera.

The linear separation between two points resolvable by static fiber optics is not greater than  $2d + 3t$  nor less than  $d+2t$ , where d is the diameter of the fibers and t is the spacing between them. It is convenient to stipulate that this displacement is roughly 3d. The resolution is then  $(1/3d)$  for the fiber plate. In order to prevent color effects and leakage between the fibers, it is necessary that d be greater than, or equal to,  $\pi \lambda$  for fibers of unit numerical aperture. This provides for the propagation of approximately 20 modes of wavelength  $\lambda$ . It also stipulates that the static resolution obtainable with fibers is in the neighborhood of:

$$R_{\text{Fibers}} = \frac{1}{3 \pi \lambda} \simeq 220 \text{ lines/mm at } \lambda = 0.5 \mu$$

This condition may be somewhat relaxed and it is believed that resolution up to 400 lines/mm is achievable with present fiber components without dynamic scanning.<sup>(2)</sup> Thus, the linear resolution obtainable with a static fiber bundle is equivalent to that of a diffraction-limited f/3.5 camera. Since both the linear resolution and the speed of a conventional camera are governed by 1/F (linearly and quadratically, respectively) it is clear that any gains

in speed of a diffraction-limited system effected by using fibers in decreasing the f /number below f/3.5 are accomplished at the cost of resolution. This does not mean that a fast fiber optics camera cannot be made better than an equivalent f/number ordinary camera. But if the camera is f/3.5 or less, its resolution will not be diffraction-limited in the conventional sense.

The curves of Figure 1 indicate the resolution obtainable using fiber conical condensers with conventional cameras of a given f/number. Each curve corresponds to a conical condenser of given numerical aperture. The maximum speed increase available for that numerical aperture is also given. This is based on the assumption that the term  $\sqrt{N_1^2 - N_2^2}$  for the conical element is equal to unity.

The formula used to generate these curves is:

$$\frac{1}{R} = \left[ (1.22 F \lambda)^2 + \left( \frac{3 \pi \lambda}{NA_{cf}} \right)^2 \right]^{1/2}$$

In this equation, R is the resolution of the compound system. The first term under the radical is the square of the reciprocal of the resolution of the diffraction limited objective. The second term is the square of the reciprocal of the resolution obtainable from a conical condenser of numerical aperture  $NA_{cf} = \frac{r_2}{r_1} \left[ N_1^2 - N_2^2 \right]^{1/2}$ . Here  $N_1$  and  $N_2$  represent the indices of refraction of core and coating, respectively, and  $r_2$  and  $r_1$  are the radii of the exit and entrance ends of the fibers in the cone. The photographic speed of the compound system is equal to  $(r_1 / r_2)^2$  times the speed of the lens.

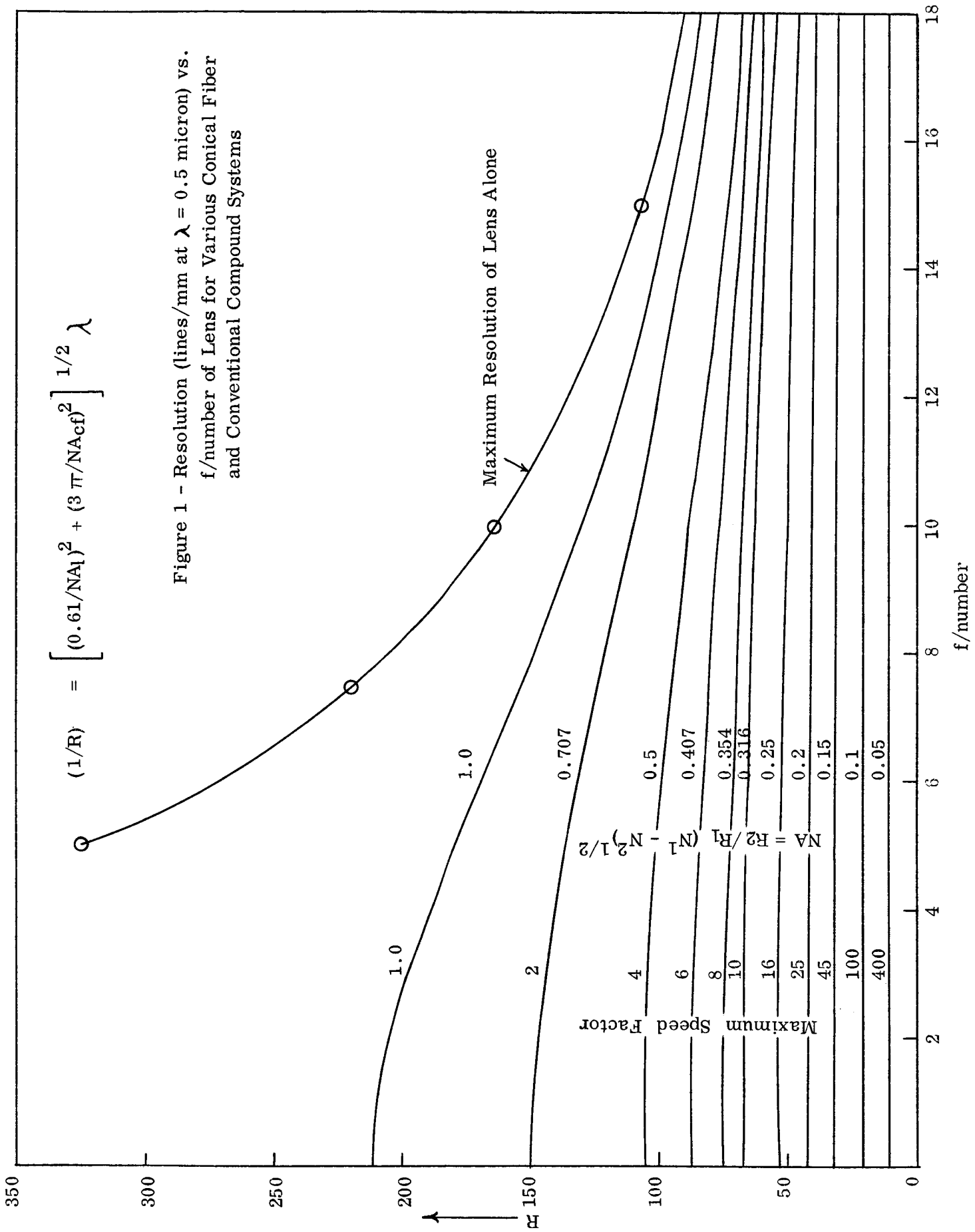


Figure 1 - Resolution (lines/mm at  $\lambda = 0.5$  micron) vs. f/number of Lens for Various Conical Fiber and Conventional Compound Systems

It is clear from these curves that, without much loss in resolution, one may considerably increase the speed of conventional lens systems of f/number greater than 10-20 by using fiber components. The curves are based on the assumption that fiber resolution is  $1/3d$ , which is a conservative assumption. Furthermore considerable gains in resolution can be achieved using dynamic scanning.<sup>(3)</sup>

Another interrelation between resolution and photographic speed in a wide angle camera employing fiber optics is that which involves the overall dimensions of the image format. In designing a conventional photographic telescope, for example, one might begin by specifying the desired photographic speed, i.e. the f/ratio, and then set the overall dimensions of the systems according to the size of the linear resolution element of the film. Since the film can be conveniently made to different sizes, large field angle can be covered and one need not consider the field angle requirements of the system when the size is to be determined. For fiber optics systems, the state-of-the-art at the end of this development program is such that fiber plates larger than 5 inches in diameter cannot be fabricated conveniently and economically. Therefore, the use of mosaics of such plates would have to be made with consequent grid structure on the recording film. The linear dimension of the system are therefore fixed by the fiber optics element in conjunction with the field angle requirements. The maximum focal length is thus:

$$f_{\max} = d \text{ inches} / 2 \tan \phi$$

where  $\phi$  is the field angle and d the diameter of fiber optics plate available.

This restriction in turn sets the aperture dimension, according to the photographic speed requirements, and thus the maximum angular resolution.

B. Correction of Aberrations in Cameras Employing Fiber Optics, Image Correctors.

In the foregoing section only perfect optical systems, ones yielding spherical wavefronts in image space, were considered to draw some general conclusions concerning the ultimate correction of optical systems that employ fiber optics. The relative correctibility of optical systems with and without fiber optics will now be examined on the basis of geometrical aberration theory.

The aberrations of a centered optical system may be expressed either by specifying the deviations of the actual wavefront from a reference spherical wavefront in the exit pupil or, equivalently, by enumerating the deviations, in the image plane, of the intersection points of all rays from those of the principle ray. Either of these aberration functions is expressible in terms of an infinite series of terms in ascending powers of  $r$ ,  $\cos(a)$ , and  $t$ , where  $r$  and  $a$  are the polar coordinates of the ray in the exit pupil, and  $t$  is proportional to the off-axis distance of the object. The particular form which these aberration polynomials takes depends on the choice of image plane or reference spherical wavefront. But whatever the form, there is generally a group of terms which describe distortion, a condition in which all the rays from a point object meet at some point other than the Gaussian image point. Another group of terms describes uniform discs of light which arise because the rays from different points in object space do not come to focus

at the same plane. Both of these aberrations, distortion and field curvature may be eliminated by using fiber optics components.

Thus the fibers in a bundle may be arranged to provide for the compensation of distortions introduced by the lens. Similarly, a fiber plate may have its entrance end ground and polished to the curvature of the best focal surface of the lens, thereby eliminating the need for correcting the lens for field curvature. Fiber optics components thus provide the optical designer with two extra degrees of freedom which, in many cases, permit significant improvements in the state of correction of given objectives and may even allow for the accomplishment of the same photographic performance with simpler objectives.

There are certain examples of systems in which fiber optics can provide significant improvements. The well-known Schmidt camera and photographic objectives of the Sutton type<sup>(4)</sup> are systems in which the image of an extended object is formed on a spherical or near-spherical surface. Fiber optics field flatteners greatly increase the usefulness of these systems.

It is perhaps less generally recognized that almost all conventional cameras, even though they are designed to work over flat fields, would provide a better average correction over their entire field if a curved rather than a flat, image surface were employed. This is because, in the presence of astigmatism, a curved surface placed between the sagittal and tangential focal surfaces provides better average imaging than any flat surface.

In Section III of this report, the relative correctibility of five

particular objectives with and without fiber optics will be examined in detail, on the basis of third order aberration theory. Some numerical verification of the general conclusions derived here are reported. Before presenting this data, however, it is necessary to describe in some detail the methods and criteria used in making comparisons. The next two sections are devoted to these descriptions



C. Selection of Merit Function - Root Mean Square Deviation as a Criterion for Comparison

Before any comparative study of the relative correctability of optical systems can be initiated, it is necessary to define some standard measure of the state of correction of such systems. As anyone familiar with the area of optical image evaluation will know this choice of a standard involves some arbitrariness, and no single number can completely specify the performance of an optical system. For this comparative study, however, it was decided that a statistical description of the point spread function (image of a point source) would be both physically meaningful and numerically convenient.

According to this statistical description, the value of the merit function for an optical system is found by first computing, for each point in the object field, the root mean square(rms) deviation, at a specified focal surface, of the intersection points of all rays through the exit pupil from the intersection point of the central ray, and then averaging (in the mean square sense) these rms values over the entire object field. The central ray, in this context, is the ray which intersects the focal surface at the center of gravity of the point image. By averaging over the field one obtains a single number specifying the state of correction of the system.

For a better understanding of this statistical description of the point image, Table I has been compiled. An inspection of this table allows one to compare the rms values for four symmetric flux distributions (Gaussian, uniform disc, third order spherical aberration and airy disc) of approximately

equal overall dimension. In addition, the corresponding "30 and 50 per cent points" are given, these being the radii of circles centered on the center of gravity of the distribution, through which 30 and 50 per cent of the energy collected by the optical system passes. All distributions are normalized to give unit flux through the system.

In the case of the Gaussian distribution ( $I = (1/\pi\sigma^2)e^{-r^2/\sigma^2}$ ), 99 per cent of the total flux passes within a circle of radius  $2.15 \sigma = C$  where  $\sigma$  is the rms deviation of the ray interreccion points. For the uniform disc and spherical aberration distributions all energy passes within a circle of radius  $C$ .

Table I

	<u>Gaussian</u>	<u>Uniform Disc</u>	<u>Third Order Spher. Aberr.</u>	<u>Airy Disc.</u>
RMS	0.465 C	0.707 C	0.5 C	0.2 C
30%	0.256 C	0.55 C	0.16 C	0.06 C
50%	0.39 C	0.35 C	0.35 C	0.08 C
99%	C	0.995 C	0.985 C	C

In the case of the Airy distribution,  $C$  is the radius of a circle bounding 99 per cent of the total flux. If all the flux were considered ( $C = \infty$ ) then the rms radius would be infinite.

An examination of the table leads to the obvious conclusion that one cannot directly infer the resolving power of an optical system from either the rms values or the 30 or 50 per cent values. Rather a knowledge of the actual distribution is needed for each point in the object field. Nevertheless, one can

come within a factor of two of the actual average resolution from either of these criteria and, for comparative purposes, either is useful.

#### D. Algebraic Formulation of Merit Function for Third Order Study

In this section the analytic statement of the form of the merit function will be formulated. Expressions will be derived which give the value of this function, to third order accuracy, for the general optical system having known amounts of third order aberrations. The theoretical methods are essentially those of Linfoot.<sup>(5)</sup> The methods of calculation of aberration coefficients, on the other hand, are those of Feder.<sup>(6)</sup>

Let a ray of light of wavelength  $\lambda$  pass through the point  $(r, \phi)$  in the exit pupil where  $0 \leq r \leq 1$ . The ray is assumed to originate from a point in object space a distance  $H$  from the optical axis. If the distance to the edge of the field, in object space, is given by  $h$ , and the quantity  $\sigma$  is used to denote the ratio  $H/h$ , then in the Gaussian image plane, the ray is displaced from the Gaussian image by a distance

$$\Delta r = \sqrt{(\Delta z)^2 + (\Delta y)^2}$$

where

$$\Delta y = h' \left[ Br^3 \cos \phi + F\sigma r^2(2 + \cos 2\phi) + 3C\sigma^2 r \cos \phi + (D-C)\sigma^2 r \cos \phi + E\sigma^3 + A_1(\lambda)r \cos \phi + A_2(\lambda)\sigma \right]^{(1-a)}$$

and

$$\Delta z = h' \left[ Br^3 \sin \phi + F\sigma r^2 \sin 2\phi + C\sigma^2 r \sin \phi + (D-C)\sigma^2 r \sin \phi + A_1(\lambda)r \sin \phi \right]^{(1-b)}$$

where  $h'$  specifies the distance from the optical axis of the Gaussian image of the object point at  $h$ . The quantities  $B$ ,  $F$ ,  $C$ ,  $(D-C)$  and  $E$  specify, respectively, the amounts of spherical aberration, coma, astigmatism, Petzval curvature, and distortion in the system. The quantities  $A_1(\lambda)$  and  $A_2(\lambda)$  give the

deviations of the rays caused by longitudinal chromatic aberration and chromatic difference of magnification. The values for all of these quantities may be found from the data obtained by tracing two paraxial rays, the marginal and the principle paraxial rays, through the system. The algebraic paraxial ray trace procedure and the equations used to calculate the various coefficients in equations one are given by Feder<sup>(6)</sup>. The coefficients  $A_1$  and  $A_2$  are exceptions. The way in which these coefficients, which are necessary to the theoretical development of Linfoot, are incorporated into the computational scheme of Feder will be described at the end of this section. First, a brief description of Linfoot's methods is in order.

Equations 1-a and 1-b describe the third order aberrations of the general ray. In order to find the rms deviation for all rays at a particular field angle and wavelength, it is necessary to integrate Eqs. 1-a and 1-b over the exit pupil. If bars ( — ) are used to denote averages, we have:

$$\begin{aligned}\overline{\Delta y^2} &= 1/\pi \int_0^{2\pi} \int_0^1 \Delta y^2 r dr d\phi \\ \overline{\Delta z^2} &= 1/\pi \int_0^{2\pi} \int_0^1 \Delta z^2 r dr d\phi \\ \overline{\Delta r^2} &= \overline{\Delta y^2} + \overline{\Delta z^2}\end{aligned}\quad (2)$$

Having found the rms spot size for given field angle and wavelength the field average spot size for that wavelength is obtained by integrating  $\overline{\Delta r^2}$  over the field, i. e.,

$$G(\lambda) = 2 \int_0^1 \overline{\Delta r^2} \sigma d\sigma \quad (3)$$

By weighting the various  $G(\lambda)$  according to the spectral density distribution of the light and integrating the product of  $G(\lambda)$  and the weighting function over all wavelengths, one obtains the merit function  $G$  given by

$$G = \int_0^{\infty} W(\lambda) G(\lambda) d\lambda \quad (4)$$

Since Eq. 1 defines the ray aberrations on the Gaussian plane, the value of  $G$  in Eq. 4 refers to that plane. In general, the Gaussian image plane will not yield the smallest value of  $G$ . In this study, the performance of a given lens type working on its "best" plane image surface will be compared with the performance on its "best" curved surface. By "best" surface, in either case, is meant the surface giving the smallest value of  $G$ .

The best flat image surface may be found by adding to Eqs. 1-a and 1-b the terms  $br \cos \phi$  and  $br \sin \phi$ , respectively. These terms describe the effect of defocusing the objective by an amount  $bR/a$  from the Gaussian image plane, where  $a/R$  is the numerical aperture of the lens in image space. By proceeding as before through the steps described by Eqs. 2 through 4, one obtains a function  $G(b)$ . This function is then minimized with respect to  $b$ , thereby yielding both the amount of defocusing which minimizes  $G$  and the value for this "best" plane surface.

To find the value of  $G$  on the "best" curved surface, a procedure described by Linfoot is followed. In this case, the term  $\epsilon(\sigma) r \cos \phi$  is added to Eq. 1-a and  $\epsilon(\sigma) r \sin \phi$  is added to Eq. 1-b. These terms specify an amount of defocusing which is a function,  $\epsilon$ , of the field position,  $\sigma$ .

One proceeds as before, obtaining from Eq. 4 an expression which is an integral function of the choice of  $\epsilon$ . An infinitesimal variations  $\delta\epsilon(\sigma)$  then changes G by an amount which vanishes when the choice of  $\epsilon(\sigma)$  is such as to minimize G. In the work of Linfoot previously referenced, a number of examples that illustrate this procedure are given. Here it is only necessary to state the pertinent results. In particular, the "best" curved surface is found to be spherical. On this surface, the value of G is given by Eq. 5.

$$G = \frac{h'^2}{36} \left[ B^2 + 12 F^2 + 6 C^2 + 18 d_1^2 + 18 d_2^2 \right] \quad (5)$$

This expression is equivalent to that given by Linfoot's Eq. 1.42 on page 14 of the reference. The quantities  $d_1$ , and  $d_2$  will be defined at the end of this section.

For the best flat field it is found that:

$$b = -\frac{2}{3} h' B - h' C - \frac{h'}{2} (D - C)$$

For this value of b, G is given by Eq. 6.

$$G = \frac{h'^2}{36} \left[ B^2 + 12 F^2 + 12 C^2 + 1.5 (D - C)^2 + 6 C (D - C) + 18 d_1^2 + 18 d_2^2 \right] \quad (6)$$

With Eqs. 5 and 6, which define the value of G on the "best" curved and flat focal surfaces, it is possible to compare the correctibility of lens types with and without fiber optics components in image space. A few more remarks are necessary to clarify these equations.

First of all it may be noted that, while Eq. 1 contains a terms  $E \sigma^3$ , specifying the distortion, Eqs. 5 and 6 are independent of E. In this sense these

equations do not follow from Eqs. 1 through 4. To obtain Eqs. 5 and 6, the distortion term must be ignored. In this study, therefore, the distortion aspects of the imaging process are neglected. Since these aspects do not contribute to the blurring of the point image, no information is lost in their presence.

Secondly, Eqs. 5 and 6 give G in terms of deviations from the center of gravity of the image patch rather than from the principle ray. The center of gravity is located by calculating from Equations 1-a and 1-b the average values of  $\Delta y (=h'F)$  and  $\Delta z (=0)$ . The aberrations of a ray are then taken with respect to the center of gravity rather than the principle ray. The difference between the two, insofar as Eqs. 5 and 6 are concerned, is found in the coefficient of  $F^2$ . For aberrations defined on the principle ray, as in Eqs. 1-a and 1-2, the coefficient is 30; for aberrations defined on the center of gravity it is 12, as in Eqs. 5 and 6.

Finally it is necessary to define the terms  $d_1$  and  $d_2$  in Eqs. 5 and 6, in terms of the computational scheme of Feder. In the integration over the wavelength described by Eq. 1, one obtains terms in  $\overline{A_1}$ ,  $\overline{A_1^2}$ ,  $\overline{A_2}$ , and  $\overline{A_2^2}$  which denote the weighted  $\lambda$ -means of  $A_1(\lambda)$ , and  $A_2(\lambda)$ . To obtain these in a particular case one would have to completely specify the spectral distribution of the light under consideration. The quantities  $d_1^2$  and  $d_2^2$  are given by  $(A_1 - \overline{A_1})^2$  and  $(A_2 - \overline{A_2})^2$ . They thus represent the mean square deviations of the coefficient  $A_1(\lambda)$  and  $A_2(\lambda)$  from their mean values  $\overline{A_1}$  and  $\overline{A_2}$ . For a particular wavelength  $\lambda$ , the coefficient  $A_1(\lambda)$  is proportional to the distance along the optical axis by which the focus for rays of this wavelength is separated from that of a reference wavelength  $\lambda$ , for which  $A(\lambda) = 0$ .

This distance is given by  $h' A_1 (\lambda) \frac{R}{a}$  where  $a/R$  is the numerical aperture. Similarly,  $h' A_2 (\lambda) \sigma$  denotes the lateral displacement of the focus of rays of wavelength  $\lambda$  from that of the reference wavelength.

It is obviously impractical to consider a continuous spectral distribution of radiation at the third order design stage. Generally only two colors, those of the F and C lines, are considered, along with that of the D line, which is used as reference. The third order chromatic aberrations are thus given by Feder in terms of the longitudinal displacement ( $\Sigma a/N' u'^2$ ) between the foci of the F and C colors and the lateral displacement ( $\Sigma b/N' u'$ ) between the intersection points of the principle rays in the two colors at the paraxial image plane. Here  $N'$  is the index of refraction and  $u'$  is the numerical aperture in image space. The equations used to calculate  $\Sigma a$  and  $\Sigma b$  from the paraxial ray trace data are given by Feder in the paper previously referenced.

The usual three color scheme may be incorporated into Linfoot's continuous color analysis by taking mean and mean square deviations for the three colors F, C, and D, assuming each receives a weighting such that the mean values of  $A_1 (\lambda)$  and  $A_2 (\lambda)$  for the three colors are zero. If the D line is used as reference, the square deviations of  $A_1 (D)$  and  $A_2 (D)$  are also zero. The deviations of the F and C foci from the D focus, due to longitudinal and lateral color errors, are then  $\pm 1/2 (\Sigma a/N' u')$  and  $\pm 1/2 (\Sigma b/N' u')$ . The means square deviations for the three colors are



thus  $d_1^2 = 2/3 (\sum a/2N'u')^2$  and  $d_2^2 = 2/3 (\sum a/2N'u')^2$

In the notation of Feder, therefore, the values of the error function on the "best" curved and flat image surfaces are given by Eqs. 5-a and 6-a.

$$G_{\text{curved}} = \frac{1}{36} \left\{ h'^2 [B^2 + 12F^2 + 6C^2] + 3 \left( \frac{\sum a}{N'u'} \right)^2 + 3 \left( \frac{\sum b}{N'u'} \right)^2 \right\} \quad (5-a)$$

$$G_{\text{flat}} = \frac{1}{36} \left\{ h'^2 [B^2 + 12F^2 + 12C^2 + 1.5(D-C) + 6(D-C)] + 3 \left( \frac{\sum a}{N'u'} \right)^2 + 3 \left( \frac{\sum b}{N'u'} \right)^2 \right\} \quad (6-a)$$

In the third order design studies of Section III of this report, the object of the investigation of each lens type was to minimize expressions 5-a and 6-a with respect to the design parameters. The functions G of Eqs. 5-a and 6-a specify actual meansquare distances on the appropriate image surface. The square root of their inverses, therefore, are directly proportional to resolution.

### III. RESULTS OF DESIGN STUDY

This section of the report is devoted to the presentation and discussion of the results of the design studies. Five simple refracting objectives were studied numerically in terms of the merit function described in Section II. D. The objectives were: (1) cemented telescope doublet, (2) uncemented telescope doublet, (3) landscape doublet - stop in front, (4) Hypergon, and (5) Pantoskop. Each of these will be discussed here in a separate subsection. In addition, a trigonometrical design study of a system consisting of a spherical

mirror with a decentered elliptical stop in the plane of its center of curvature, and an incomplete study of this same system with a cylindrical mirror corrector, will be reported. A few remarks common to the presentation of the results of each of the third order analyses will first be made.

For each third order system, an initial design was taken from the literature. The design was then studied as a function of the bending of the first element. Specifically the curvature of first refracting surface was altered, that of the second (and third in the case of the cemented doublet) being adjusted to keep the power of the first element constant. The aberration coefficients B, F, C, D, E, and the two color coefficients of Eq. 5-a and 6-a were then recalculated. The value of each coefficient was then adjusted to preserve its pertinence to a system of the required focal length and f/ratio. (Such adjustments are necessary because the overall focal length of a multi-lens objective is changed in the process of bending a single component). With these values of the aberration coefficients, those of the merit functions, as defined by Eqs. 5-a and 6-a of Section II-D were generated. These provided a measure of the performance of an objective of the altered design working over the 60° field angle originally specified. In the same way, the performance of the altered design working over field angles of 32, 16, 8 and 4° was evaluated. The first curvature was then bent again and the values of the merit functions for each of the five field angles generated. Through a series of such calculations, the values of the merit functions for each of the third order systems working over each of five different total field angles were obtained as a function of the bending of the first component. Sufficient numerical data was thus generated to provide 50 plots (5 systems x 5 field

angles x 2 image surfaces) of merit function vs. curvature of the first refracting surface. The minimum of each such plot provided the value of the bending, giving optimum design for an objective of the type under consideration working over the specified field and imaging on the desired surface (flat or curved). Since the principal objective was to find the minimum value of the merit function for each of the 50 cases rather than to study the way in which the minimum is approached only ten plots of merit function vs. curvature are shown in this report. These pertain to the cemented landscape doublet and are shown in Figure 5, of Section III.C.

For each of the five systems studied the optimum average resolution (defined as the square root of the reciprocal of the minimum value of the error function) is plotted as a function of total field. Two curves are thus obtained for each system, one pertaining to a flat image surface without fiber optics and the other to a curved image surface coincident with a fiber optics field flattener. Equation 7, which follows the next paragraph, gives the formula by which the resolution for the coupled objective - field flattener system was computed. A figure giving the two plots pertinent to a particular system is contained in the appropriate subsection.

The optimum designs for imaging on a flat surface (as defined above) were then studied as a function of f/number. This was done by recalculating the merit functions after weighting the aberration coefficients so as to adjust their values for the desired aperture dimensions. From this data, curves that give the average resolution (as defined above) as a function of f/number for

each system, working over a specified field and imaging on a flat surface, were obtained.

The curve for a given system is shown in a figure to be found in the appropriate subsection. In each such figure may also be found curves giving the average resolution of various lens-fiber optics combinations working at the same effective f/number. The latter curves are obtained by calculating the effective resolution of the combination specified by two elements: (1) an objective designed to work on a curved surface at a specified f/number; and (2) a fiber optics conical condenser with its entrance end curved to fit this surface and its exit diameter sufficiently diminished to provide the desired increase in photographic speed. This effective resolution is obtained from the formula.

$$\left(\frac{1}{R_{eff}}\right)^2 = \left(\frac{1}{R_{lens}}\right)^2 + \left(\frac{1}{R_{fiber}}\right)^2 \quad (7)$$

where the approximate resolution of the fibers is given by:

$$R_{fiber} = \frac{1}{3\pi\lambda} \sqrt{n_1^2 - n_2^2} \leq \frac{1}{3\pi\lambda}$$

In this equation,  $\lambda$  is the wavelength,  $r_1$  and  $r_2$  are the entrance and exit radii of the conical fibers, and  $N_1$  and  $N_2$  are the indices of refraction of core and coating materials.

Since the data for particular cases discussed in the following subsections are derived from third order theory, the accuracy of the results in describing the actual performance of the objectives studied when working over wide field angles or low f/numbers is certainly to be questioned, for in either case it is true that a third order study provides only the beginning of a

complete design study. It must also be mentioned that the quantity called "resolution" in this report may differ from actual resolution, as measured experimentally, by as much as a factor of two. This should not, however, severely affect the validity of conclusions based on the comparison of the resolution capabilities of the objectives with and without fiber optics. Finally it may be noted that, while the objectives considered were optimized with respect to the bending of the first component, they were not optimized with respect to every parameter, nor were they optimized for each f/number for which they were studied. Complete optimization in every case would have been prohibitively time consuming, and unwarranted at the preliminary design phase, which a third order study constitutes. In spite of these considerations, the data obtained undoubtedly indicate the magnitude of the gains in speed and performance that combinations of conventional objectives and fiber optics components can provide.

#### A. Cemented Telescope Doublet

The initial design for this objective is given by Van Heel. <sup>(7)</sup> If a focal length of 10 is assumed, the data are as follows:

$$C_1 = 0.2697557$$

$$t_1 = 0.11111, n_D = 1.51806, V = 33.42$$

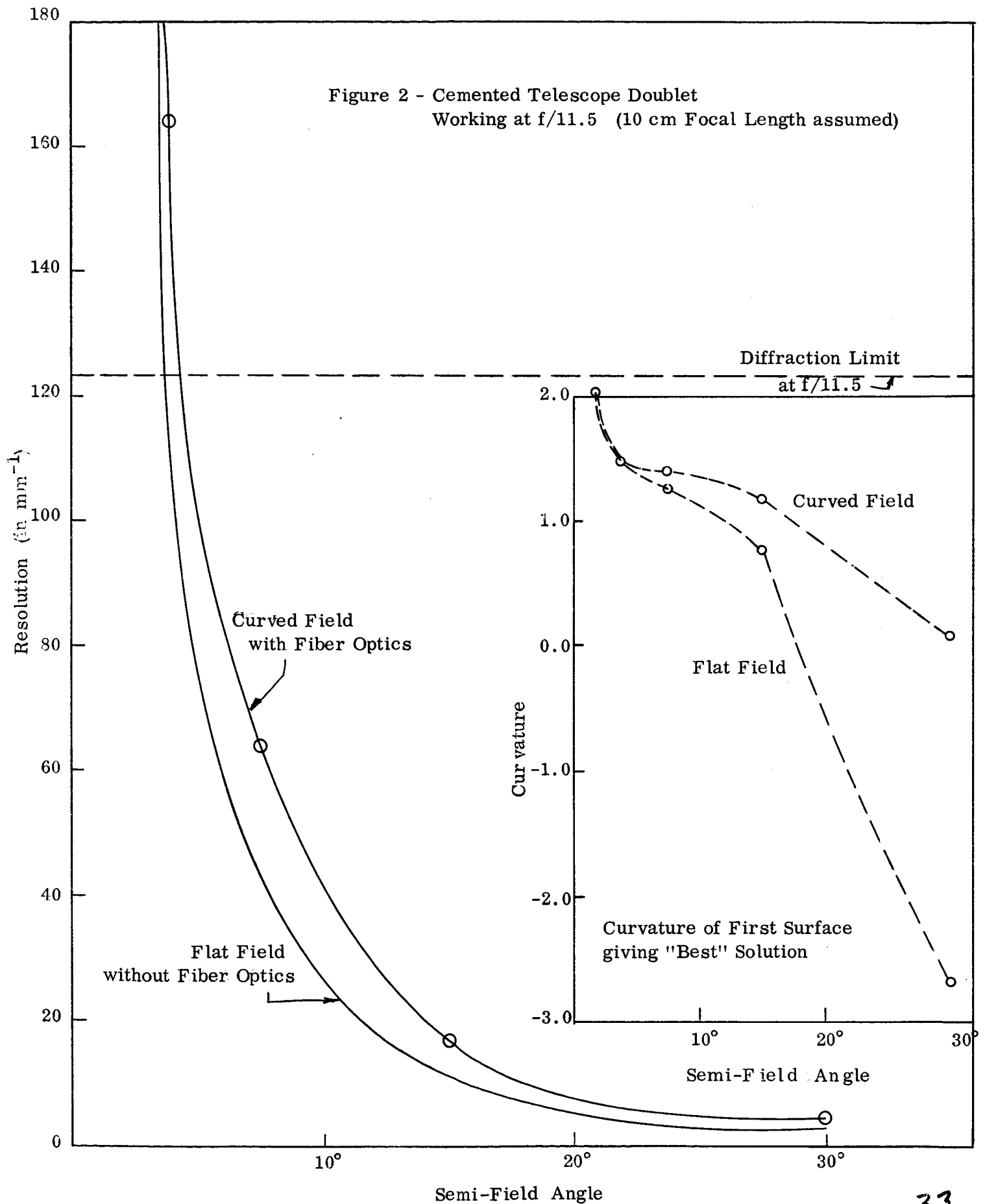
$$C_2 = -0.2628717$$

$$t_2 = 0.6945, n_D = 1.61358, V = 21.20$$

$$C_3 = 0.0246527 \text{ where } V = (n_D - 1)/(n_F - n_C)$$

The curves of Figure 2 indicate the best "resolution" (as defined above) as a function of semi-field angle, which can be obtained by bending

Figure 2 - Cemented Telescope Doublet  
Working at  $f/11.5$  (10 cm Focal Length assumed)



the doublet. For these curves, the systems are assumed to be working at  $f/11.5$ , with a focal length of 10 cm. For semi-fields less than  $4^\circ$ , both systems are diffraction-limited. The curves indicate that the fiber optics field flatteners can provide 20 to 30 per cent increases in resolution in most cases. The plots at the right of Figure 2 give the curvature of the first surface as a function of semi-field angle for the design yielding the resolution values plotted. Since the curves cannot be expected to be smooth, the points are connected by dashed straight lines. The lines should not be read to imply the curvature values for intermediate points.  $C_2$  and  $C_3$  may be found from  $C_1$  with the aid of the thick lens bending formula.<sup>(8)</sup>

$$C_{i+1} = \left( C_i - \frac{1}{f(N-D)} \right) / \left( 1 - \frac{N-1}{N} t_i C_i \right)$$

where  $\frac{1}{f}$  is the power of the lens and  $N$  is its index of refraction.

In the left half of Figure 3 plots are shown which indicate the comparative merits of this type of lens with and without fiber optics conical condensers. All systems are assumed to be working over a full field of  $16^\circ$ , and the designs are those appropriate for this field coverage, as given in Figure 2. The lower curve of the same figure shows the resolution for the flat-field design working at various  $f$ /ratios. The three upper curves give the resolutions of three lens-fiber optics-conical condenser systems for the same  $f$ /ratios. The  $f$ /ratio of the lens alone in each of these combinations is indicated alongside the appropriate plot. It may be seen that in order to obtain the best performance at given effective  $f$ /ratio, one must study a number of different combinations. For example at effective  $f/4$  the

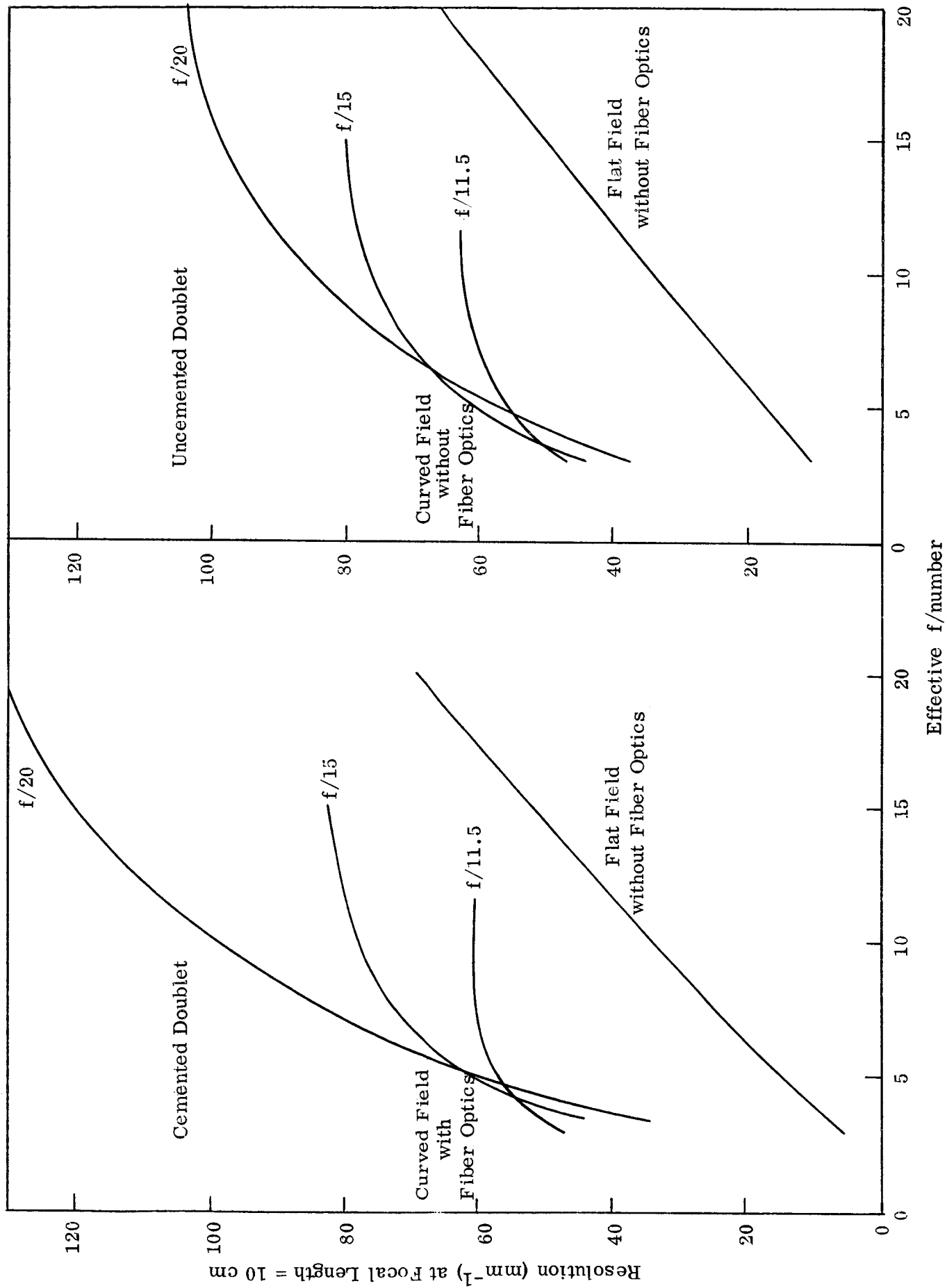


Figure 3 - Average Resolution over 16° Full Field as a Function of Effective f/number



the combination in which the lens works at  $f/11.5$  is better than those for which the lens works at  $f/15$  or  $f/20$ . It is clear from these curves that very significant increases in performance can be achieved through the use of fiber optics. The explanation may be found in the fact that there are not enough design parameters available to allow for correction of astigmatism. Since a large amount of astigmatism is present, the curved field imaging is much better.

#### B. Uncemented Telescope Doublet

The initial design for the uncemented telescope doublet is given by Stephens.<sup>(9)</sup>

This objective, which is corrected for spherical aberration, coma, and primary chromatic aberrations, is described by the following data:

$$C_1 = 0.16367$$

$$t_1 = 0.0826, n_D = 1.517, V = 64.5$$

$$C_2 = -0.27933$$

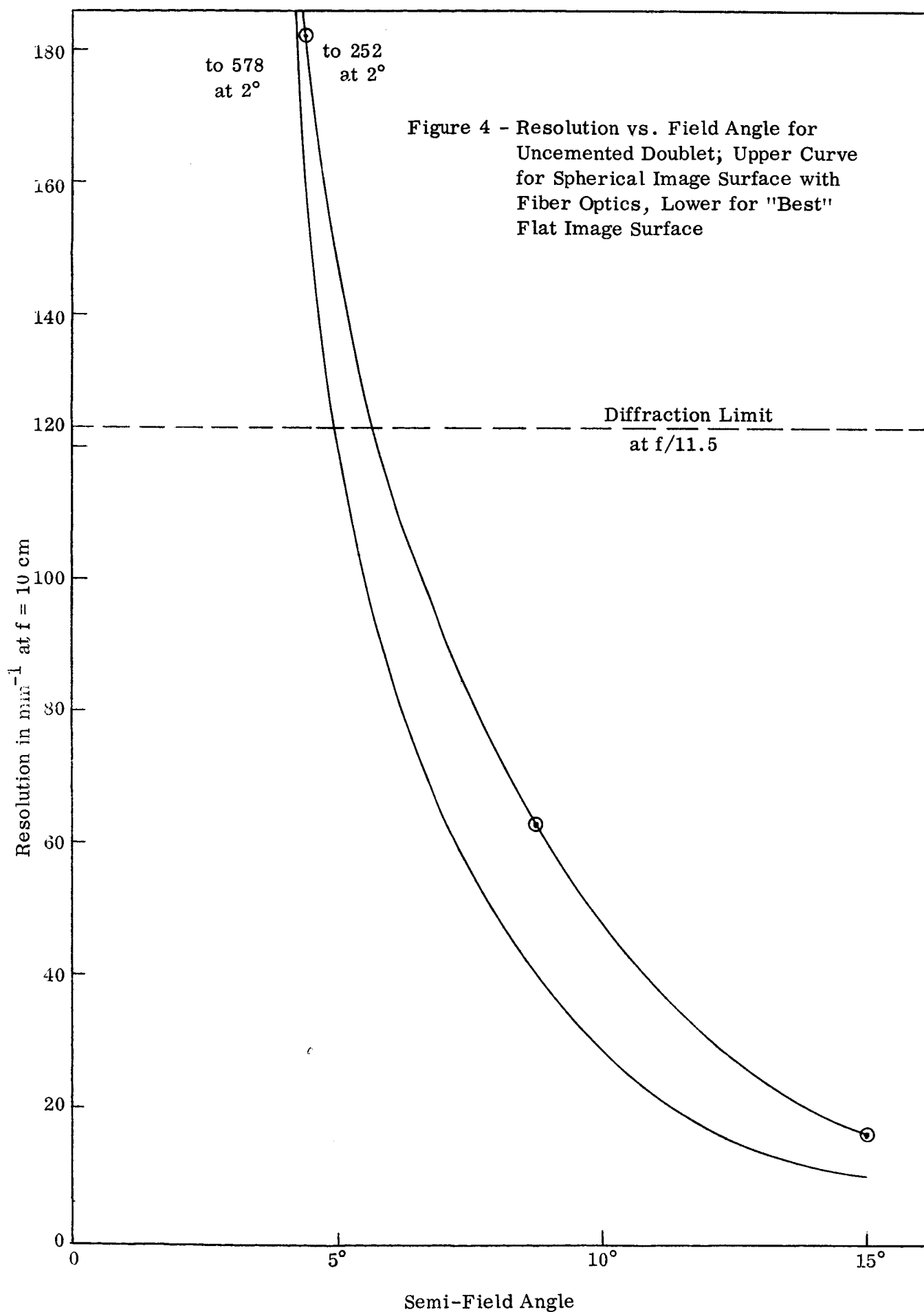
$$t_2 = 0.0198, n_D = 1$$

$$C_3 = -0.27824$$

$$t_3 = 0.0703, n_D = 1.621, V = 36.2$$

$$C_4 = -0.069798$$

The lens was studied as a function of the bending of the first element as well as the second. For all field angles and both focal surfaces the initial design provided the best performance. Figure 4 shows that comparative merit of the design, at various semi-field angles, for imaging on a plane surface and



on the spherical entrance face of a fiber optics field flattener. To obtain these curves, a focal length of 10 cm and an f/ratio of 11.5 was assumed.

In the right half of Figure 3 may be found the plots that indicate the comparative performance of this design, with and without fiber optics conical condensers and working at various f/ratios. The f/ratio of the lens alone, in combination systems, is given along the appropriate plot.

C. Cemented Doublet Landscape Lens

The initial design for the cemented doublet landscape lens system is taken from Conrady.<sup>(10)</sup>

$$C_1 = -0.450$$

$$t_1 = 0.10, n_D = 1.5472, V = 45.8$$

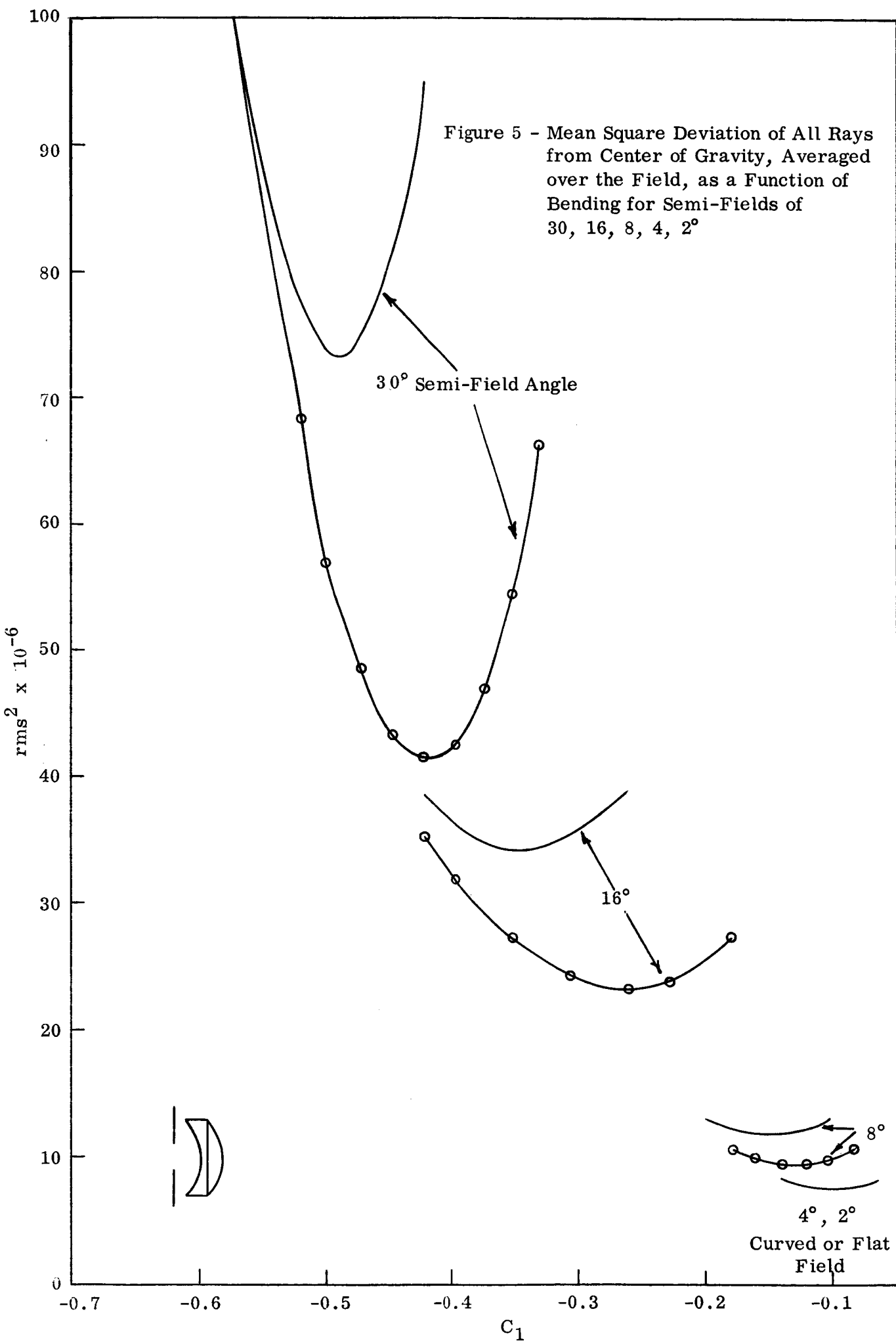
$$C_2 = 0.1314$$

$$t_2 = 0.25, n_D = 1.6118, V = 59.0$$

$$C_3 = -0.5040$$

(Stop is located at a distance 0.8176 in front of first surface).

In Figure 5 the mean squared deviation, averaged over the field, of all rays from the central ray (as explained in the introduction to this section) is plotted as a function of the curvature of the first surface for fields of semi-angle 30, 16, 8, 4 and 2°. From the minima of these curves the plots of Figure 6, which show the optimized resolution as a function of field angle, were obtained. In these curves a focal length of 10 cm and f/11.5 are assumed. The curves plotted at the upper right of the figure show the curvatures of the first surface yielding the resolutions plotted. From the



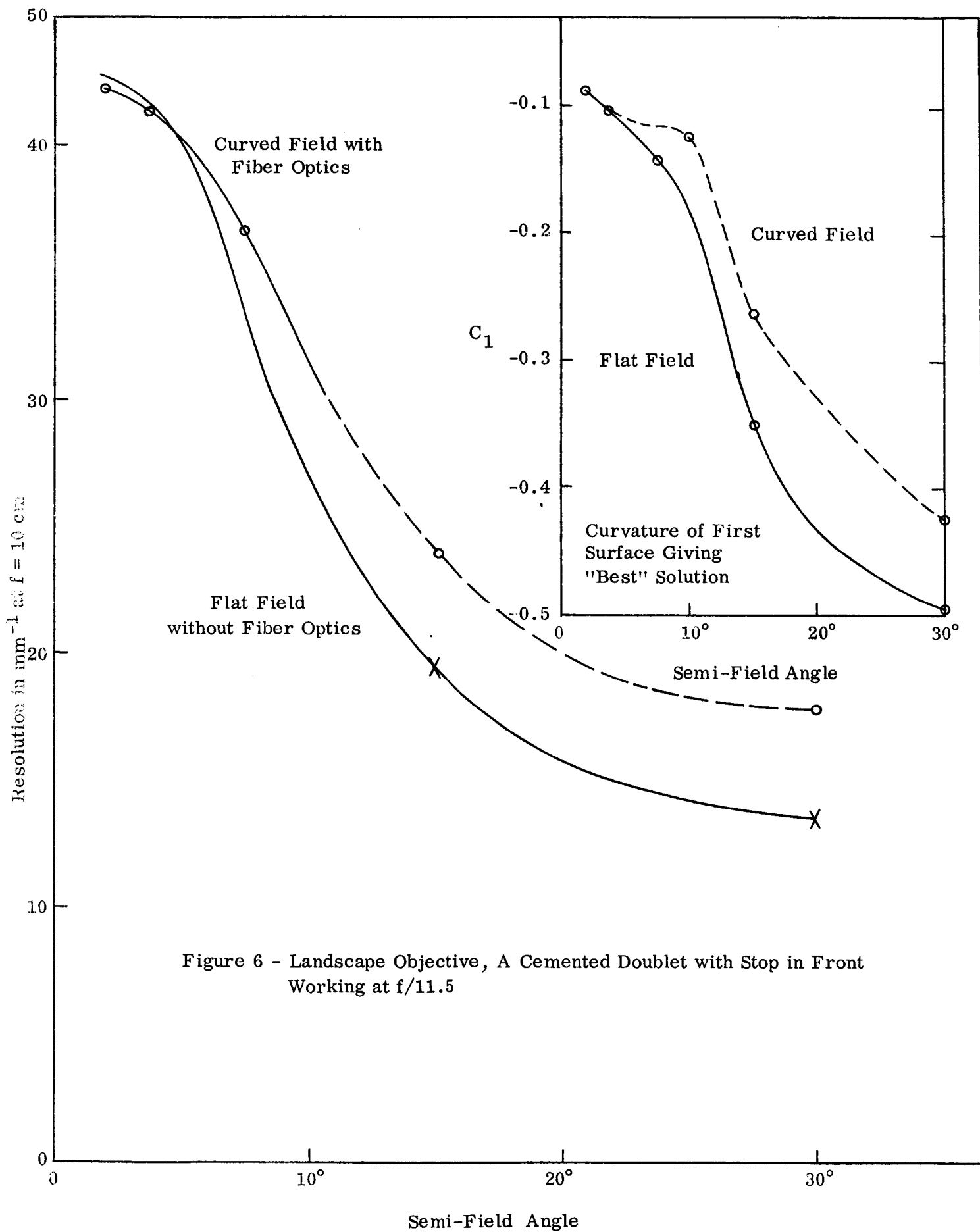


Figure 6 - Landscape Objective, A Cemented Doublet with Stop in Front Working at  $f/11.5$

curves of Figure 7, the performances of the system with and without fiber optics conical condensers are compared.

D. Hypergon

The initial design for the Hypergon lens is given by Conrady.<sup>(11)</sup>

The data are as follows:

$$C_1 = 1.167$$

$$t_1 = 0.2200, n_D = 1.5101, V = 63.4$$

$$D_2 = 1.158$$

$$t_2 = 1.3800, n_D = 1.000$$

$$C_3 = -C_2$$

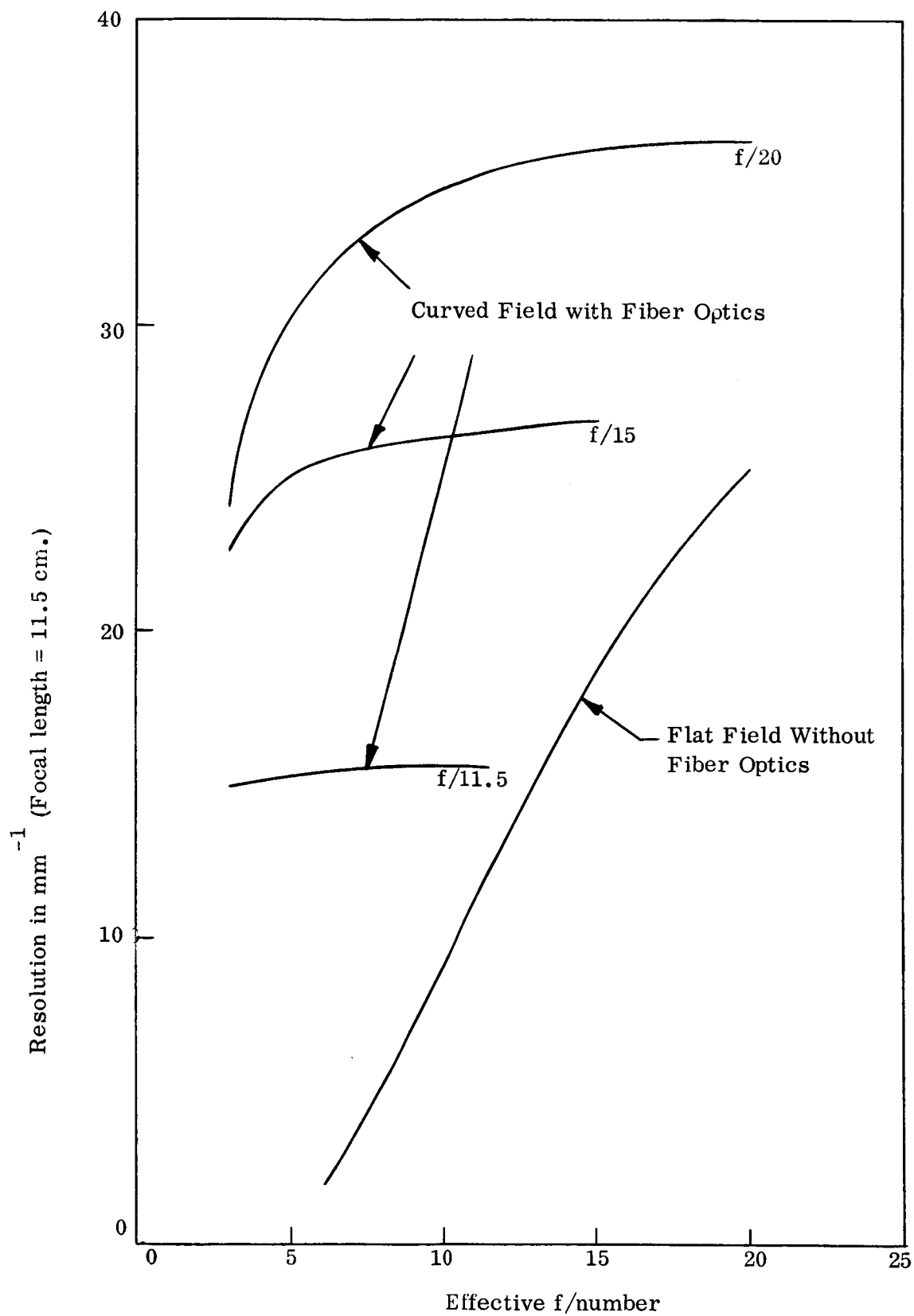
$$t_3 = 0.2200, n_D = 1.5101, V = 63.4$$

$$C_4 = -C_1$$

(The stop is located at a distance 0.690 from the second surface.)

The resolution of the system working at  $f/10$  and 10 cm focal length was studied as a function of bending of the first element. The second element was adjusted at all time to preserve the symmetry. In Figure 8, the best resolutions obtainable for various semi-field angles are shown. The advantage offered by fiber optics field flatteners is very marked in this case. Even more pronounced are the increases in performance which result from the use of conical condensers. These are shown by the curves of Figure 9 for systems working over  $60^\circ$  fields.

Figure 7 - Resolution vs. Effective f/Number for Landscape Doublet



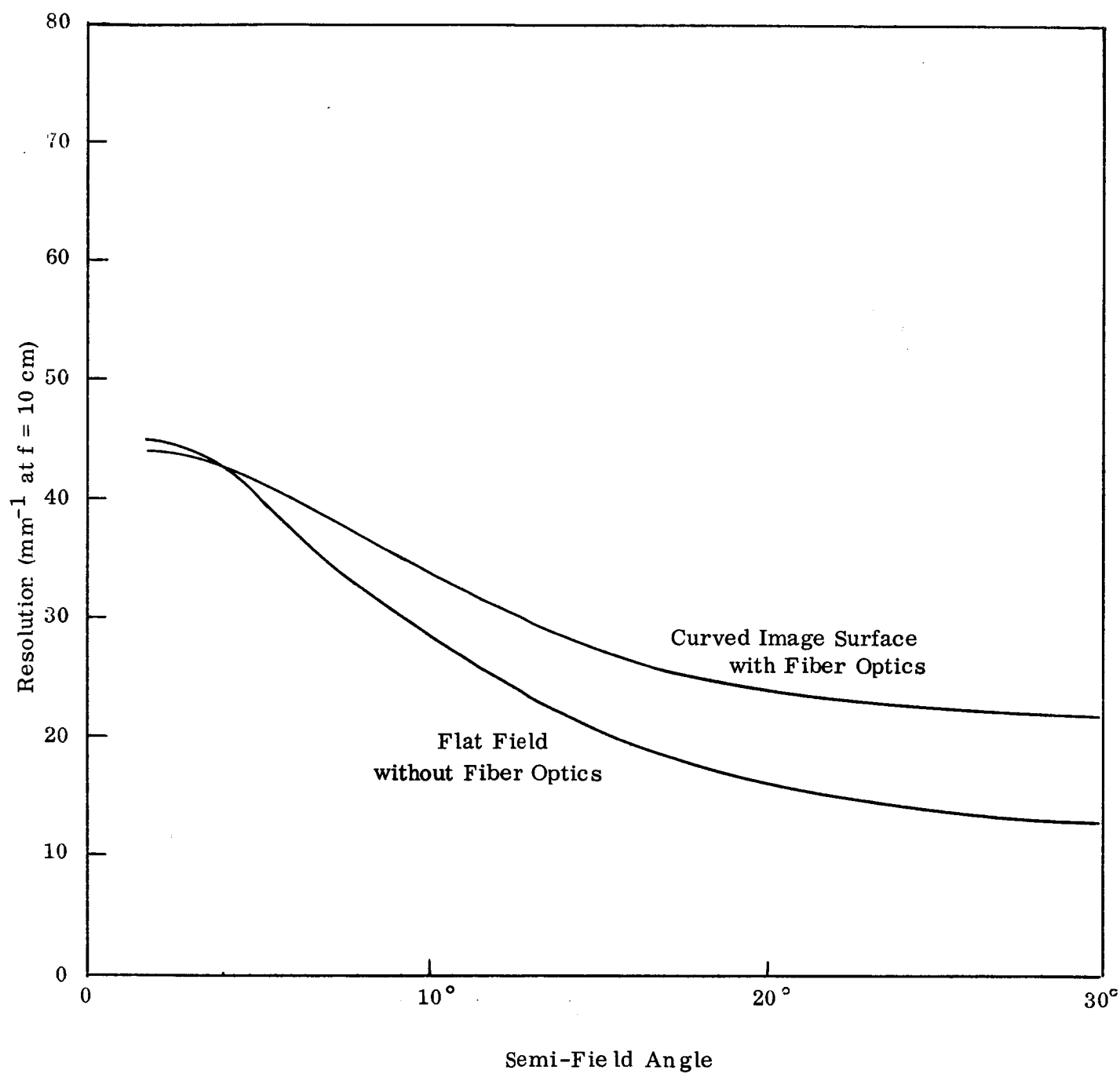


Figure 8 - Hypergon at  $f/10$ , Best Correction with Bending as a Function of Field Angle



E. Pantoskop

The initial design for the Pantoskop system is given by Conrady.<sup>(12)</sup>

The data are as follows:

$$C_1 = 1.343$$

$$t_1 = 0.1740, n_D = 1.5317, V = 48.9$$

$$C_2 = 0.0625$$

$$t_2 = 0.0190, n_D = 1.6034, V = 38.0$$

$$C_3 = 1.310$$

$$t_3 = 1.240, n_D = 1$$

$$C_4 = -C_3$$

$$t_4 = t_3, n_D = 1.6034, V = 38.0$$

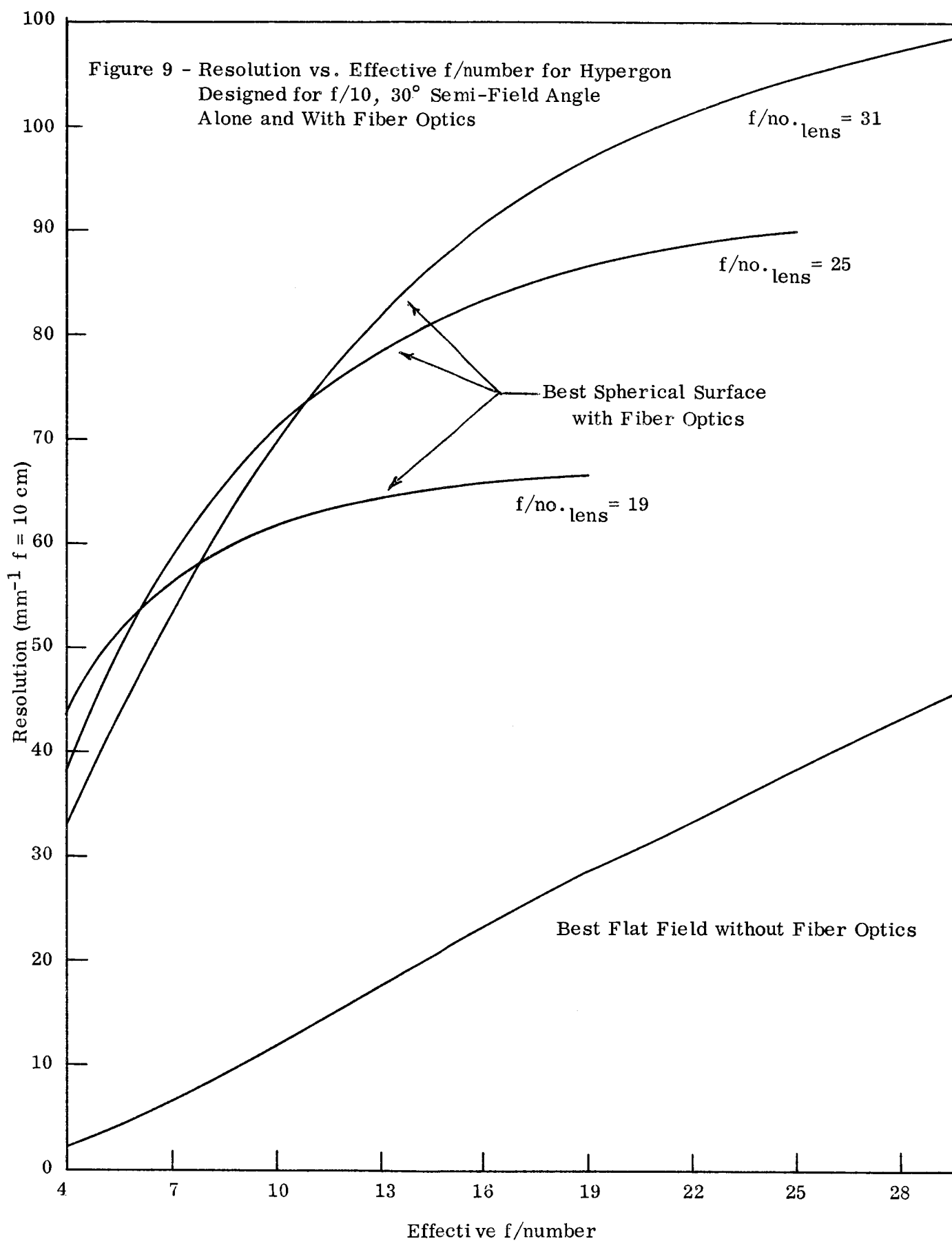
$$C_5 = -C_2$$

$$t_5 = t_2, n_D = 1.5317, V = 48.9$$

$$C_6 = -C_1$$

(The stop is located at a distance 0.620 behind the third surface).

The design was studied at  $f/10$  as a function of bending of the first glass, the second being adjusted to preserve symmetry. For a focal length of 10 cm, the best obtainable resolution for various field angles is given by the curves of a Figure 10. As with the Hypergon lens, fiber optics field flatteners provide substantial improvements. The curves of Figure 11 give the average performances of various lens-fiber optics - conical condenser systems working over  $60^\circ$  full fields. The lowest curve gives the resolution as a function of  $f/\text{ratio}$  for the best flat field design.



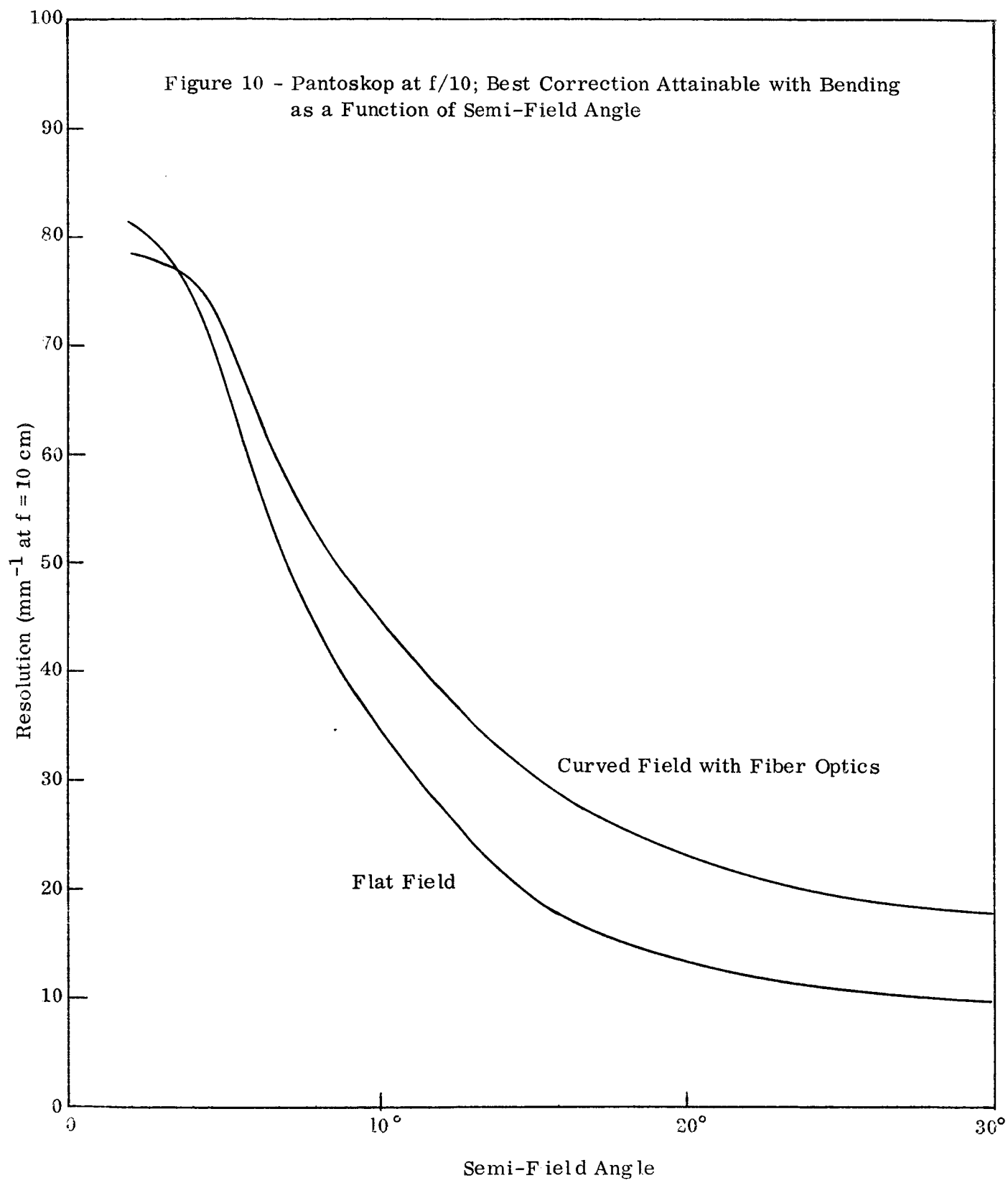
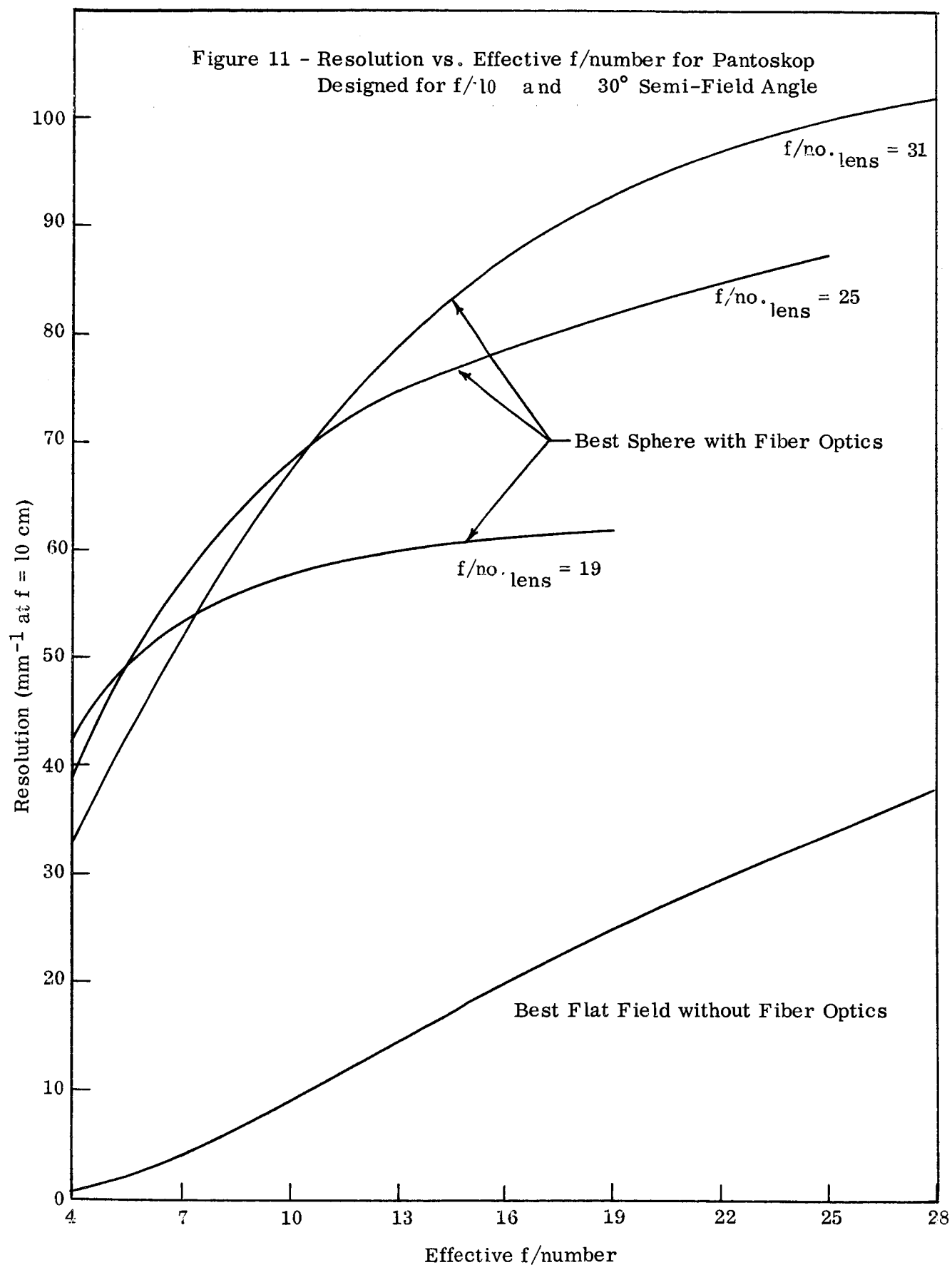


Figure 11 - Resolution vs. Effective f/number for Pantoskop  
Designed for  $f/10$  and  $30^\circ$  Semi-Field Angle



#### F. Wide Angle Reflecting System

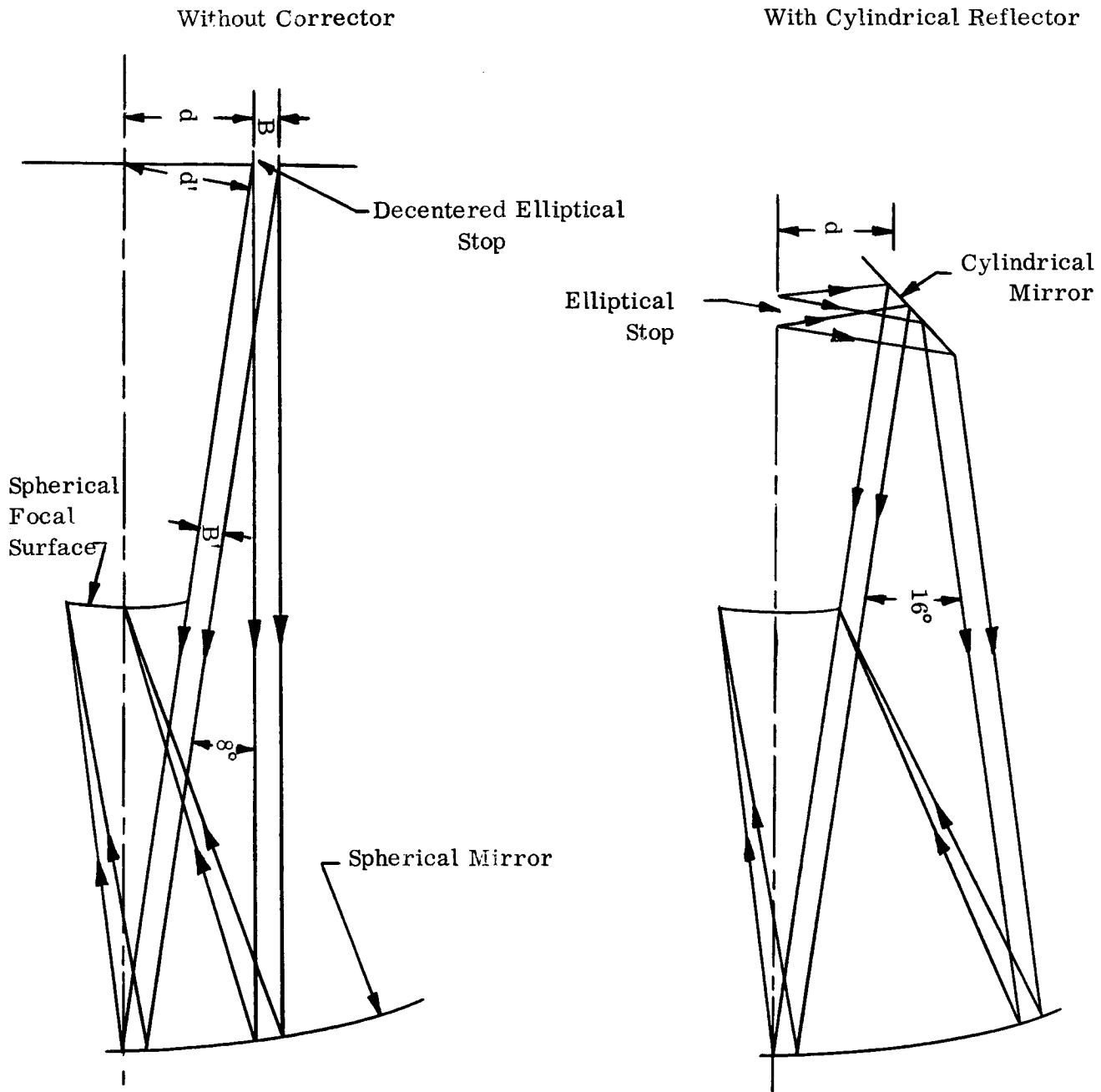
The desirability of reflecting optics in space exploration is obvious. The advantages of lightweight and broad spectral range are significant. Centered reflecting system, however, cannot provide wide angle coverage except at very low f/ratios, because of the obstruction of light by the film plane and/or secondary mirrors. At these low f/ratios reasonable correction can be obtained only by using complicated correcting elements, generally refracting. As a result one would expect that a wide angle reflecting system of simple design would not be possible. That such a design may nevertheless exist was suggested by Dr. James Baker, who proposed the general form of the system.

The system proposed by Dr. Baker is essentially a variation of the Schmidt camera in that it consists of a spherical mirror with a stop located in the plane of its center of curvature and forms an image of an extended object on a spherical focal surface. It differs from the Schmidt camera in that the stop is decentered to provide wide angle coverage and is made elliptical to reduce the effect of the spherical aberration of the mirror. The system is presented schematically in Figure 12. The lower edge of the stop is located a distance  $d$  from the optical axis. This distance specifies the angular field which may be covered without any vignetting of the off-axis pencils. This angular field is given by  $2\tan^{-1}(d/R)$ , where  $R$  is the radius of the mirror. Thus the field of view may be extended by increasing  $d$ .

The aberrations of the fan of rays that enter the system parallel to optical axis are determined by  $d$  and by  $B$ , the aperture dimension in this

Figure 12

f/8 Wide Angle ( $16^\circ \times 60^\circ$ ) Reflecting Camera with Decentered Elliptical Aperture



plane. The aberrations of the upper ray of the fan are given by a series of terms in powers of  $(d+B)$ , while those of the lower ray are given in powers of  $d$ . In terms of the customary aberration polynomial that describes the performance of centered systems, these aberrations are given by the spherical aberration terms. Clearly, any increase in field coverage (and, therefore,  $d$ ) is obtained at the cost of increased aberrations. These aberrations may be reduced somewhat by decreasing  $B$  by using an elliptical aperture which provides the same total flux to the system.

Up to this point the aberrations of the system have been considered only in terms of rays that enter the camera in a direction parallel to the optical axis. The off-axis aberrations may be seen to be slightly less. Consider, for example, a parallel pencil of rays that enter the system in such a way as to have no component in the direction perpendicular to the plane of Figure 12. The aberrations of the fan which lie in the plane of the figure depend only on the distances  $d'$  and  $B'$ . These distances are the projections of the lengths  $d$  and  $B$  onto a plane perpendicular to the path of the rays. Since  $d' < d$  and  $B' < B$ , the aberrations of the fan are less than those of the on-axis pencil. It may also be seen that it is sufficient to study only those pencils that have no component of direction perpendicular to the plane of Figure 12. This is because, except for a foreshortening of the cross sectional dimension of a pencil inclined at any azimuth to this plane, the choice of the plane is arbitrary since the system is symmetric about a line through the center of curvature perpendicular to the optical axis. The system

is thus capable of covering a wide field of view in the direction perpendicular to the plane of Figure 12. For the determination of the choice of eccentricity of the aperture and focal surface that would provide the best compromise between resolution and field coverage, a numerical design study of the system was made.

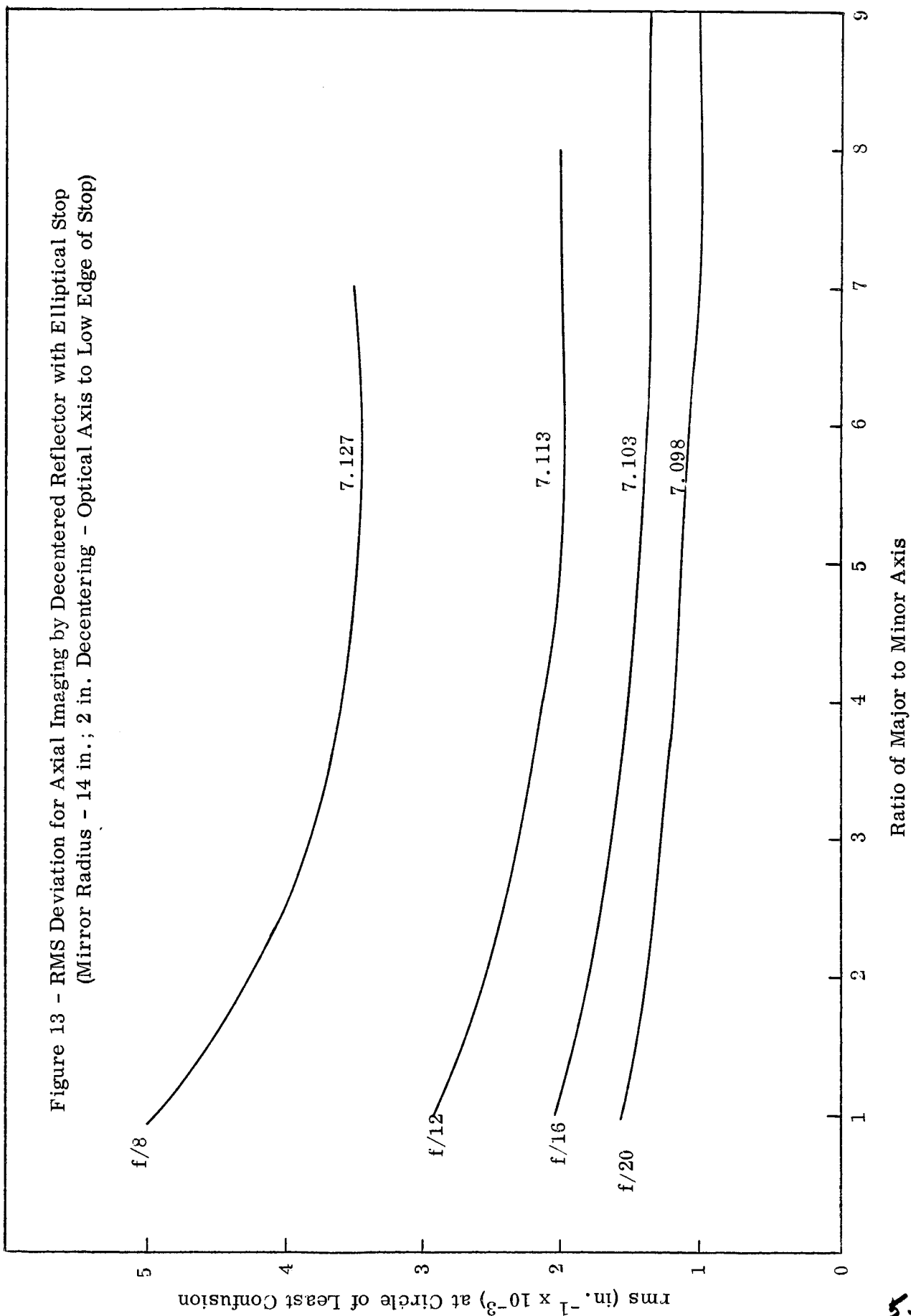
A computer ray trace program for the IBM 7090 was written to determine which combination of aperture eccentricity and focal surface would provide the best imaging over 16 x 16, 12 x 16 and 8 x 16 degree fields at f/ratios of 8, 12, 16, and 20. The program was designed so that it can be used to trace an arbitrary number of rays from points at the centers of mass of equal area portions of an elliptical aperture of arbitrary eccentricity. The rays are traced to one or more spherical focal surfaces concentric with the mirror. Several types of results may be obtained, including sagittal and tangential fans and complete spot diagrams. The rms deviations of all ray intersections from the center of gravity of the image patch on the chosen focal surface for any desired field angle may be obtained, as well as the rms deviations in two perpendicular directions at the focal surface. For the study, best images were taken to be those that gave symmetric image patches. Thus if  $\Delta y$  and  $\Delta z$  specify the deviations of a ray from the center of the image patch, in two perpendicular directions, the best images are those for which  $\overline{\Delta y^2} = \overline{\Delta z^2} = \overline{\Delta r^2} / 2$ , where the superscribed lines indicate averages.

One expected result of the study was that the rms deviations for on-axis and off-axis pencils differed slightly from one another, the latter



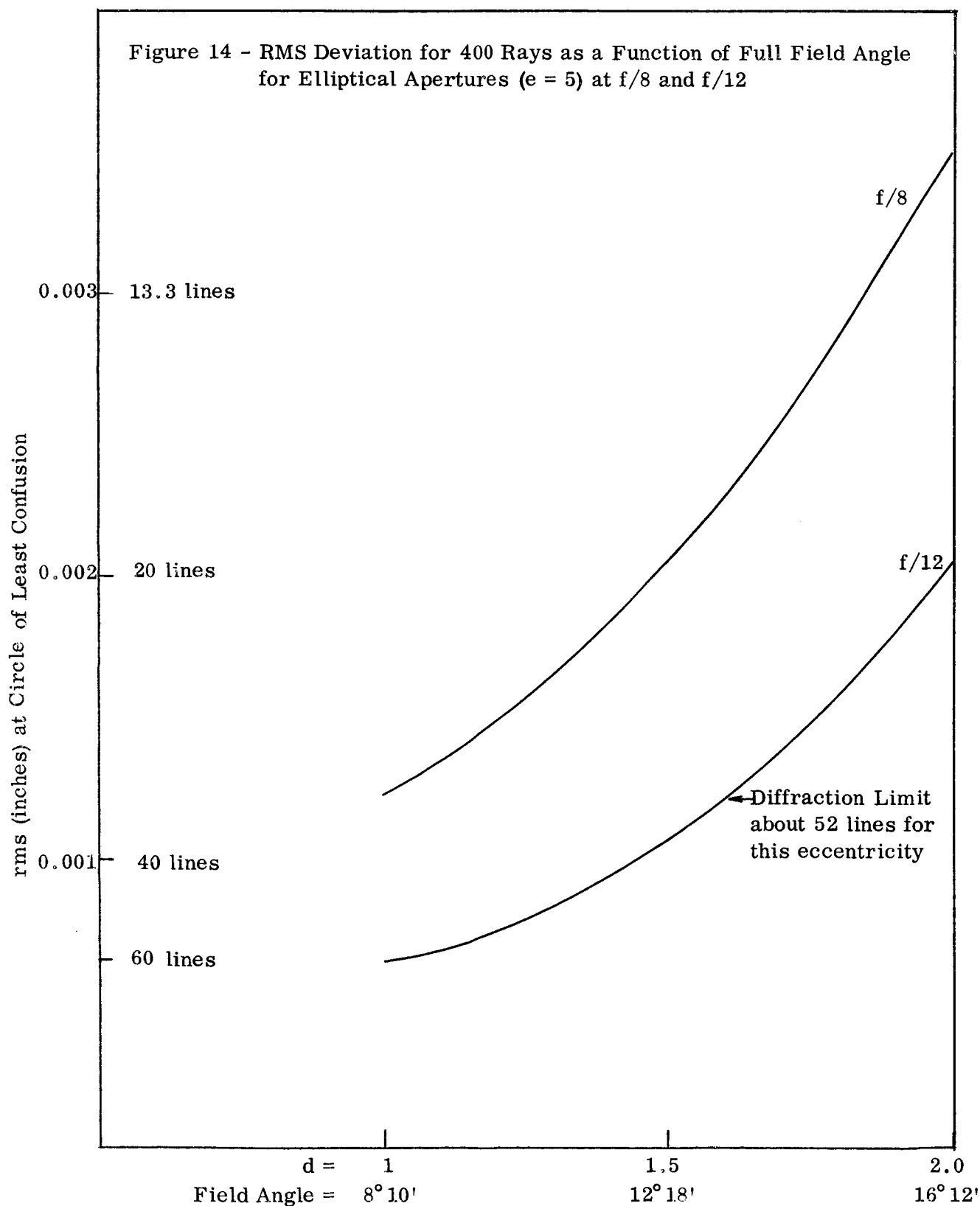
being less than 5 per cent better for the field angles considered. It was therefore possible to make a complete study of the system by evaluating in detail only the on-axis pencil. The best design is thus found by determining the combination of focal surface and the aperture eccentricity which gives a symmetric image patch with a minimum value of rms deviation. The results of this study are shown in Figure 13. The curves give the values of the rms deviation of rays that form a symmetric image patch as a function of the ratio of major to minor axis of the elliptical aperture. The lower edge of the aperture is assumed to lie at a distance  $d = 2$  inches from the optical axis. The radius of curvature of the mirror is 14 inches. The four curves are labeled according to the effective  $f$ /number of the system under study. The ordinate is scaled in thousandths of inches. If the reciprocal of the rms is taken as the measure of resolution, an rms of two thousandths provides a resolution of about 20 lines/mm. The radius of curvature of the focal surface that gives the minimum rms is indicated above the appropriate curves. It is clear from these curves that not much is gained by reducing the speed below  $f/12$ . Since the value of  $d$  is fixed at 2 inches for all the curves, they describe only the performance of a system designed to work over an unobstructed  $16^\circ$  field.

To determine the improvements that might be obtained by reducing the field angle requirements, the system was further studied for values of  $d$  between 1 and 2 inches at  $f/8$  and  $f/12$ . The results are shown in Figure 14. For these curves the eccentricity of the aperture was fixed;



a ratio of major to minor axis of 5 was assumed. The curves give, for this eccentricity, the rms deviation of rays that form a symmetric image patch as a function of the unobscured field that the system can cover. The lower curve indicates that a field of  $12^\circ$  (by 60 or more degrees in the other direction) can be covered by this system at  $f/12$  with approximately uniform resolution of 4 /mm. Such a system would be diffraction-limited for red and infrared radiation. The diffraction limitation is imposed by the narrow dimension of the elliptical aperture. It is clear that a final design of even this simple system cannot be made without precise specification of the desired spectral range, since diffraction limitations arise with longer wavelengths for those choices of eccentricity that the geometrical theory predicts as optimum. For a system designed to work in the visible, the design with  $d = 1.5$  and  $f/12$  appears to provide the best compromise.

Figure 14 - RMS Deviation for 400 Rays as a Function of Full Field Angle  
for Elliptical Apertures ( $e = 5$ ) at  $f/8$  and  $f/12$



G. Improvement of Performance of Wide Angle Reflecting System Using a Cylindrical Reflector

The data plotted Figure 13 and 14 of the previous section indicate that a high state of correction at low  $f$ /ratios is not attainable with this simple system. To obtain better correction, a number of obvious correcting elements suggest themselves. First among these is the Schmidt corrector plate designed to eliminate the spherical aberration in a system working at the  $f$ /number governed by the off-axis distance of the outer edge of the elliptical aperture. Such a plate would completely eliminate the monochromatic aberrations on axis, and would provide good imaging for all pencils of moderate obliquity. However, for those pencils having large components in the direction perpendicular to the plane of Figure 12, the aberrations would be serious. The chromatic errors introduced by the corrector plate would also limit its usefulness.

A second possible means of correcting the aberrations of the system is the incorporation of a concentric refracting element such as is used in Brower's concentric systems. This element would also be limited by color effects, but has the advantage of preserving the symmetries of the original system. It would, therefore, not introduce serious errors for pencils of large obliquity, as would a Schmidt plate. In addition the element provides the obvious constructional advantage of spherical surfaces.

The possibility of incorporating refracting elements of zero first order power, with spherical surfaces, in the immediate region of the aperture was

also suggested. The difficulty in these cases lies primarily in the fact that such correctors completely destroy all the symmetries of the system. This is because the only spherical surfaces symmetric about the optical axis of the original system which provide zero power are plane surfaces, perpendicular to the optical axis. It would seem that spherical surfaces with their centers of curvature removed from the optical axis would be required; however, it is difficult to visualize what might be expected from such refracting elements.

Unfortunately, the time and funds allotted for this program did not allow a comparative study of these possibilities. While each element was being studied in a rough quantitative manner in terms of the aberrations of the original system, a novel type of corrector element suggested itself. This element was one which was peculiar to a decentered system of this type and might provide significant improvement.

A cross-section of the system with this corrector is shown in the right side of Figure 12. The cross-section is taken through the minor axis of the elliptical aperture.

Consider the aberrations of the original system for the pencil parallel to the optical axis. Rays in the fan through the minor axis of the elliptical aperture cross the optical axis at points which depend on the height at which they strike the main mirror, the higher rays crossing closer to the mirror. At a short distance off axis and at a point considerably closer to the mirror than the intersection points of any of these rays with the optical axis, all the rays of the fan come within a very small distance of one another. Since the tangential fan is quite narrow (the minor axis being short) the depth

of focus of this fan is comparatively great. If we now examine the sagittal fan of rays, it is clear that its depth of focus will be comparatively small, since the major axis is about five times as long as the minor axis. Since the fan is effected only by the spherical aberration of the mirror, all rays will cross the axis at almost the same point. This point lies within a negligible distance from the point where the upper ray of the tangential fan crosses the optical axis. This qualitative discussion points up the fact that, although the aberrations of the original system are formally called spherical, they manifest themselves in a manner much more akin to astigmatism.

The purpose of the cylindrical mirror is now obvious. The intent is to impart sufficient power to the rays of the sagittal fan to cause them to converge in the region of focus of the tangential fan. The exact radius of curvature for the cylindrical mirror can be found only by ray tracing. A first approximation may be readily obtained analytically from the algebraic description of the path of the edge rays of the major fan.

A computer ray trace program was written in order to completely study the design of the corrector system. The program is designed to provide for the tracing of an arbitrary number of rays from the centers of mass of equal area portions of an elliptical aperture of arbitrary eccentricity and size. The rays are traced through reflection from a cylindrical mirror of any specified radius, and subsequent reflection from the main mirror to any specified focal surfaces concentric with the main mirror. Rays in any specified direction may be traced.

The program was used to study the imaging of the axial pencil for

an  $f/1.8$  elliptical aperture with ratio of major to minor axis of five and a series of different radii for the cylindrical corrector. For this  $f$ /ratio and eccentricity, best imaging was obtained for a cylindrical mirror radius of 395 inches. The rms deviation of all rays was equal to 0.00147 inch, compared with an rms of 0.00345 inch for the uncorrected system. The image for the corrected system, however, was not symmetrical, the rms deviations in perpendicular directions being in the ratio of about 2:1. For symmetric imaging an rms of about 0.002/inch might be expected. A better performance for this particular value of eccentricity is impossible, since the rays of the tangential fan never are any closer together than 0.00136 inch in the rms sense. However, data for an eccentricity of three on the original system indicate that a symmetric image patch with an rms radius of 0.001 inch should be possible. Unfortunately, time and funds prevented the investigation of this and other possibilities. The study did indicate, however, that a resolution ( $1/\text{rms radius}$ ) of 40 lines/mm at  $f/1.8$  over a 16 by 16 degree field should be possible. With a 5:1 conical condenser, this system could be made to provide 40 lines/mm at effective  $f/1.6$  in the visible, infrared or ultraviolet. Though the corrected system was not studied numerically for off-axis pencils, it is not expected that a cylindrical mirror of such large radius of curvature will change the off-axis pencils in a manner significantly different from that of the axial pencil. This conclusion requires verification, however.



#### IV. EXPERIMENTAL DATA

##### A. Refracting System

For the refracting system the concentric system of Sutton was chosen as a promising lens type. The particular design used in this program was suggested by Dr. James J. Baker. The design was selected because of its curved field, simplicity, vibrational stability and relatively low f/number ( $f/3.5$ ) and it was diffraction-limited over a very wide angle ( $120^\circ$  total field). The design specifications of the system are given in Figure 15.

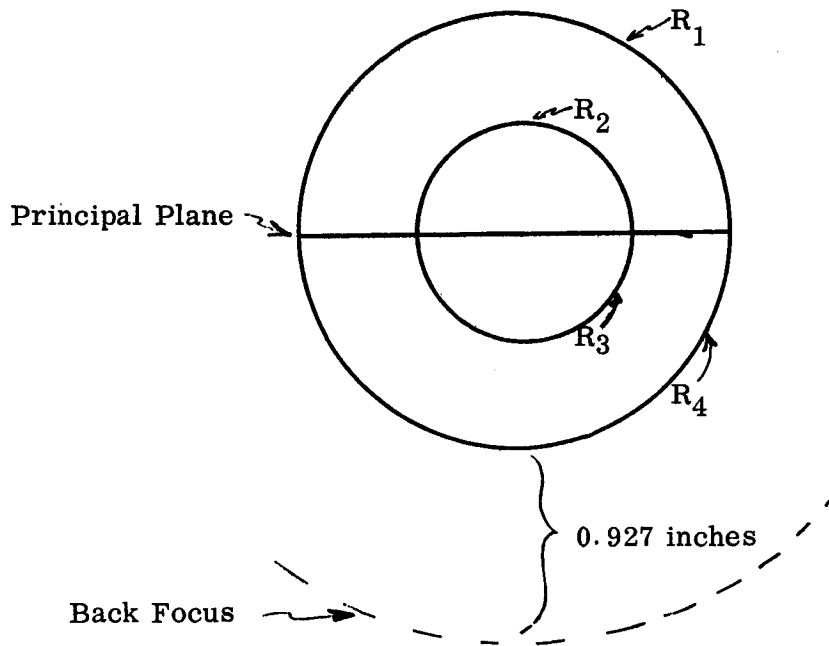
The finite conjugate, point spread function of the Sutton lens was inspected and found to be asymmetric; the asymmetry rotated with the lens when it was turned about its optical axis. Therefore, the point spread function asymmetry is attributable primarily to a slight misalignment of the two glass hemispheres when they were cemented together.

Frequency response measurements were made of the Sutton lens and the Sutton lens-field flattener combination. Special apparatus was needed for these measurements, particularly because of the very high spatial frequencies involved. A detailed description of the apparatus has been included in Appendix B. The measurements are summarized in Figure 16 and further details are given in Figures 17 and 18.

Figure 16 shows the following frequency responses:

- (a) Perfect  $f/3.5$  lens system using monochromatic  $550\text{ Å}$  light.
- (b) Sutton lens on-axis using light transmitted through a green filter peaked at  $550\text{ Å}$  and whose half-width was  $40\text{ Å}$ .

Figure 15 - Sutton Lens Specification



Glass Separation		Glass Type	
$R_1 = 1.073$ inches		EDF-3	$n_D = 1.720$
	0.537		
$R_2 = 0.536$ inches		C-1	1.523
	1.071		
$R_3 = 0.536$ inches		C-1	1.523
	0.537		
$R_4 = 1.073$ inches		EDF-3	1.720

Back Focus = 0.927 inches

The radius of the spherically curved image surface is the same as the EFL, namely 2 inches.

▽ Airy Disc

⊙ Sutton Lens - 0°

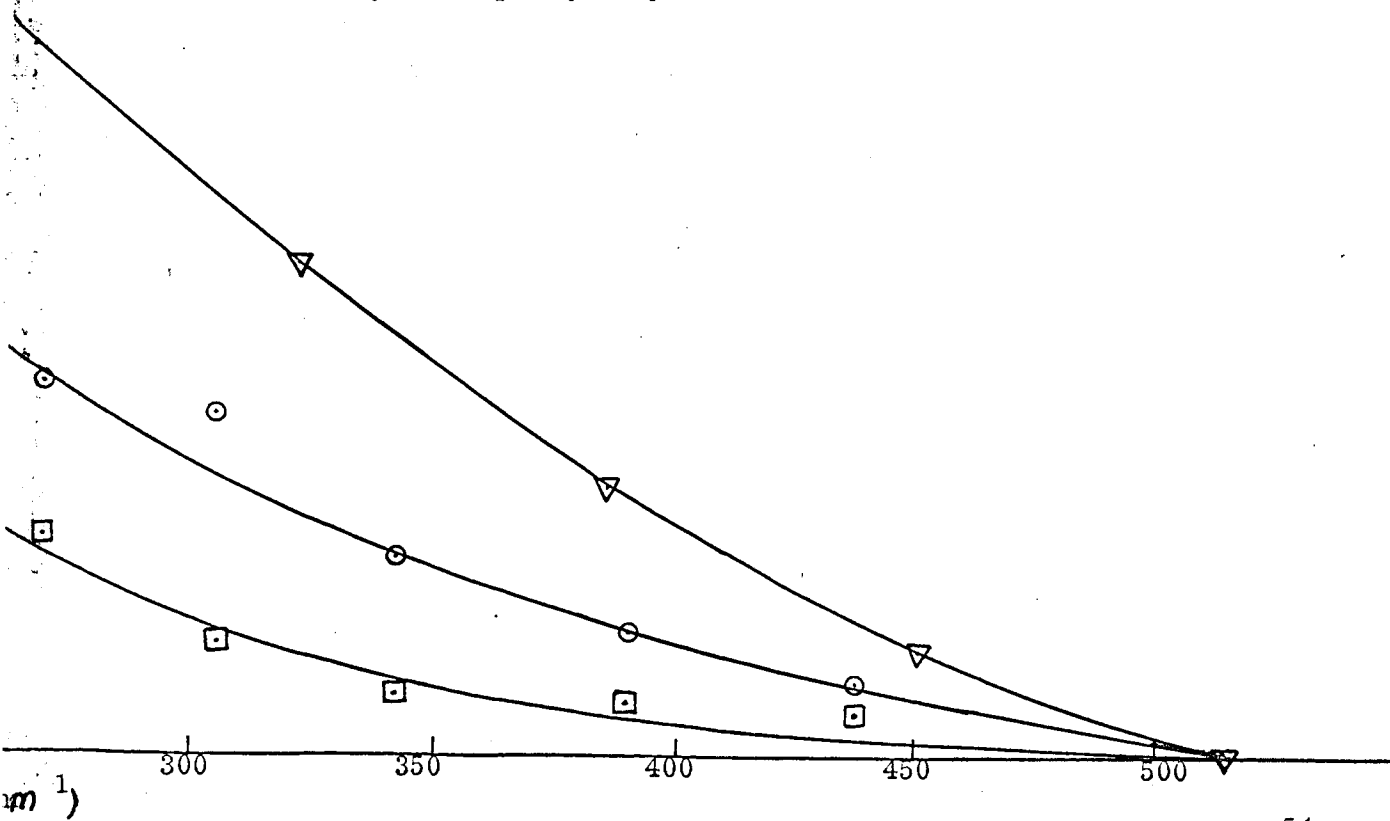
▣ Sutton Lens - 50°

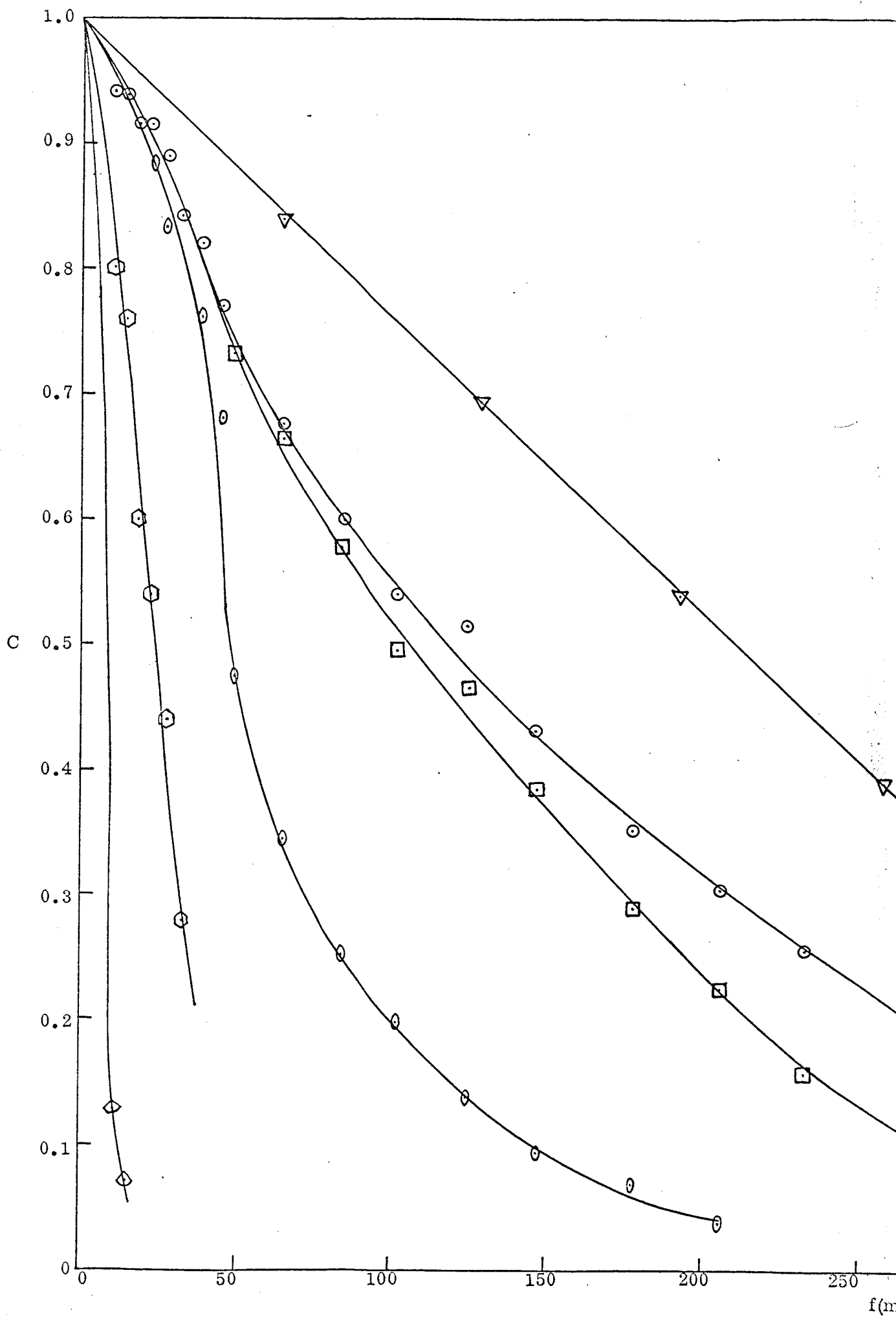
⊖ Sutton Lens with field flattener - 0°

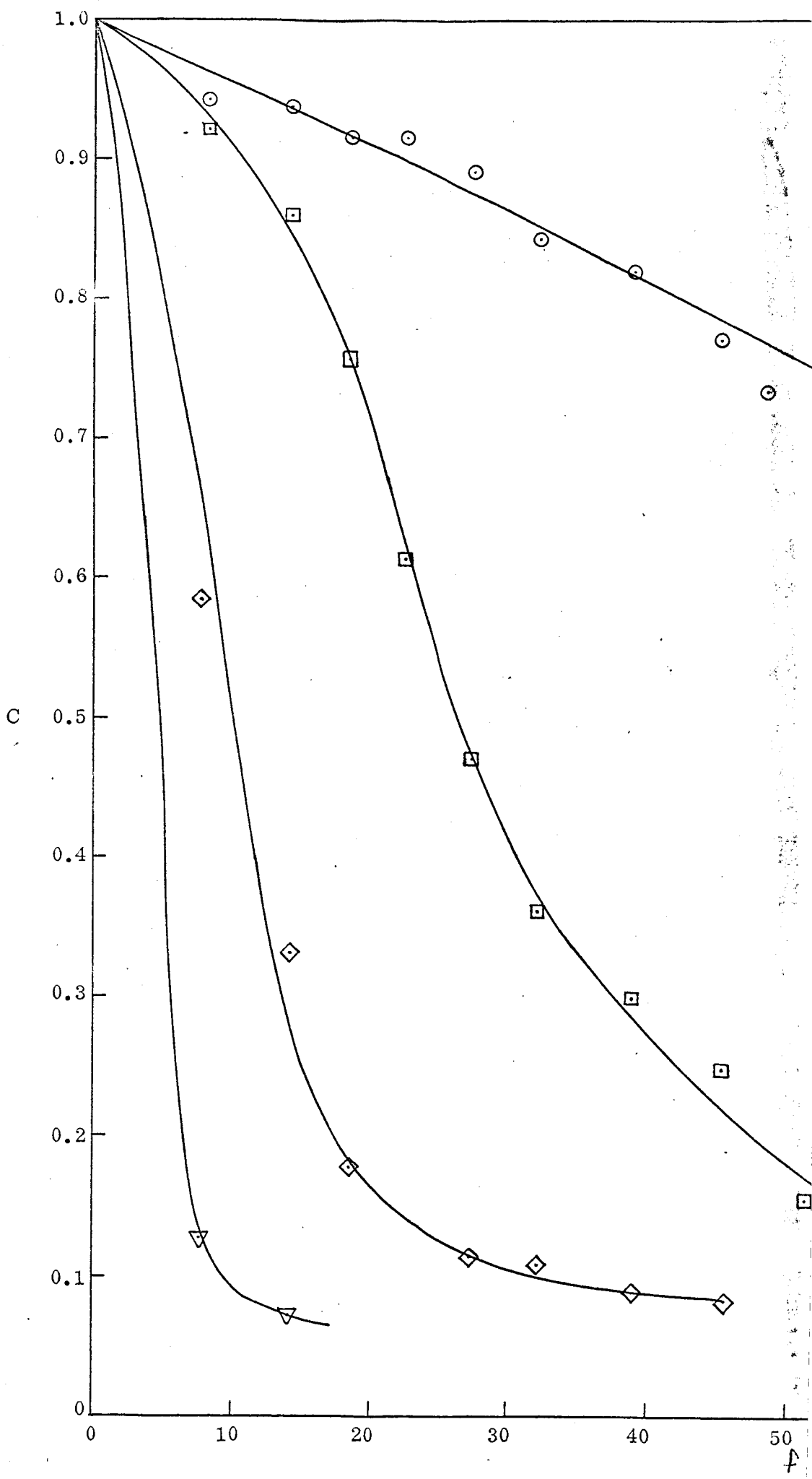
⬠ Sutton Lens with field flattener - 27°

⬡ Sutton Lens at Gaussian Focus - 10°

Figure-16.- Summary of Frequency Response Data







- Sutton Lens at Gaussian Focus -  $0^\circ$
- Sutton Lens at Gaussian Focus -  $5^\circ$
- ◇ Sutton Lens at Gaussian Focus -  $7.5^\circ$
- ▽ Sutton Lens at Gaussian Focus -  $10^\circ$

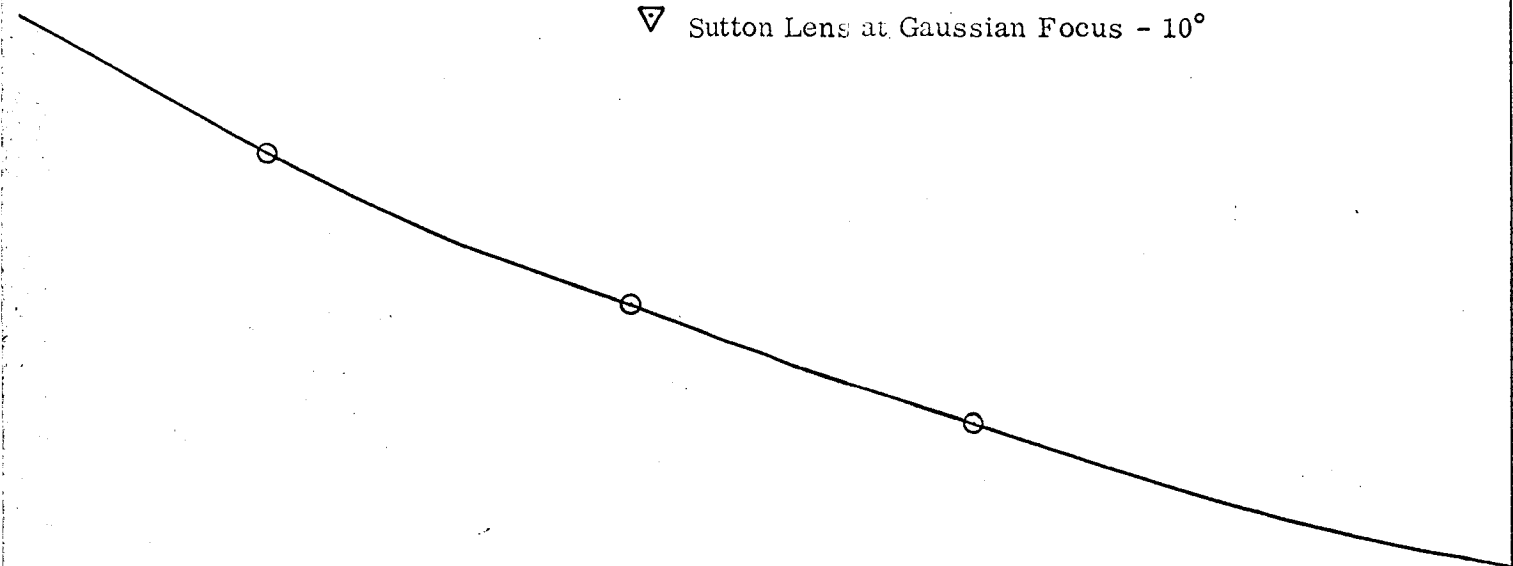
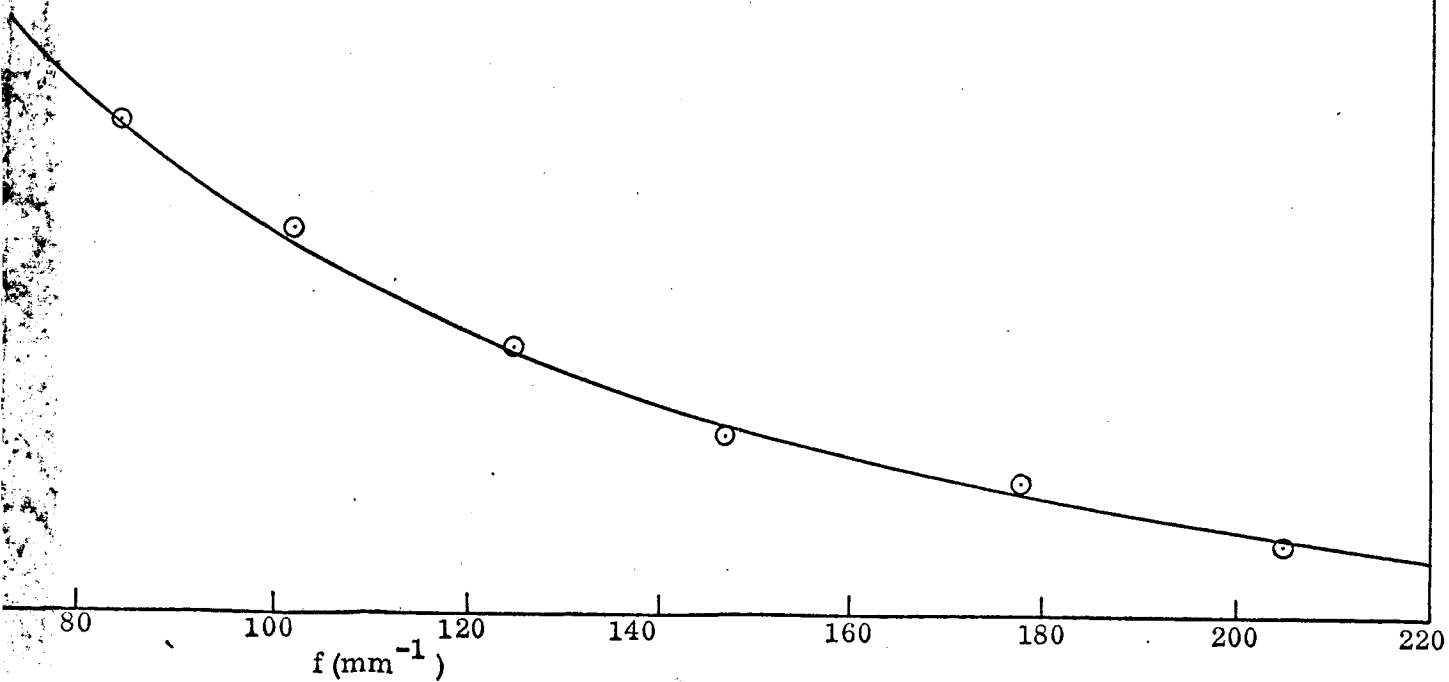


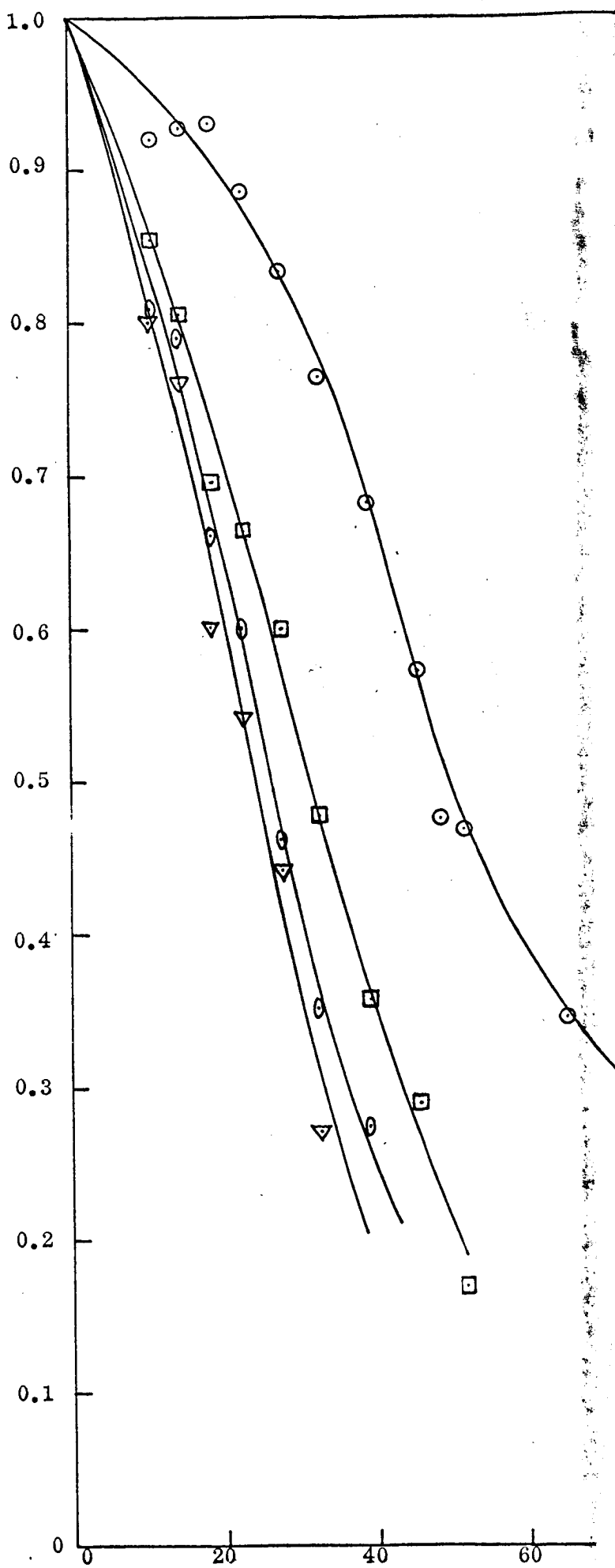
Figure 17 - Frequency Response of Sutton Lens at Gaussian Focal Plane

- Sutton Lens with field flattener -  $0^\circ$
- ◻ Sutton Lens with field flattener -  $15^\circ$
- ◊ Sutton Lens with field flattener -  $20^\circ$
- ▽ Sutton Lens with field flattener -  $27^\circ$

Figure 18 - Frequency Response of Sutton Lens -FieldFlattener Combination



64



C



- (c) Sutton lens-field flattener combination on axis.
- (d) Sutton lens-field flattener at  $27^\circ$  half angle.
- (e) Sutton lens at the Gaussian focus,  $10^\circ$  half angle.

It should be noted that the frequency response of the Sutton lens is noticeably lower than that of a perfect lens. There are several reasons for this. In general, the measuring apparatus only sets a lower limit on the frequency response and any refinements of the measuring technique would tend to raise the frequency response curve. In particular, the point spread function has a slight asymmetry. The aluminized stop caused the introduction of extraneous reflected and scattered light; there were also a number of pinholes or perforations found in the aluminized stop. Also, the deterioration in frequency response at  $50^\circ$  half angle is caused, at least in part, by vignetting (the change in effective f-number as a function of field angle). That is, deterioration is caused by the transformation of the circular aperture of  $0^\circ$  into an elliptical aperture off-axis.

Figure 17 shows the frequency response of the Sutton lens at its Gaussian focal plane for 0, 5, 7.5 and  $10^\circ$  half angles. The deterioration here is due primarily to the defocused image in the Gaussian plane.

Figure 18 shows the frequency response of the Sutton lens-field flattener combination at 0, 15, 20 and  $27^\circ$  half angles. It will be noted that the frequency response is a function of angle as well as spatial frequency. The lower response at large field angles is caused by light leakage out of the fibers into the interstices. As the field angle increases for a given numerical aperture fiber, the lower rim ray first begins to leak out, then the principal ray, and finally at very large angles all rays leak out and are scattered. Although the field

flattener causes a deterioration in the frequency response from that of the Sutton lens only, it should be pointed out that even for a  $10^\circ$  half angle the frequency response of the Sutton lens at the Gaussian focus is much inferior to that of the Sutton lens-field flattener combination. Furthermore, it is possible to eliminate this effect entirely by "Fresnelizing"<sup>(13)</sup> the entrance end of the field flattener. Further developments along these lines seem highly justified.

#### B. Camera

A camera which incorporated the Sutton lens-field flattener combination was built and tested. An exploded view of this camera is shown in Figure 19, and Figure 20 shows the camera completely assembled. Photographs of various targets were taken using this camera and are shown in Figures 21, 22 and 23. Figure 21 is a photograph of some homes in the hills of San Carlos; Figure 22, a photograph of a test object in the Optics Technology laboratory; and Figure 23, a photograph of the same test object with the field flattener removed from the camera.

#### C. Reflecting System

The construction of a reflecting system capable of high resolution in the ultraviolet, visible and infrared regions of the spectrum was also decided upon. With the assistance of Dr. Baker, a system was selected which consisted of a large spherical mirror, a decentered elliptical aperture and a fiber optics field flattener. This particular system was selected since it appeared to offer wide field angle at a relatively low f-number.

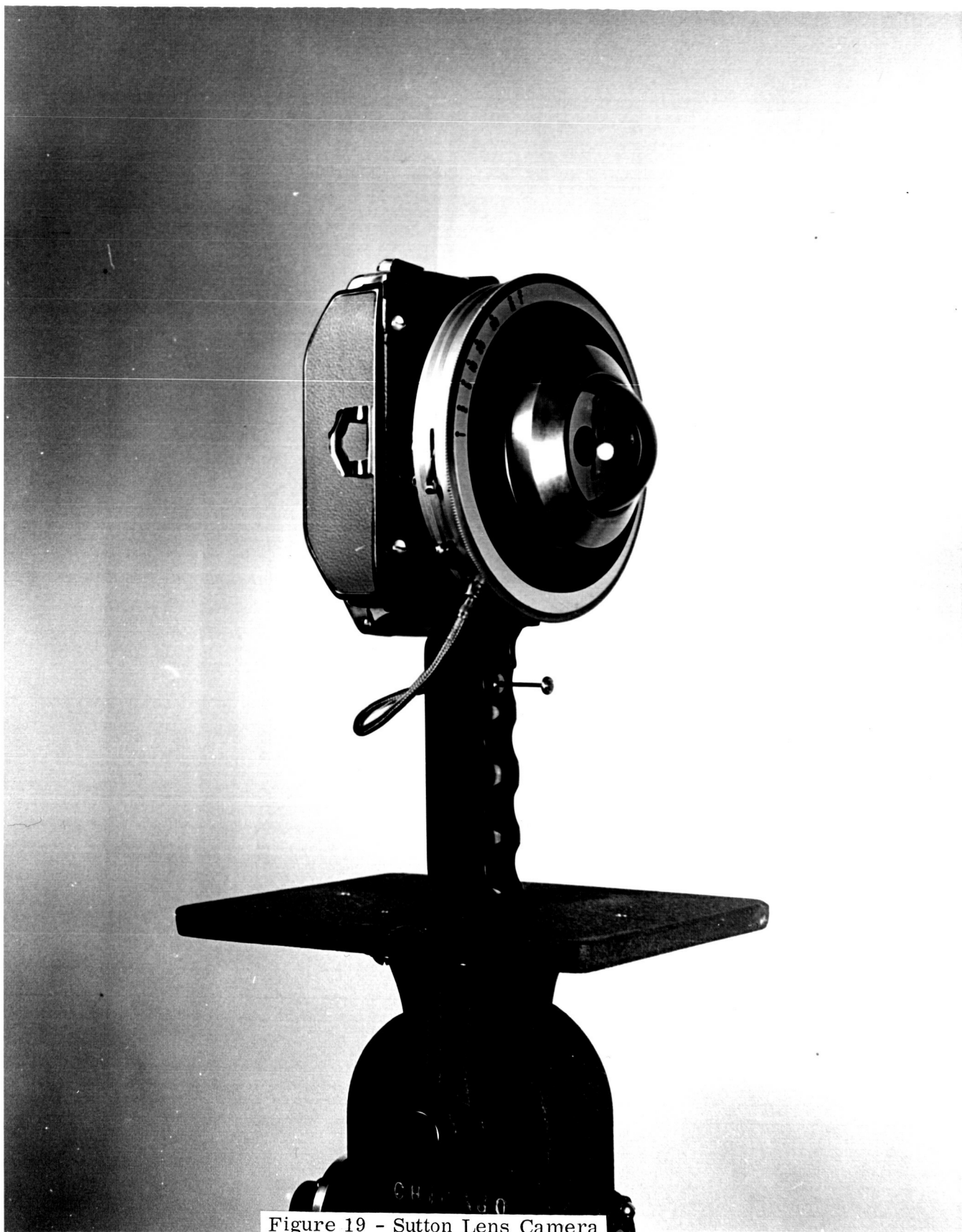


Figure 19 - Sutton Lens Camera

67

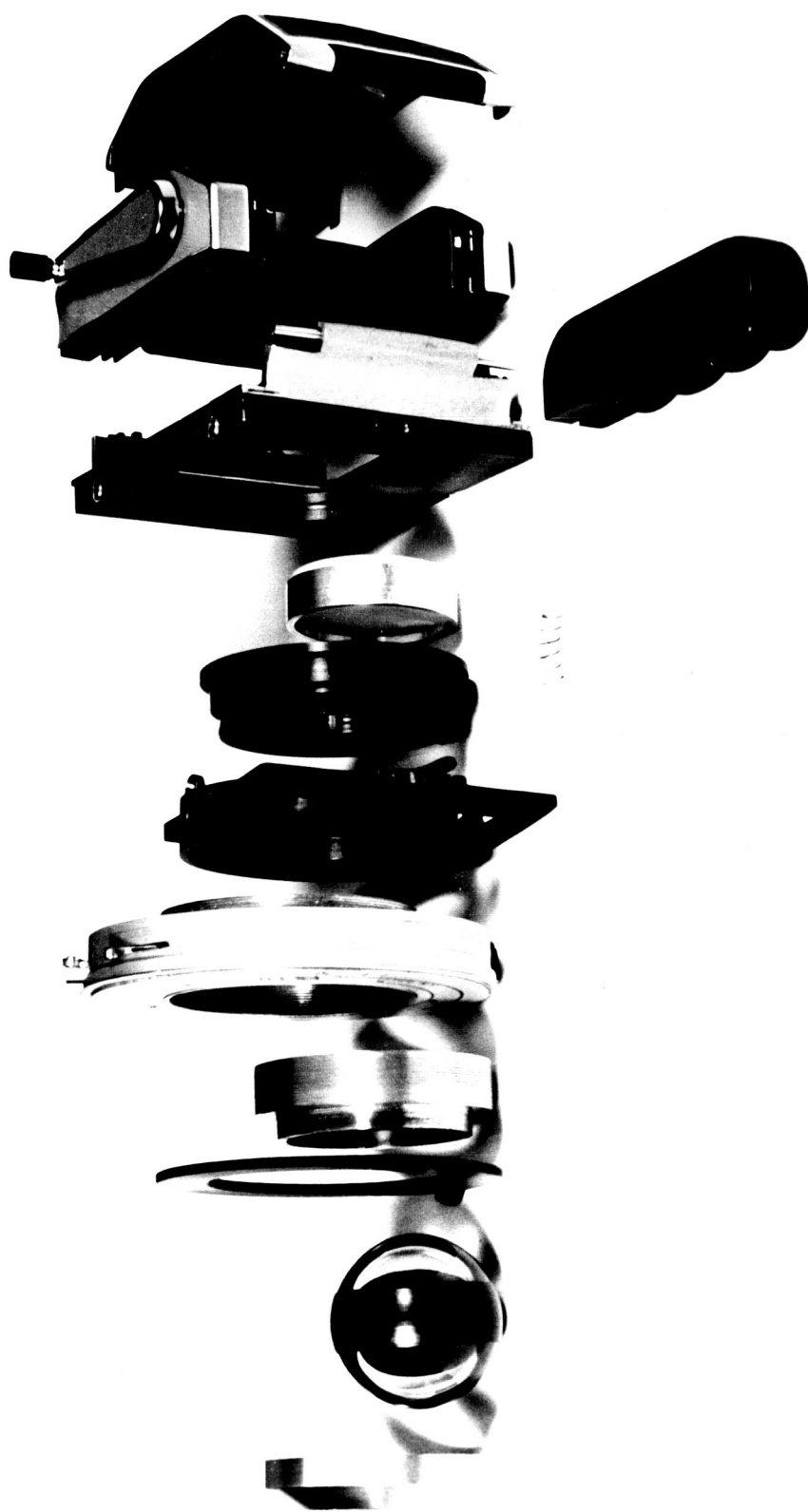


Figure 20 - Sutton Lens Camera Exploded View

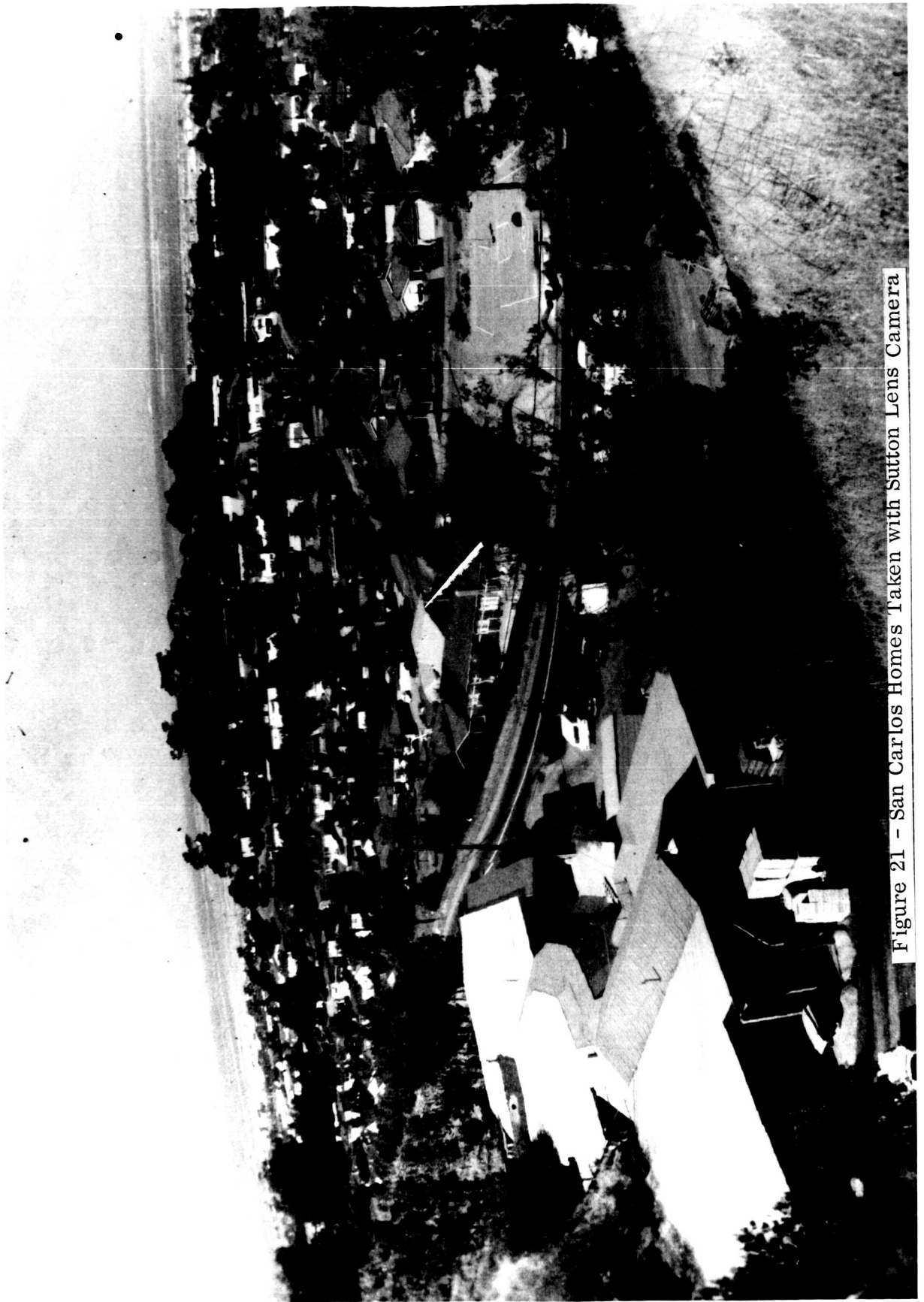


Figure 21 - San Carlos Homes Taken with Sutton Lens Camera

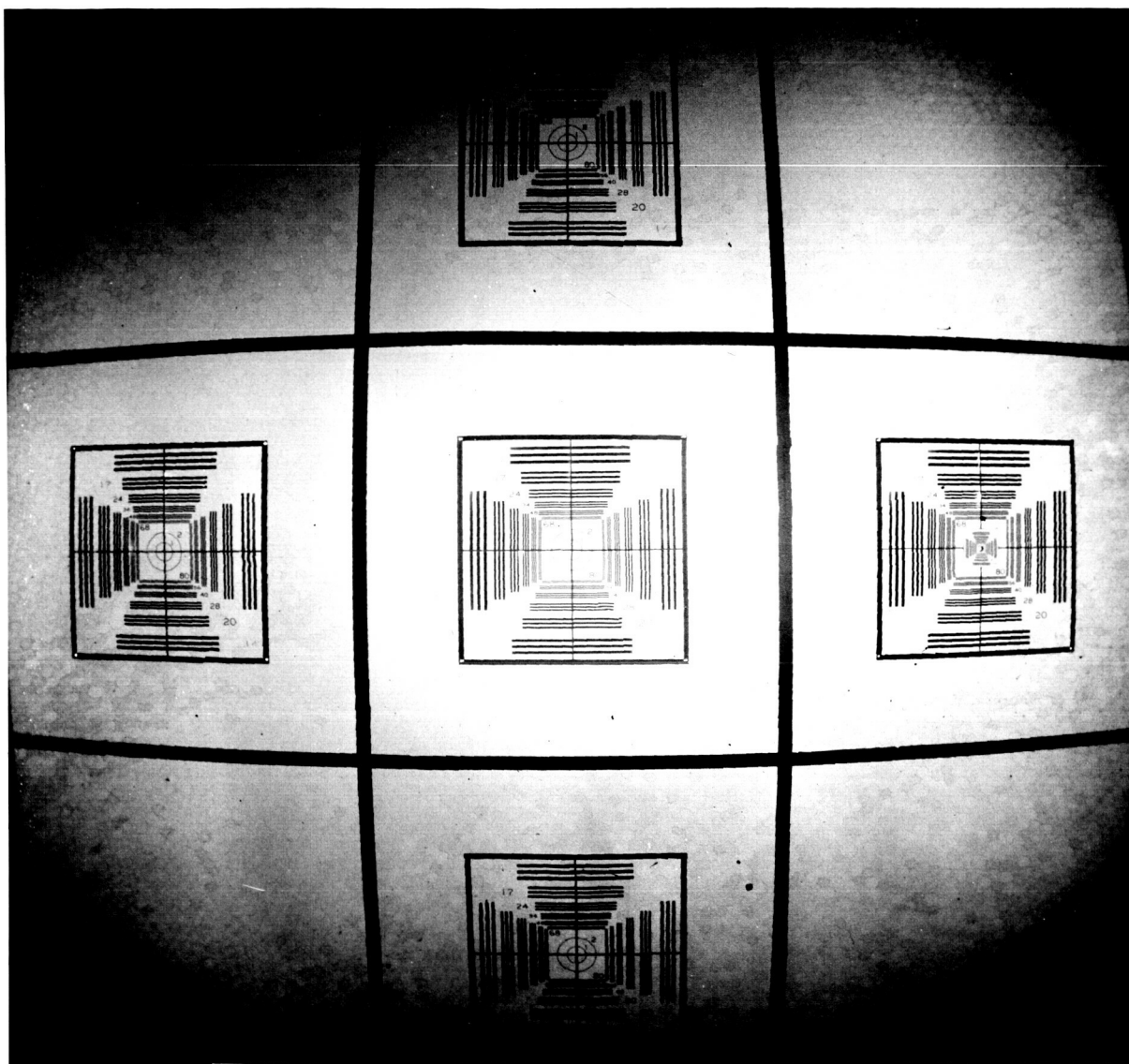


Figure 22 - Test Object Taken with Sutton Lens Camera

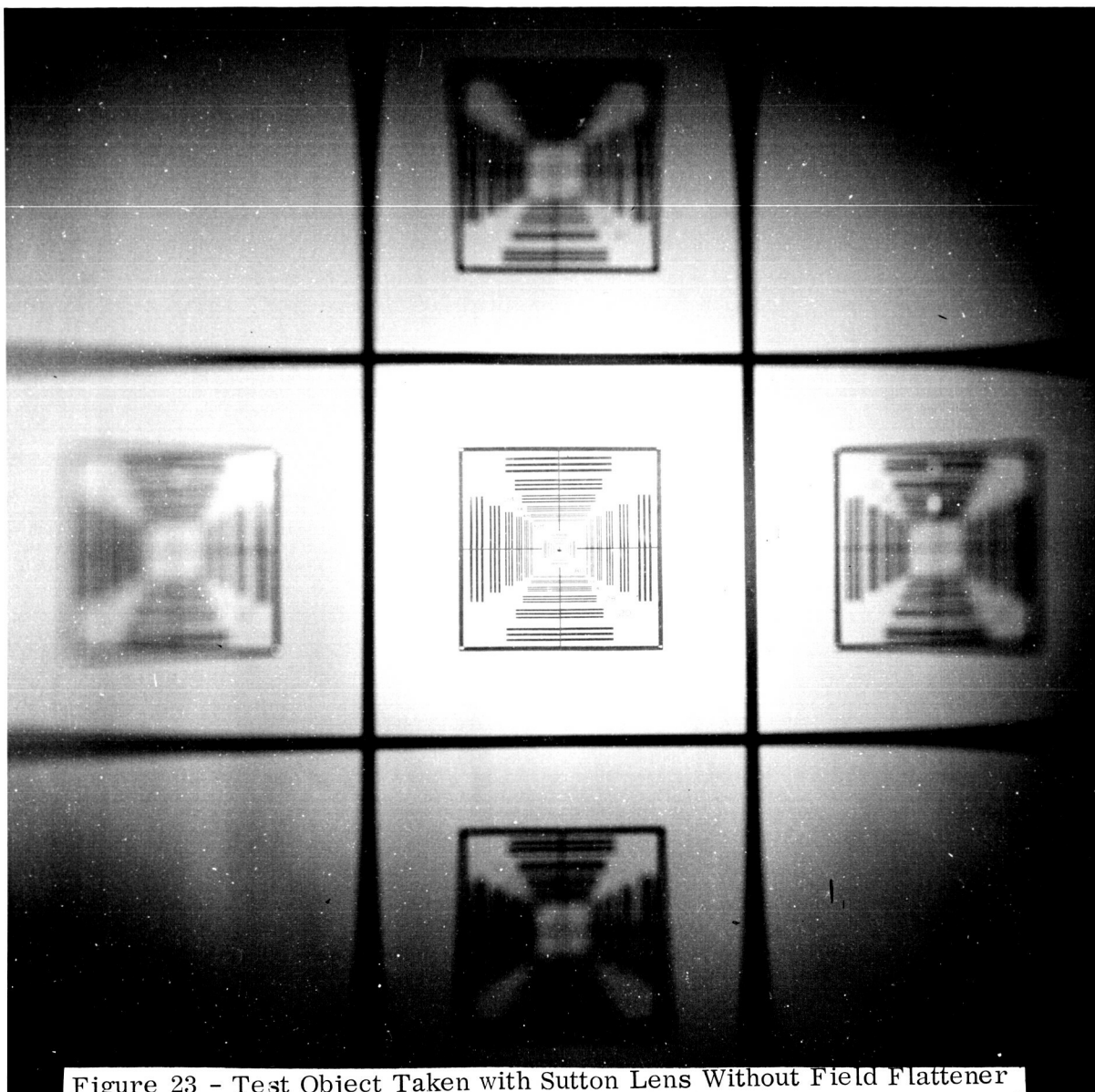


Figure 23 - Test Object Taken with Sutton Lens Without Field Flattener

Figure 24 shows the camera with an aperture-shutter on the front, a film holder-field flattener assembly and bolts on the side which control the four degrees of freedom of the mirror mounts. The film holder-field flattener assembly also had four degrees of freedom. While a single degree of freedom is normally used in focusing a camera, with this camera the degrees of freedom of a given component were not independent, thus focusing by only one degree of freedom was impossible.

Unfortunately, at the time the decision was made to construct the reflecting system, the computer studies were not complete, therefore allowances were made for the position adjustments of all components. This made the alignment of the components difficult since in an experimental design configuration there are a large number of unnecessary degrees of freedom. Also, the radius of curvature of the fiber optics field flattener was not necessarily the optimum since the results of the computer studies were not available at the time of its fabrication.

The system having the following design data was tested:

f-number	f/12
d	1.47 inches
$\epsilon$	5
$R_m$	13.7 inches
$R_{ff}$	7.02 inches

where d = distance from the axis of the system to the edge of the stop

$\epsilon$  = ratio of major axis to minor axis of the elliptical aperture

$R_m$  = radius of the mirror

$R_{ff}$  = radius of the field flattener





Figure 24 - Reflecting System Camera

For preliminary quantitative analysis on the performance of the system a bar chart was placed 70 ft from the camera and the image which was formed on the field flattener was inspected visually. The resolution was in excess of 30 lines/mm; the best resolution which could be photographically recorded was approximately 20 lines/mm. This is possibly due to the fact that the high numerical aperture fibers captured scattered light from a large portion of that mirror which was not used for imaging. Furthermore, it is possible that movement of the camera, which was used outdoors under windy conditions, could have affected the resolution.

The type of reflecting system used, however, seems to hold considerable promise. Unfortunately not sufficient effort could be expended on this phase of the program because of time and fund limitations. Further theoretical and experimental investigations of different configurations of this type of systems seem highly justified.

## V. FIBER OPTICS

The work in this area has been directed primarily toward the construction of three types of fiber optics elements, the fiber optics field flattener, the conical condenser and the fiber optics distortion corrector. For convenience these three areas will be discussed separately.

### A. Fiber Optics Field Flattener

In order to fabricate the fiber optics field flattener it was only necessary to obtain a suitable size of the material presently being used for fused fiber optics elements. The first field flattener constructed utilized fiber optics material of high numerical aperture and small individual fiber diameter. Our standard plates at that time had the properties of a numerical aperture nominally equal to one and with an individual fiber diameter of about 8 microns. However, being of necessity constructed of a glass of high refractive index, a certain amount of coloration of the fibers was inevitable, which contributed slightly to a fall in intensity at the edge of the field due to the thickness of the field flattener. However, this first field flattener was incorporated in the camera and provided the initial data.

As the techniques of fabrication of fused fiber optics employed at Optics Technology developed, together with improvements in the optical clarity of the glasses employed, the fused fiber plates became of a correspondingly higher quality and a second fiber optics field flattener was fabricated. The second field flattener was used to extend the data obtained from the first. Both the field flatteners had similar optical qualities in that they had the high numerical aperture

and small fiber diameter. The detailed experimental measurements on these field flatteners are contained elsewhere in this report.

#### B. Fiber Optics Conical Condenser

On a small scale the fabrication of fused fiber optics conical condensers is a routine process evolving from the procedures used in the fabrication of multiple fibers. It was thought that to extend this process to the fabrication of conical condensers of major diameter two to three inches would involve a considerable outlay both in new equipment and in basic raw material in that a large fiber boule would need to be suspended in a vertical cylindrical furnace in such a fashion as to allow one end to become sufficiently molten to allow it to form a cone while the other end remains sufficiently rigid to support the complete weight of the boule. In the drawing of multiple fibers this is simply accomplished by having a boule whose length is ten to twelve times as great as its diameter, the low heat conduction of glass being sufficient to maintain the required conditions.

The first experiment performed in the production of larger cones was tried using a one-inch diameter fused fiber boule of about five inches in length. This was held by metal wires which allowed it to hang through the center of a small, short cylindrical furnace. This whole assembly was constructed within a large annealing oven, through the baseplate of which a wire joined to the lower end of the boule could pass. In performing the experiment the annealing oven was heated to a temperature somewhat above the annealing temperature of the glass. Fairly intense local heating was then applied to the center of the boule through the action of the small furnace surrounding it. As the boule softened, it was possible to draw it apart into two cones by lightly pulling the wire attached

to its lower end. On completion of the process the small furnace was switched off and the whole assembly allowed to cool within the annealing oven under strictly controlled thermal conditions.

The cone produced by this technique was somewhat unsymmetrical caused by the boule not being located precisely in the center of the small heating furnace, one side thus becoming more fluid than the other. However, it appeared from the preliminary results, which were quite encouraging, that the technique was sound in principle and could be applied to larger assemblies. Consequently the experiment was redesigned in order to accept boules of two inches in diameter.

The first experiment using the revised apparatus and a two inch boule pointed out several important limitations in the apparatus and the process. The first of these was the fact that the two-fold increase in diameter demanded a disproportionately large increase in the power dissipation of the small heating furnace. As a result the furnace being used was run at the utmost limit of its capability and several hot spots could be seen upon its surface. This resulted in a non-uniform heating of the boule causing an unsymmetrical cone to be produced. Nevertheless, it was felt that with an improved boule and minor furnace modifications it would still be possible to produce a good quality cone.

The second boule, somewhat larger than the previous one, was also somewhat shorter, being a little under five inches in length. In forming a cone from this boule, the same limitations observed in the first experiment existed although to a lesser degree but, more important, it was found that the decreased length was insufficient to keep the two ends of the boule cool enough during the process

and a tendency was noticed for the boule to pull apart at the points of its support. To overcome this, it was necessary to apply what was later found to be excessive heat at the center of the boule resulting in an extremely steep thermal gradient between the center and the surface of the boule. Thus, while a mechanically sound cone was formed, on examination it was found that the central portion of the fibers was comparatively undeformed while the outer layers had fused sufficiently to merge together and lose their optical identity.

In the experiments on the next boule it soon became apparent that even though further precautions had been taken to prevent the softening of the ends, sufficient rigidity was not being maintained to allow a satisfactory cone to be drawn. The experiment was therefore stopped and the boule allowed to pass through its annealing cycle. In order to prevent the softening of the boule at the point of support a massive steel cylinder was attached to the metal clamp and allowed to extend several inches above the top of the furnace. The furnace was preheated gradually and the boule slowly inserted into the hot central zone. The tip of the boule softened and was withdrawn through the bottom of the furnace. Several feet of the tip of the cone were drawn off to insure that stable conditions had been reached within it. The furnace was then closed off and the boule allowed to anneal. At the conclusion of this experiment it was found that a perfectly shaped cone had resulted and this was removed from the clamp and cut to size.

The final dimensions of the cone were: major diameter, 2.25 in.; smaller diameter, 0.5 in.; overall length, approximately 3 in.; fiber size at large end, 25 microns. The alignment exhibited within this cone appeared to be excellent, a straight edge being reproduced with little or no distortion. However, being of

high numerical aperture, the cone exhibited a certain amount of coloration and it was decided to reduce its overall length. This could be achieved with only minor losses in the overall diameters and at a possible reduction of about 0.75 in. in length. During the subsequent cutting, several cracks developed in this cone, undoubtedly due to the cumulative stresses induced into the boule by the many thermal cycles it had endured during the fabrication of the cone. At the present time this cone is at the grinding and polishing stage.

#### C. Distortion Corrector

In order to assess the relative contribution of fiber diameter variation and actual displacement of fibers at the two ends of a distortion corrector, a detailed examination of available distortion correctors was undertaken. A rectangular grid was photographed through the distortion corrector in such detail as to show the ends of the individual fibers. To establish a reference the procedure was reversed and, without moving either the grid or the distortion corrector, the fibers were photographed through the grid structure. Thus by direct observation it was possible to compare the relative positions of the input and output ends of many of the individual fibers. It was also feasible to observe any change in diameters that existed within the fibers. It was possible to show that two effects were apparent in providing the distortion corrector characteristics of the fiber optics plate. Toward the center of the plate the individual fibers were well fused and had apparently been under considerable pressure during their processing. This had resulted in a change of diameter along the length of the fiber. Conversely, at the edges of the plate where the fibers had been loose packed and not subjected to such high pressure, a tendency to change the relative positions of the fiber ends rather than their diameters was noted.

Neither of these two effects could be conclusively shown to predominate and in the absence of further samples it was assumed that a combination of both these effects may in fact be necessary at all times to produce distortion in a fiber bundle.

During these initial measurements several experiments were in progress to produce further distortion correcting devices. Two approaches were tried, each of which met with partial success in that a distortion device was obtained although no definitive technique was established. In the first of these methods of fabrication the boule of fibers was fused to form a rod with a re-entrant cavity in its lower end. This rod was held vertically in a furnace and allowed to form a cone. As the edges of the re-entrant cavity drew together, an entrapment occurred and a gradient thereby produced. By further pulling the boule into a cone, a gradient was established across the rod and, as was apparent upon subsequent examination, considerable differential movements occurred within the main body of the fibers. The distortion produced by this method was severe and non-linear across the boule. However, it did appear that the method showed some promise and could possibly have been developed had conditions permitted.

The second approach also produced results which could probably have been extended with further effort. In this method, distortion was introduced into a boule during its formation by the application of considerable pressure at different points on its circumference. The first experiments on this method were, for the sake of convenience, designed to produce distortion which was non-radial in character. Loose fibers were formed into rectangular boules by being placed into a U-shaped jig which was then heated up to the softening point of the glasses



used. Pressure was applied to the fibers by the action of a plunger inserted into the open end of the U. By suitably shaping both the face of the plunger and the opposing face of the U a deformation in the cross section of the fiber boule could be induced. Similar experiments using carbon moulds instead of metal moulds were performed. The fragility of the carbon did not allow sufficiently high pressures to be used to provide a significant amount of distortion.

At the conclusion of these experiments on the examination and fabrication of distortion correctors further work on this aspect of the program was held in abeyance in order to concentrate our efforts toward the construction of a fiber optics conical condenser. It is clear that further developments of distortion correctors are imperative before the use of fiber optics image correctors in new and unique optical systems can be optimized.

# LIST OF REFERENCES

1. N. S. Kapany, J. Opt. Soc. Am., 51, No. 1, 32-34 (January 1961).
2. N. S. Kapany, J. Opt. Soc. Am., 49, No. 8, 779-787 (August 1959).
3. N. S. Kapany, J. A. Eyer and R. E. Keim, J. Opt. Soc. Am., 47, No. 5, 423-427 (May 1957).
4. R. Kingslake, Lenses in Photography, Garden City, Carden City Books, 1951, p. 122.
5. E. H. Linfoot, Recent Advances in Optics, London, Oxford Press, 1955, pp. 1-14.
6. D. P. Feder, J. Opt. Soc. Am., 41, 630 (September 1951).
7. A. C. S. Van Heel, Optica Acta, 1, 44 (1954).
8. A. E. Conrady, Applied Optics and Optical Design, New York, Dover Publications, Inc., 1957, p. 455.
9. R. E. Stephens, NBS Circular 549, September 1954.
10. A. E. Conrady, Applied Optics and Optical Design, Part Two, New York, Dover Publications, Inc., 1960, pp. 786-787
11. Ibid., p. 801
12. Ibid., p. 800
13. N. S. Kapany and R. E. Hopkins, J. Opt. Soc. Am., 47, No. 7, 594-598 (July 1957).

## APPENDIX A

### IMAGE SYNTHESIS STUDIES

#### I. INTRODUCTION:

The technique for providing real images from the design data of hypothetical optical systems is called image synthesis.<sup>(1) (2)</sup> To synthesize an image from the lens design data the characteristic point spread function of the optical system must first be determined and represented by a "spot diagram". This representation, or spot diagram, is used with a highly convoluting optical system to produce real images of typical geometrical and pictorial test targets (transparencies). The images thus formed are almost indistinguishable from those formed by the optical system when it is constructed.

Obviously, such a technique is valuable to a lens designer, both as a means of determining the relative importance of various kinds of aberrations on image degradation and evaluating the design of an optical system before it is constructed.

In the studies under this program the accuracy of point spread function representation was 1) extended beyond the previous state-of-the-art; 2) new point spread functions were generated and represented; 3) a new technique for making small spot diagrams was developed; 4) a small versatile image synthesizer was constructed; 5) images of space targets were synthesized; 6) valuable insight into the image degrading effects of several aberrations was gained; and 7) an image formed by a real optical system was compared to the appropriate synthesized image.

## II. TECHNICAL DISCUSSION

The following technical discussion deals with theoretical and experimental aspects of the image synthesis technique. Discussed are methods, problems, solutions, possibilities and limitations of the general technique. The actual experimental work which was accomplished on this program will be reported in a later section.

### A. Theory

Equation (1) is the well known expression<sup>(3,4)</sup> for the intensity distribution in the image  $i(x,y)$  of an extended, incoherently illuminated object  $O(x_0, y_0)$ .

$$i(x,y) = \int_{-\infty}^{+\infty} \int_{-\infty}^{+\infty} O(x_0, y_0) I(x_0, y_0; x, y) dx_0 dy_0 \quad (1)$$

The optical system, including aberrations, is characterized at each image point  $(x,y)$  by the point spread function  $I(x,y; x_0, y_0)$ . If the aberrations vary slowly over a isoplanic patch, the "shape" of  $I(x,y; x_0, y_0)$  does not change rapidly and equation (1) may be rewritten as a convolution integral.

$$i(x,y) = \int_{-\infty}^{+\infty} \int_{-\infty}^{+\infty} O(x_0, y_0) I(x - x_0, y - y_0) dx_0 dy_0 \quad (2)$$

Simple arguments from first principles show that this expression also describes the intensity in the shadow cast by source S through target T onto the plane of detector D of Figure A-1.

In this case S is an incoherent diffuse light source whose intensity varies as  $I(x-x_0, y-y_0)$  and T is a transparency whose transmission varies as  $O(x_0, y_0)$ . An important experimental assumption which is implicit in the

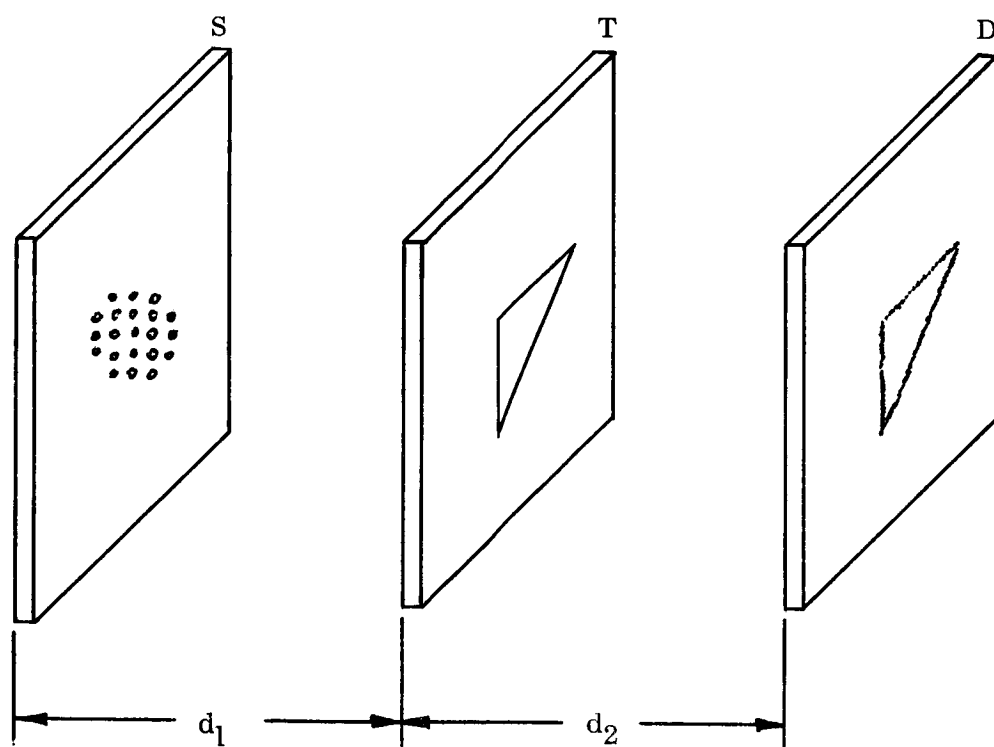


Figure A-1 - Image Synthesizer

foregoing is that if the target T were a pinhole, that is if  $O(x_0, y_0)$  were a 2 dimensional Dirac delta function, the point spread function would be reproduced exactly in the plane of the detector. This assumption can indeed be realized approximately, but a light source of special physical properties is required. This particular point will be discussed later.

It would seem appropriate to discuss the calculation of point spread functions. There are, however, excellent sources <sup>(3,5)</sup> on the subject of both geometric and diffraction aberrations. The Zernike-Nijboer theory of diffraction aberrations is discussed by Born and Wolf and details of the calculations are given in a paper by Kapany and Burke <sup>(4)</sup>. Furthermore, Born and Wolf devote all of Chapter 5 of their book to the discussion of geometric aberrations.

There is a real possibility of extending the image synthesis technique to image degrading effects other than aberrations. For example, in a real optical system vibrations degrade the image in much the same way as aberrations. Consider the image of a point source formed by a vibrating lens which suffers from aberrations. If the aberrations can be described mathematically, a probability  $P(\eta, \beta)$  can be calculated such that  $P(\eta, \beta) d\eta d\beta$  describe the probability that the Gaussian point in the image plane will be at  $(\eta, \beta)$ .

The image  $T_{VA}(x_i, y_i)$  formed by the lens is given by

$$T_{VA}(x_i, y_i) = \int_{-\infty}^{+\infty} \int_{-\infty}^{+\infty} T(x_i, \eta, y_i, \beta) P(\eta, \beta) d\eta d\beta \quad (3)$$

where  $T(x_i, y_i)$  is the point spread function for aberrations. Since  $T_{VA}(x_i, y_i)$  is the response of the system to a point source it is by definition the point spread function of the vibrating lens. Moreover, since it is expressible as a convolution integral the image synthesizer can be used to generate this resultant

point spread function. That is, either  $T_{VA}(x_i, y_i)$  can be computed beforehand and represented by a single spot diagram or spot diagrams representing  $T(x_i, y_i)$  and  $P(\eta, \beta)$  can be cascaded so that  $T_{VA}(x_i, y_i)$  can be generated in the image synthesizer.

The possibility of simulating other image degrading effects such as atmospheric turbulence, film graininess and granularity, electronic noise, etc. would seem to be feasible.

## B. Experimental Considerations

It is a simple matter to construct the image synthesizer of Figure A-1. However, if the integration expressed by Equation (2) is to be accurate, careful attention must be given to experimental technique. In particular, the physical representations of mathematic point spread functions must be carefully determined and constructed and the synthesizer must be designed in such a way that accuracy is not destroyed by experimental limitations. Some experimental techniques have been discussed in the literature<sup>(1, 2)</sup>. These will be reviewed and new techniques will be introduced.

### 1. Representation of Point Spread Functions

The ideal representation is a transparency whose transmission varies continuously according to the intensity in the point spread function. Unfortunately, it is an extremely difficult task to construct transparencies of anything but very simple functions (one dimension variations in transmission as the sine of the angle, for example). However, a good approximation to a transparency can be made by placing a large number of transparent holes on a opaque background in such a manner that the transmission averaged over a small area containing

several holes is proportional to the intensity in the point spread function.

If the holes in such a "spot diagram" do not overlap, this approximation approaches the ideal representation as a number of holes becomes arbitrarily large.

There are a number of obvious ways of constructing spot diagrams. The drilling of tiny holes in a thin metal sheet is straightforward, but the method can only be used for slowly varying functions because the maximum number of holes per unit area which can be drilled is quite small.

On the other hand, one can use photographic techniques to accurately represent more rapidly varying functions by preparing first a large scale drawing of a spot diagram and then recording it to the desired scale on high contrast film in the form of transparent spots on an optically dense background. Unfortunately, even when film is developed for maximum density the transmission of the background is finite. Thus, in cases where the ratio of the area of the holes to the area of the background is small, the amount of light transmitted by the background may be comparable to the light transmitted by the holes. This background "noise" is not characteristic of the point spread function and thus constitutes an appreciable error.

To avoid the problem of background noise, a background of infinite optical density may be selected at the outset. For example, a thin, vapor-deposited film of copper on a glass substrate constitutes such a background. A standard photoresist technique can be used to place an image of a spot diagram on the copper and the holes can be etched through after the image is developed.



Cathode ray tube display of spot diagrams appears to offer some advantages over the photographic techniques cited above. In this method, the co-ordinates of the spots are calculated by a high speed digital computer and are stored on magnetic tape or cards at the time of computation. The pattern is then generated automatically by passing the tape or cards through a digital-to-voltage converter whose output voltages deflect the electron beam of the cathode ray tube to the positions specified by the co-ordinates. If the cathode ray tube itself were used in an image synthesizer, application to semi-automatic lens design becomes apparent. The input to such a system would be optical system design data and the output would be a visual or photographic record of the image which would be generated by the hypothetical optical system. Obvious disadvantages of this technique of display are low light intensity and low resolution from the cathode ray tube as well as the possibility of overlapping of spots generated on the tube.

## 2. Image Synthesizer

Strictly speaking, in order for the spot diagram of Figure A-1 to be exactly reproduced in the plane of the detector for a pinhole target, it is necessary for the radiation pattern from an individual spot to be isotropic. Although no radiating surface has this property, opal glass or a ground glass screen approach it over very small angles. It should be pointed out in this regard that the radiation pattern from a patch of area on a diffuse surface ceases to be a characteristic of the entire surface and becomes a characteristic of a particular location on the surface when the size of the patch sampled approaches

the size of the diffusing elements on the surface. It is therefore necessary that the diffusing elements be made small enough so that, for areas small compared to the size of the spot diagram, the radiation pattern remains approximately isotropic over small angles.

For practical reasons then it is necessary that the synthesizer be designed in such a way that the solid angle subtended by the target at any spot in the spot diagram be small. This is equivalent to requiring that the dimensions of the spot diagram and target both be small compared to their separation  $d_1$ .

From the geometry of the device it is easily seen that the magnifications of the spot diagram and the target in the plane of the detector are  $d_2/d_1$  and  $(d_1 + d_2)/d_1$  respectively.

### III. EXPERIMENTAL WORK

#### A. Apparatus

A photograph of the particular instrument used in the study is shown in Fig. A-2 and its essential features are depicted graphically in Fig. A-3. Condensing lens  $L_1$  collimates light from source S so that the ground glass diffusion screen  $D_1$  is uniformly illuminated. The position of lens  $L_2$  is adjustable so that, if desired, a slightly defocused image of the spot diagram SD can be formed on the thin (0.020 in.) ground glass diffusion screen  $D_2$ . The defocusing produces a closer approximation to the point spread function. The target wheel contains several targets and can be transported along its axis or rotated about its axis. A ground glass screen is normally located in the film plane FP and the image on it can be viewed through eyepiece E with the aid of mirror M. For photographic work a film holder is inserted in the film plane and the ground glass screen is pushed aside. S,  $L_1$ ,  $D_1$ , SD, and E are external to the light tight enclosure which surrounds the other components. Lens  $L_2$  is provided with a shutter.

In particular, source S is a 100 watt projection lamp enclosed in a Cenco incandescent lamp illuminator (PG 2015). Diffusion screen  $D_1$  is a 2" x 2" microscope slide which has been ground with 600 grit grinding compound. Lens  $L_2$  is a 44 mm. Bolsey lens and shutter, with a shutter release provided outside the light tight enclosure. This lens can be translated along its axis by means of a lever located outside the enclosure, but for accurate integration the best position for the lens is such that the image on  $D_2$  is demagnified and slightly defocused. Screen  $D_2$  is about 0.020 in. thick and was ground with 600 grit

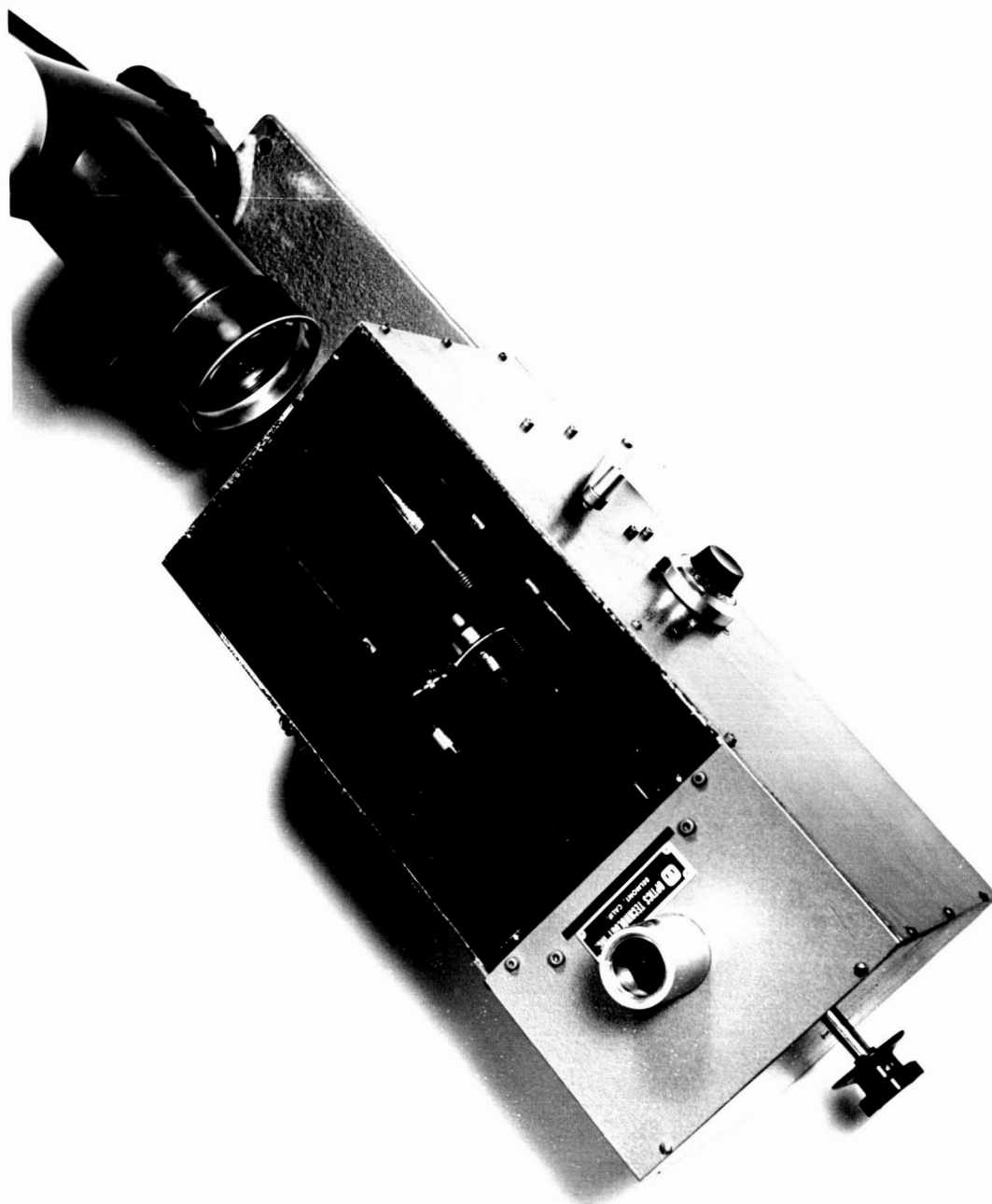
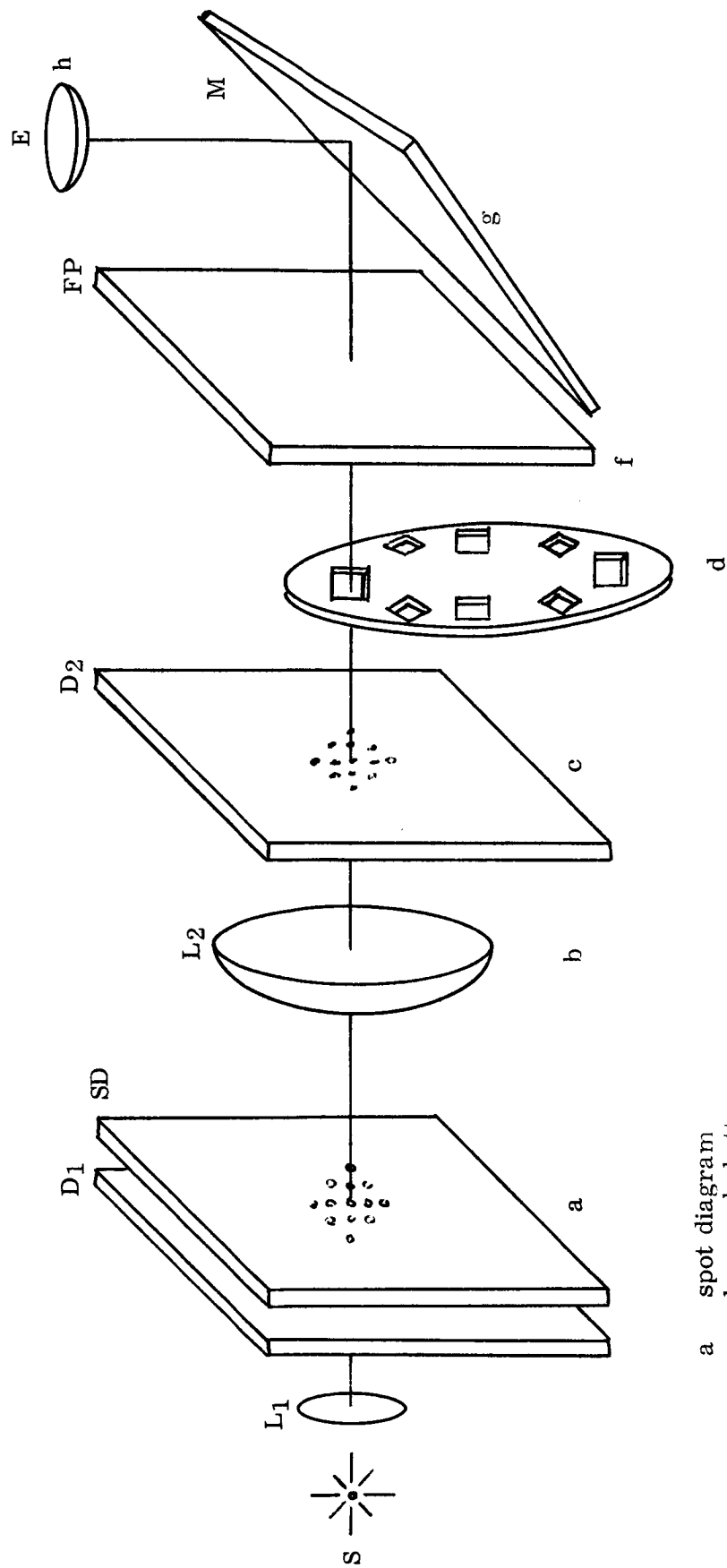


Figure A-2 Laboratory Image Synthesizer

Figure A-3 - Schematic of Laboratory Image Synthesizer



- a spot diagram
- b lens and shutter
- c ground glass screen
- d target wheel which can be rotated and translated
- e target
- f ground glass screen or photographic plate
- g mirror
- h viewing eyepiece

grinding compound. The target wheels accepts 12 x 12 mm transparencies and can be translated along its axis by means of calibrated 1 - turn helipot. Eight different targets can be rotated into position by turning a knob at the end of the enclosure. The magnifications of spot diagram  $M_S$  and the magnification of the target  $M_t$  are related to the arbitrary units on the helipot in Figures A-4 and 5, respectively.

The film holder accepts 2-1/2 in. x 3-1/2". cut film. Baffles were placed appropriately such that only light which passes through the lens reaches screen  $D_2$ .

For some spot diagrams which were used, the diameter of an individual spot on  $D_2$  was approximately 150 microns. Because of the particular geometric configuration some of these spots were required to radiate at angles up to 8°, a single spot of diameter 150 microns was investigated and is shown in Fig. A-6. The relative transmitted intensity is plotted as a function of angle measured from the normal to the screen  $D_2$ . The curve has an half width of over 20 degrees, although the pattern in anything but isotropic the variation over 8 or 9 degrees is not too large. The pattern was not changed grossly for different locations of the spot on the screen.

#### B. Procedure

The information on the point spread functions was generated by a computer, which specified the intensity in the image at a large number of points given by their polar coordinates. For the purpose of representing this intensity distribution, a 40 x 60 in. white display board was divided into small areas by first drawing concentric circles and then drawing radial lines at equal

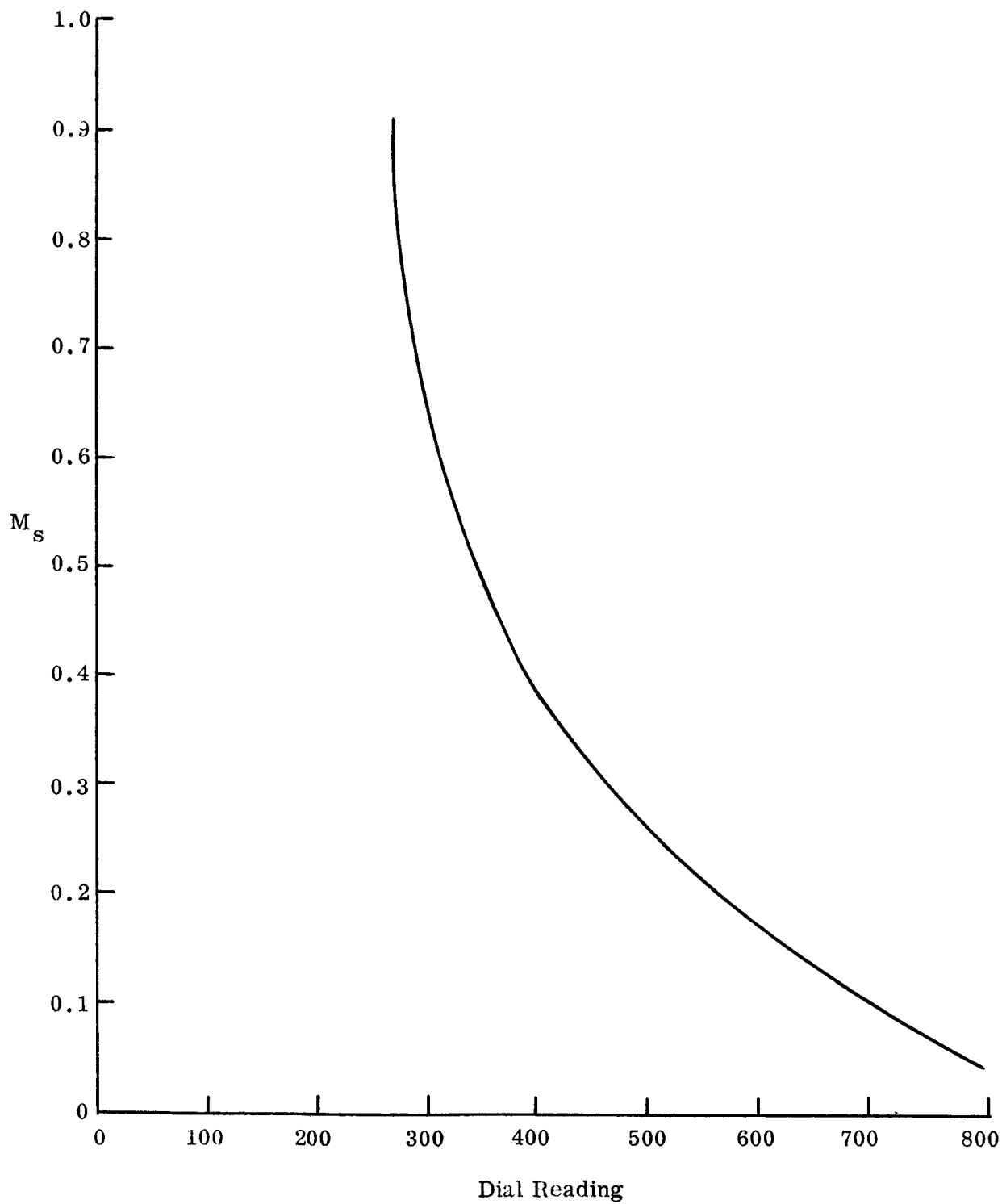


Figure A-4 - Magnification of Spot Diagram vs. Dial Reading

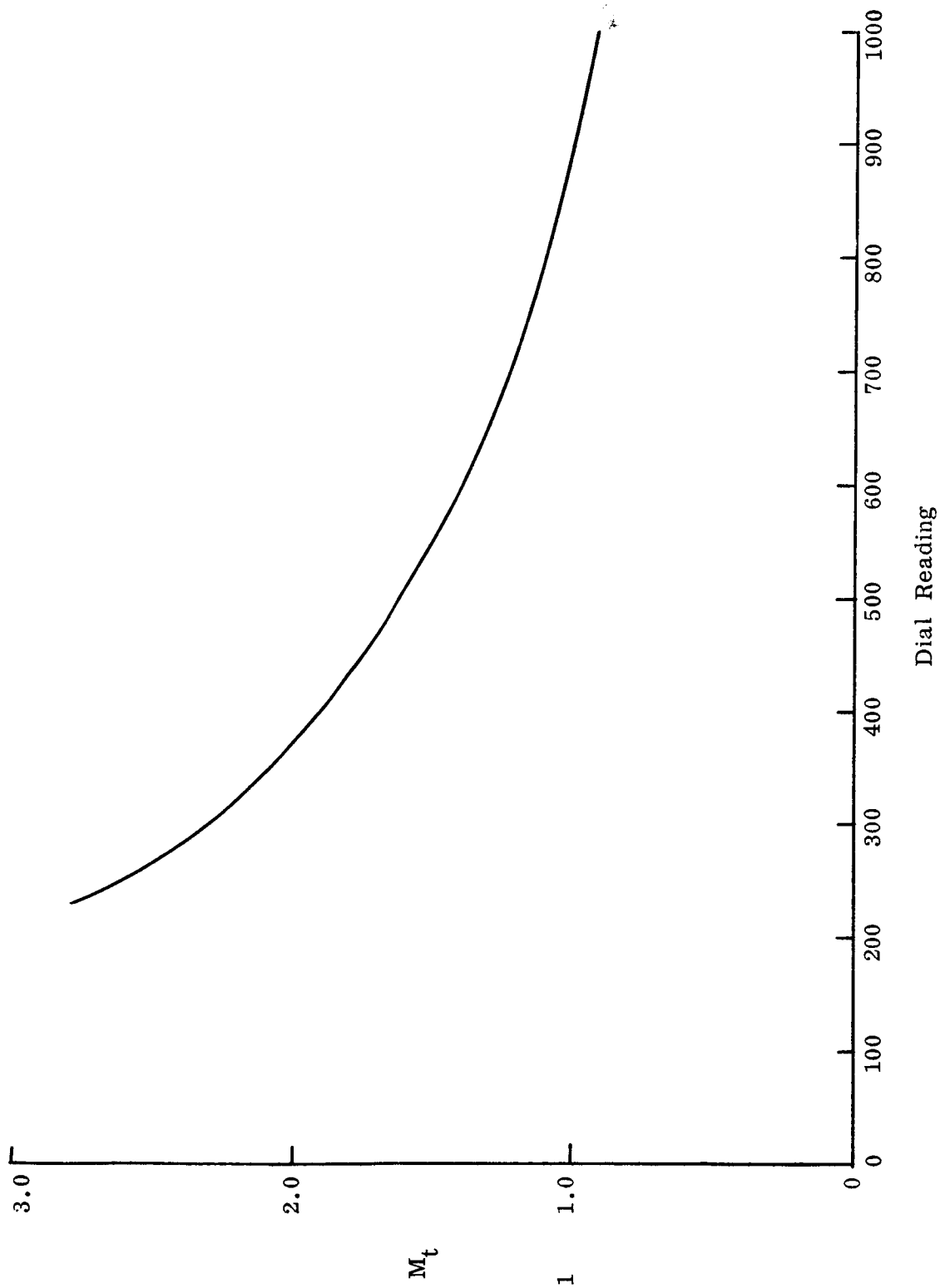


Figure A-5 - Magnification of Target vs. Dial Reading



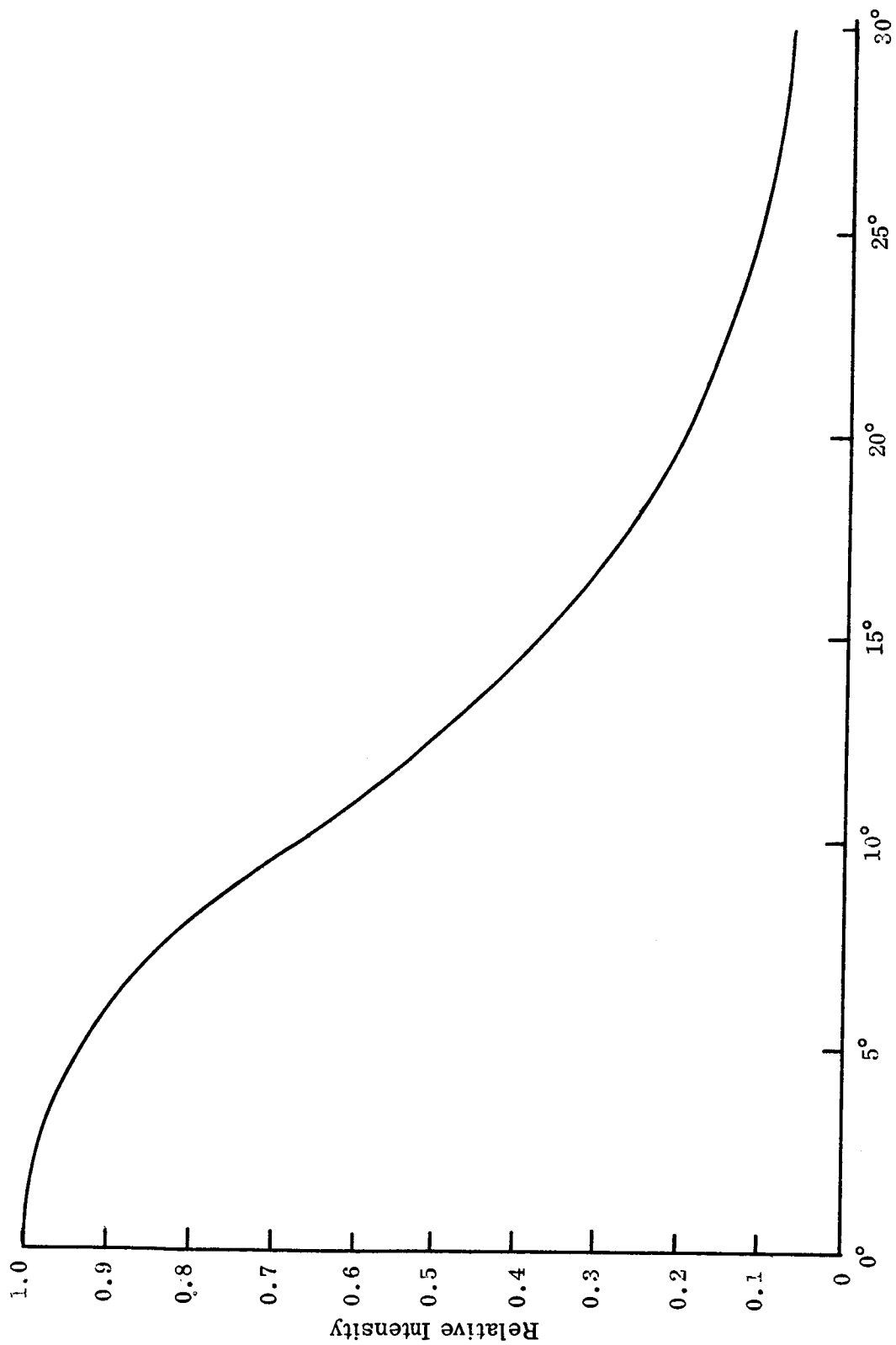


Figure A-14 - Magnification of Target vs. Dial Reading

angle intervals. The radii of adjacent circles differed by a constant amount. The intensity data was then transposed graphically to specify the flux associated with a particular element of area on the display board. Adhesive-backed, black terminal circles 0.093" in diameter were placed on the display board to represent the flux. A scale was selected such that the highest total number of terminal circles was used without overlapping in the high intensity regions.

The representation was photographed with Kodalith Ortho Film and reduced in size to fit into an area approximately 2 x 2 in. The final form of the spot diagrams consisted of transparent holes etched through a vapor deposited copper film on a glass substrate. In order to eliminate pinholes, it was necessary to deposit three thin ( $\approx 10^{-5}$  in.) layers of copper on the glass and to do the photochemical processing in a clean room.

The relative transmissions of the spot diagrams were determined by focusing the light transmitted through each and in turn onto a phototube. These measurements were used to establish an exposure time such that the time-integrated exposures through the various spot diagrams could be made identical.

An experimental H and D curve was obtained for the film which was used, and an exposure value was selected for the synthesis such that the linear portion of this curve was used. In principle, this was not necessary for a meaningful comparison of the synthesized photographs to be made. It was desirable for practical reasons, however, that the photographs be developed under controlled conditions of time and temperature. Care was exercised to insure that all photographs were treated in exactly the same manner.

C. Results

Table I shows the aberrations associated with the nine spot diagrams which were constructed and Fig. A-7 shows the spot diagrams along with several images which were synthesized from them. Some images are obviously better than others. However, close inspection reveals that the "quality" of an image associated with a given aberration depends upon the type of object. Moreover, in comparing the images associated with two different aberrations, one may find that depending on the shape of the test object different magnitudes of various aberrations are tolerable. Obviously, no general conclusions can yet be drawn from these images. Nevertheless, they do point out the potential of the image synthesis technique for a study of this type and further work is indicated.

There is one conclusion that can be drawn from the results so far. When the aberrations under consideration are small, there is a gross difference between the geometric point spread functions and the diffraction point spread functions. Therefore, for accuracy, diffraction effects must be taken account of in calculating the point spread functions. It should also be noted in this respect that the images synthesized using diffraction theory were, in general, better than those found using geometric theory, which agrees with the general observations of other workers in the field.

For comparison Fig. A-8 shows a synthesized image which was made using the airy disc representation, and Fig. A-9 shows a photograph of the same target made through the Sutton Lens whose point spread function is nearly an airy disc.

TABLE A - 1

TYPES OF SPOT DIAGRAMS CONSTRUCTED

<u>No.</u>	<u>Aberration</u>	<u>Amount</u>
1	Airy Disc (Diffraction)	--
2	Pinhole (Geometric)	--
3	Coma(Diffraction)	1.11 wavelengths
4	Coma(Geometric) Gaussian Plane	1.11 wavelengths
5	Spherical (Diffraction) Circle of Least Confusion	0.50 wavelengths
6	Spherical (Geometric) Gaussian Plane	0.50 wavelengths
7	Astigmatism (Diffraction) Central Plane	0.96 wavelengths
8	Astigmatism (Geometric) Central Plane	0.96 wavelengths
9	Coma and Astigmatism (Diffraction) Central Plane	0.96 wavelengths each aberration

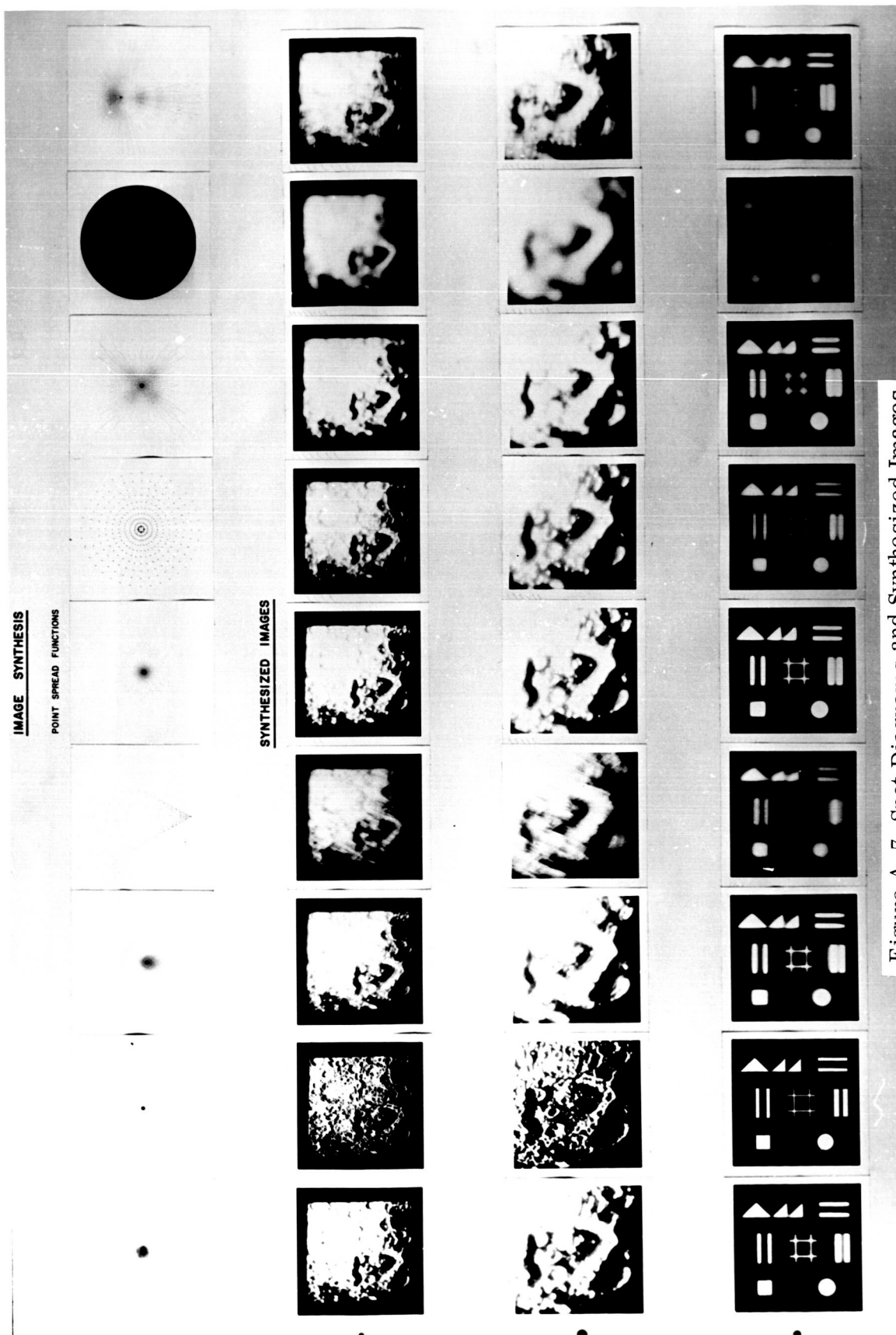


Figure A-7 Spot Diagrams and Synthesized Images

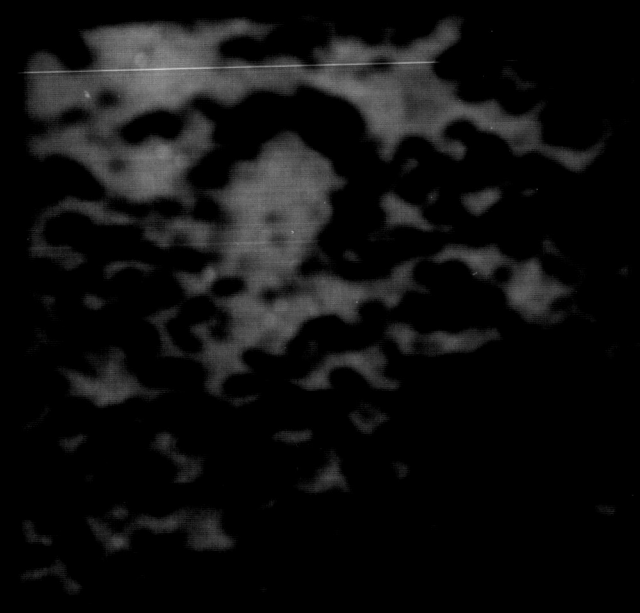


Figure A-8 Synthesized Image Using Airy Disc Spot Diagram

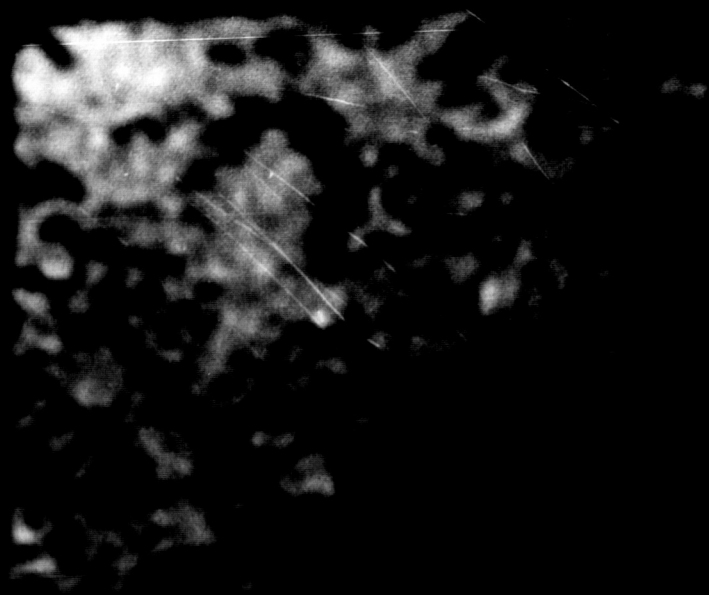


Figure A-9 - Real Image Using Sutton Lens

# LIST OF REFERENCES

1. R. E. Keim and N. S. Kapany, "Image Synthesis and Lens Response Using Spot Diagrams," J. Opt. Soc. Am. 48, 351-353 (1958)
2. N. S. Kapany, "Optical Image Assessment," Nature, 188, 1083-1086 (Dec. 24, 1960)
3. M. Born and E. Wolf, Principles of Optics, London, Pergamon Press, 1959.
4. N. S. Kapany and J. J. Burke, "Various Image Assessment Parameters," to appear in J. Opt. Soc. Am., 52, No. 12 (1962)
5. B. R. A. Nijboer, The Diffraction Theory of Aberrations, Groningen - Batavia, 1942.



## APPENDIX B

### APPARATUS FOR MEASURING VERY HIGH SPATIAL FREQUENCY RESPONSE

Figure 1 is a photograph of the special apparatus which was used for measuring the very high spatial frequency response of the Sutton lens. It is similar to the apparatus which was described by Kapany.<sup>(1)</sup> The essential features of the apparatus are illustrated in Figure 2.

Light from the slit is rendered parallel by the collimator and the test lens forms a real image corresponding to line spread function,  $A(x)$ , of the slit at its focal point. The optical design is such that the corresponding Gaussian image of the slit is smaller than the line spread function of the test lens, and diffraction effects due to the presence of the collimator are not appreciable. The microscope objective magnifies this image onto a sine wave mask which is located on the inside of a rotating glass drum. The time modulated intensity is detected by a photomultiplier tube and the signal is displayed on the oscilloscope. Several sets of masks, each having 25 cycles of a given frequency, are positioned along the circumference of the drum. The signal on the oscilloscope is photographed and the frequency response is calculated from the measurements taken directly from the photographs.

---

(1) N. S. Kapany, "Optical Image Assessment", Nature, 188, pp. 1083-1086 (December 24, 1960).

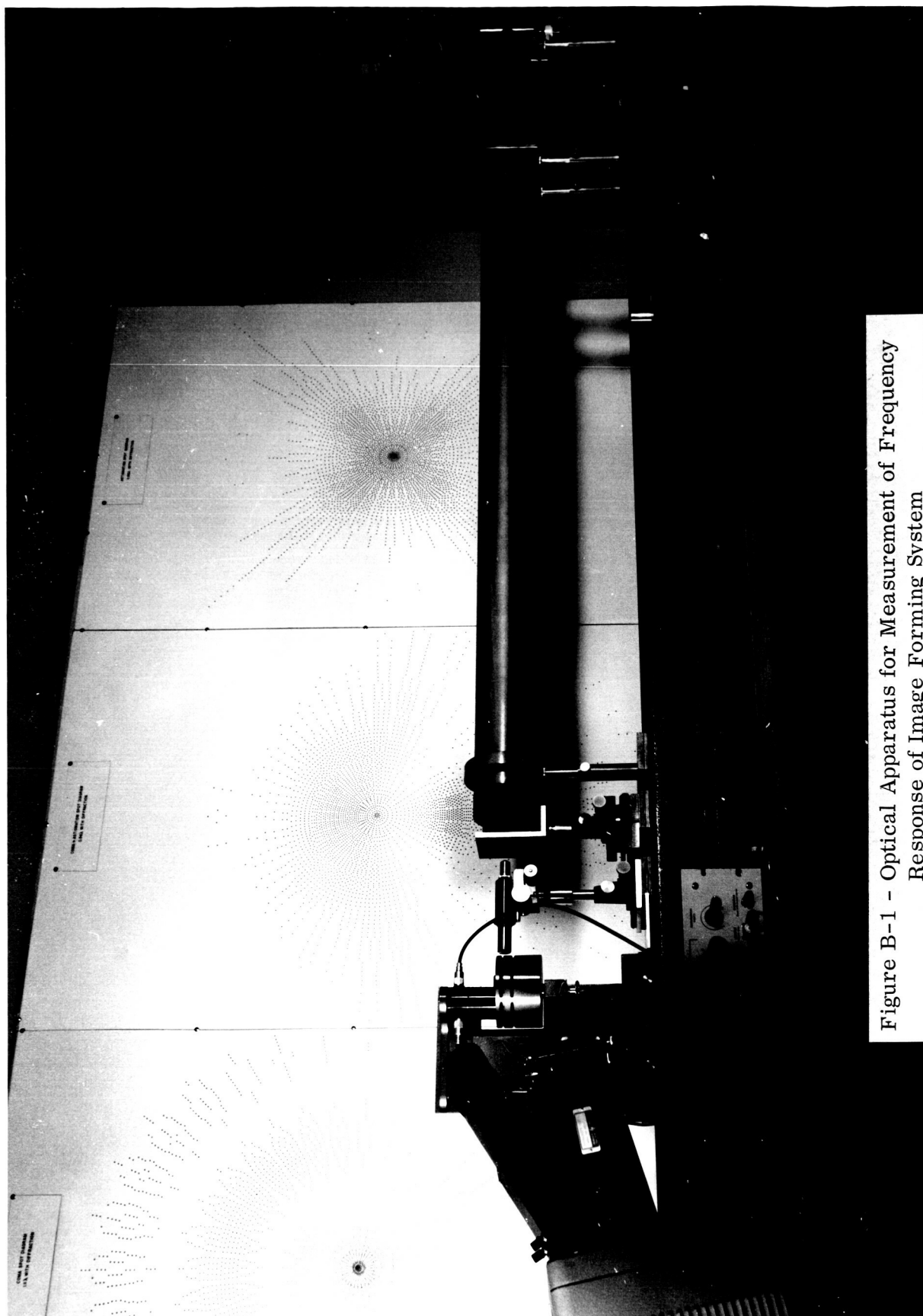


Figure B-1 - Optical Apparatus for Measurement of Frequency  
Response of Image Forming System

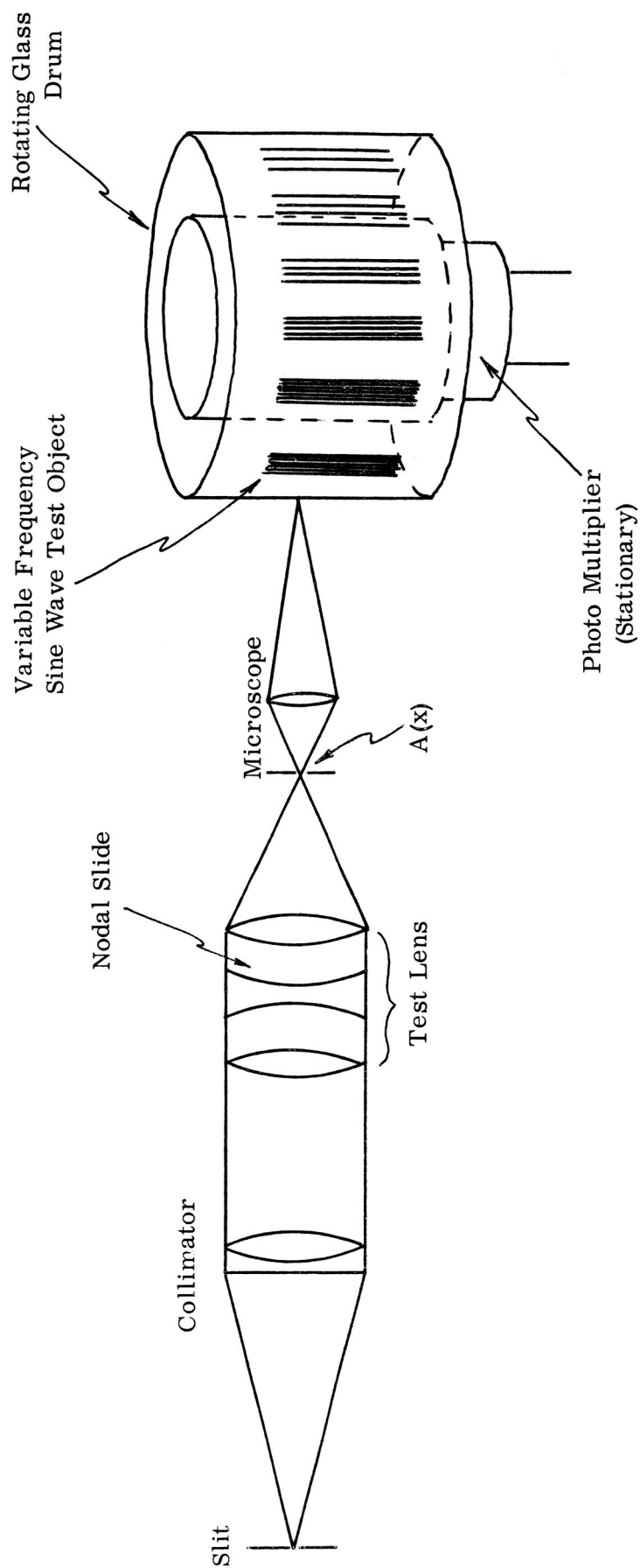


Figure B - 2 Optical Set Up for Measurement of Frequency Response of Image Forming System